



Platelets as modulators of blood-brain barrier disruption and
inflammation in the pathophysiology of ischemic stroke

• • •

Thrombozyten als Modulatoren der Blut-Hirn-Schrankenstörung und
Inflammation in der Pathophysiologie des ischämischen Schlaganfalls

Doctoral thesis for a doctoral degree at the Graduate School of Life Sciences

Julius-Maximilians-Universität Würzburg

Section: Neuroscience

submitted by

Lena Zimmermann née Papp

from Werneck, Germany

Würzburg 2022



Submitted on:

Members of the Thesis Committee

Chairperson: Porf. Dr. Thomas Dandekar

Primary Supervisor: PD Dr. Michael K. Schuhmann

Supervisor (Second): Prof. Dr. David Stegner

Supervisor (Third): Prof. Dr. Katrin G. Heinze

Supervisor (Fourth): Prof. Dr. Mirko Pham

Date of Public Defence: _____

Date of Receipt of Certificates: _____

Table of contents

Summary**Zusammenfassung**

1. Introduction	8
1.1 Ischemic stroke	8
1.2 Experimental models of ischemic stroke	10
1.3 The blood-brain barrier in health and ischemic stroke.....	12
1.4 The role of platelets in cerebral ischemia	14
1.5 Immune responses following ischemic stroke.....	18
1.6 Aim of the study.....	21
2. Material and Methods	23
2.1 Material	23
2.2 Methods.....	23
2.2.1 Murine experiments.....	23
2.2.1.1 Preparation of murine brain tissue.....	23
2.2.1.2 Brain tissue lysates.....	23
2.2.1.3 Endothelial cell lysates	24
2.2.1.4 Western blot analysis.....	24
2.2.1.5 Platelet isolation, washing, and generation of platelet releasate.....	25
2.2.1.6 Isolation of primary brain microvascular endothelial cells (MBMECs).....	26
2.2.1.7 Transendothelial electrical resistance (TEER) measurements of MBMECs.....	27
2.2.1.8 Isolation of lymphocytes from murine lymph nodes	28
2.2.1.9 Transmigration of lymphocytes over MBMEC monolayers	28
2.2.1.10 Flow cytometric analysis of lymphocytes after transmigration.....	30
2.2.1.11 Staining and quantification of gaps in MBMEC monolayers.....	30
2.2.1.12 Measurement of intracellular Ca ²⁺ in MBMECs.....	31
2.2.1.13 Murine PDGF-AB ELISA	33
2.2.2 Human experiments.....	33
2.2.2.1 Analysis of leukocyte subpopulations in human ischemic stroke patients by flow cytometry	33
2.2.2.2 Determination of platelet-leukocyte-aggregates in ischemic blood using flow cytometry.....	34
2.2.2.3 Immunofluorescence staining of platelet-neutrophil aggregates in human blood smears of the ischemic brain territory.....	34
2.3 Graphical illustrations.....	35
2.4 Statistics.....	35
3. Results	36
3.1 Characterization of the temporal dynamics of secondary microthrombosis following recanalization in an experimental stroke model.....	36
3.2 Blood-brain barrier breakdown as potential pathomechanism underlying progressive infarct growth ...	38

3.2.1	Early blood-brain barrier disruption after vessel recanalization	38
3.2.2	Elevated MMP9 levels after vessel recanalization	41
3.3	The role of platelets in blood-brain barrier disruption	42
3.3.1	Platelet GPVI-deficiency sustains vascular integrity following tMCAO.....	42
3.3.2	Platelet α -granules induce the loss of endothelial cell monolayer integrity	43
3.3.3	Platelet releasate does not affect tight junction protein levels in endothelial cells	46
3.3.4	Lack of platelet α -granules, but not dense granules protect from blood-brain barrier breakdown after tMCAO.....	47
3.3.5	Screening for an endothelial harming α -granule component.....	49
3.3.6	Platelet secretion mediates Ca^{2+} signalling in cultured endothelial cells	54
3.3.7	Platelet releasate affects lymphocyte distribution in an in vitro blood-brain barrier model.....	56
3.4	Unravelling intravascular processes in patients with hyper-acute stroke.....	58
3.4.1	Large vessel occlusion is accompanied by an immediate immune response, mainly consisting of granulocytes and $CD4^{+}$ T cells.....	58
3.4.2	Increased numbers of platelet-leukocyte aggregates in the ischemic vasculature of stroke patients	60
4.	Discussion	62
4.1	Secondary microthrombosis is not causative for infarct development.....	62
4.2	Early blood-brain barrier breakdown during reperfusion is associated with the secretion of platelet α -granules	64
4.3	Local immune cell invasion and formation of platelet-leukocyte aggregates during occlusion in human hyper-acute stroke	70
4.4	Concluding remarks and future perspectives	73
5.	References	76
6.	Appendix	86
6.1	Devices	86
6.2	Consumables, Kits.....	86
6.3	Chemicals/Reagents	87
6.4	Buffers, solutions and media.....	90
6.5	Antibodies.....	95
6.6	Software.....	98
7.	Abbreviations	99
8.	Creative Commons License	103
9.	Curriculum vitae	104
10.	Acknowledgements	105
11.	Publications	106
12.	Affidavit	108
13.	Eidessattliche Erklärung	108

Summary

Ischemia-reperfusion injury (I/R injury) is a common complication in ischemic stroke (IS) treatment, which is characterized by a paradoxical perpetuation of tissue damage despite the successful re-establishment of vascular perfusion. This phenomenon is known to be facilitated by the detrimental interplay of platelets and inflammatory cells at the vascular interface. However, the spatio-temporal and molecular mechanisms underlying these cellular interactions and their contribution to infarct progression are still incompletely understood. Therefore, this study intended to clarify the temporal mechanisms of infarct growth after cerebral vessel recanalization. The data presented here could show that infarct progression is driven by early blood-brain-barrier perturbation and is independent of secondary thrombus formation. Since previous studies unravelled the secretion of platelet granules as a molecular mechanism of how platelets contribute to I/R injury, special emphasis was placed on the role of platelet granule secretion in the process of barrier dysfunction. By combining an *in vitro* approach with a murine IS model, it could be shown that platelet α -granules exerted endothelial-damaging properties, whereas their absence (NBEAL2-deficiency) translated into improved microvascular integrity. Hence, targeting platelet α -granules might serve as a novel treatment option to reduce vascular integrity loss and diminish infarct growth despite recanalization.

Recent evidence revealed that pathomechanisms underlying I/R injury are already instrumental during large vessel occlusion. This indicates that penumbral tissue loss under occlusion and I/R injury during reperfusion share an intertwined relationship. In accordance with this notion, human observational data disclosed the presence of a neutrophil dominated immune response and local platelet activation and secretion, by the detection of the main components of platelet α -granules, within the secluded vasculature of IS patients. These initial observations of immune cells and platelets could be further expanded within this thesis by flow cytometric analysis of local ischemic blood samples. Phenotyping of immune cells disclosed a yet unknown shift in the lymphocyte population towards CD4⁺ T cells and additionally corroborated the concept of an immediate intravascular immune response that is dominated by granulocytes. Furthermore, this thesis provides first-time evidence for the increased appearance of platelet-leukocyte-aggregates within the secluded human vasculature. Thus, interfering with immune cells and/or platelets already under occlusion might serve as a potential strategy to diminish infarct expansion and ameliorate clinical outcome after IS.

Zusammenfassung

Eine häufig auftretende Komplikation in der Behandlung des ischämischen Schlaganfalls ist der Ischämie/Reperfusion Schaden (I/R Schaden), welcher trotz der erfolgreichen Wiederherstellung der zerebralen Durchblutung durch ein paradoxes Fortschreiten des entstandenen Gewebeschadens charakterisiert ist. Dieses Phänomen wird durch das schädigende Zusammenspiel von Thrombozyten und inflammatorischen Zellen am vaskulären Endothel verursacht. Allerdings sind die räumlich-temporalen und molekularen Mechanismen dieser zellulären Interaktionen und deren Beteiligung am Infarktwachstum noch nicht vollständig verstanden. Daraus folgend, beabsichtigte diese Arbeit eben diese temporalen Mechanismen des fortschreitenden Infarktwachstums nach der zerebralen Gefäßwiedereröffnung aufzuklären. Die hier vorgestellten Daten implizieren, dass das anhaltende Fortschreiten des Gewebeschadens durch die Schädigung der Bluthirnschranke verursacht wird und somit unabhängig vom Auftreten sekundär gebildeter Thromben ist. In vorangegangenen Studien konnte die Freisetzung von thrombozytären Granula als molekularer Mechanismus, mit welchem Thrombozyten zum I/R Schaden beitragen, aufgedeckt werden. Basierend auf diesen Studien wurde in dieser Arbeit ein besonderes Augenmerk auf die Sekretion thrombozytärer Granula im Zusammenhang mit der Beeinträchtigung der endothelialen Barriere gelegt. Durch die Kombination eines *in vitro* Ansatzes mit einem murinen Model des ischämischen Schlaganfalls konnte gezeigt werden, dass α -Granula endothelialen Schaden verursachen, wohingegen deren Absenz (NBEAL2 Defizienz) zu einer verbesserten mikrovaskulären Integrität führte. Aufgrund dessen könnte das Adressieren der α -Granula als eine neuartige Therapieoption zum Erhalt der vaskulären Integrität und zur Verminderung des Infarktwachstums trotz Rekanalisation genutzt werden.

Neuste Erkenntnisse enthüllten, dass die dem I/R Schaden zu Grunde liegenden Pathomechanismen bereits während des Verschlusses eines großen hirnversorgenden Gefäßes zu beobachten sind. Dies deutet darauf hin, dass der Verlust von penumbralem Gewebe unter Okklusion und I/R Schädigung während der Reperfusion im engen Zusammenhang stehen. Im Einklang hiermit konnten humane Daten eine Neutrophilen-dominierte Immunantwort und lokale Thrombozyten Aktivierung und deren Sekretion, anhand der Detektion der α -Granula Hauptkomponenten, im verschlossenen Gefäßsystem von ischämischen Schlaganfall Patienten nachweisen. Diese anfänglichen Beobachtungen konnten im Rahmen dieser Arbeit anhand

durchflusszytometrischer Untersuchungen von lokal abgenommenen ischämischen Blutproben erweitert werden. Die Phänotypisierung von Immunzellen enthüllte eine bisher unbekannte Verschiebung der Lymphozyten Population hin zu CD4⁺ T-Zellen und bekräftigte zusätzlich das Konzept einer unmittelbaren intravaskulären Immunantwort, welche durch Granulozyten dominiert wird. Darüber hinaus konnte in dieser Thesis das erste Mal das erhöhte Auftreten von Thrombozyten-Leukozyten-Aggregaten in dem verschlossenen humanen Gefäßsystem nachgewiesen werden. Demzufolge könnte eine Beeinflussung von Immunzellen und/oder Thrombozyten bereits unter Okklusion als potentiell vielversprechende Strategie genutzt werden, um die Ausweitung des Infarktes einzuschränken und klinische Endpunkte nach einem ischämischen Schlaganfall zu verbessern.

1. Introduction

1.1 Ischemic stroke

Ischemic stroke (IS) is a severe neurological disease with a worldwide incidence of 12.2 million people in 2019 [1]. This clinical condition accounts for approximately 80% of hospitalized stroke patients, frequently leading to serious long-term disabilities with eminent mortality [2]. The mainstay of IS treatment aims for rapid restoration of blood flow within the occluded vasculature [3], which was until recently solely achieved by systemic thrombolysis via the application of recombinant tissue plasminogen activator (rt-PA). In 2015 the advent of mechanical thrombectomy (MT) revolutionized IS treatment [4, 5], by the addition of mechanical thrombus removal to pharmacologic thrombolysis therapy or by its individual application [6]. This novel treatment option substantially ameliorated neurological sequelae and increased successful recanalization rates, but still did not imply a favourable clinical outcome in 43.5 to 63.3% of treated patients [7].

Pathophysiologically, large-vessel occlusion (LVO) is characterized by an obstruction of a major brain-supplying artery, such as the internal carotid artery (ICA) or middle cerebral artery (MCA), via a thrombotic event or an embolus that emerged from the heart or extracranial artery stenoses [8]. This initial event subsequently blocks cerebral blood flow (CBF) and immediately deprives a specific brain territory (infarct core) of oxygen and nutrients. As a consequence, brain cells are no longer able to generate adenosine triphosphate (ATP) through their aerobic metabolism pathway and are forced to alternative anaerobic metabolism. This in turn, leads to high local concentrations of lactic acid, which disturbs the physiologic acid-base balance of the brain, and a decreased amount of available ATP. Due to the restricted amount of energy, ATP-reliant Na^+/K^+ pumps of neurons can no longer maintain their transmembrane gradient, leading to cytotoxic oedema and thereby to the impairment of neuronal signalling. Likewise, failure of $\text{Na}^+/\text{Ca}^{2+}$ pumps results in an accumulation of intracellular calcium, triggering the activation of proteases and lipases, the formation of reactive oxygen species (ROS), as well as the release of the excitatory neurotransmitter glutamate. The excessive amount of extracellular glutamate further leads to the activation of NMDA (N-methyl-D-aspartate) and AMPA (α -amino-3-hydroxy-5-methyl-4-isoxazolepropionic acid) receptors on astrocytes and neurons, which ultimately terminates in excitotoxicity [8, 9]. The extent of tissue damage, though, highly depends on the structural organization of the affected brain vasculature [10]. The infarct core

is substantially ceased from CBF and thus most prone to irreversible tissue damage. Brain tissue surrounding the infarct core, referred to as the ischemic penumbra, on the contrary, is defined as dysfunctional but metabolic active tissue, which highly relies on the nourishment through collateral anastomoses [11, 12] (Figure 1-1). This compensatory blood supply can temporally preserve the cellular structure of the tissue and therefore makes the penumbra potentially salvageable upon restoration of CBF [13]. However, if the occlusion persists, the infarct core will most likely expand and lead to penumbral tissue loss and thus infarct growth [14]. Nevertheless, even in case of successful recanalization, the salvation of tissue at risk is not guaranteed. This might be attributable to the mechanism of ischemia-reperfusion injury (I/R injury) [15], which is defined as a paradoxical harmful blood reflow. In general, five main reasons are considered to contribute to infarct growth after recanalization. First, platelet and leukocyte interactions within the microvascular compartment exert deleterious effects in the process of thrombo-inflammation [16]. Second, reperfusion itself may induce detrimental harm, leading to unfavourable tissue damage. Third, collateral blood flow that nourishes the ischemic penumbra fails [17]. Fourth, vascular complications result in haemorrhagic transformation (HT) and, fifth, due to alterations caused by the ischemic insult, vascular functions cannot be restored because of pericyte, large vessel constriction or microvascular neutrophil stalling - a multifaceted condition referred to as the no-reflow phenomenon [18, 19].

In either circumstance, initial cerebral hypoperfusion induces the conversion of the luminal endothelial surface from an anti-coagulant to a pro-coagulant state, elicits an immediate strong inflammatory response, and provokes platelet activation [20, 21]. This broad array of mechanisms is intertwined within the superordinate process of thrombo-inflammation, orchestrating secondary infarct expansion. This concept has first been proposed for I/R injury, but compelling evidence demonstrates that thrombo-inflammation commences already under occlusive conditions [22], and persists upon reperfusion [23]. Thus, enforcing a paradigm shift from two separate processes acting under occlusion - penumbral tissue loss – and reperfusion - I/R injury-, to one interrelated process sharing mechanistic similarities. Although some drivers of thrombo-inflammation could already be determined, namely platelets, immune cells, and the vascular system [24], molecular and cellular interactions that participate in the orchestration of infarct expansion remain largely unknown.

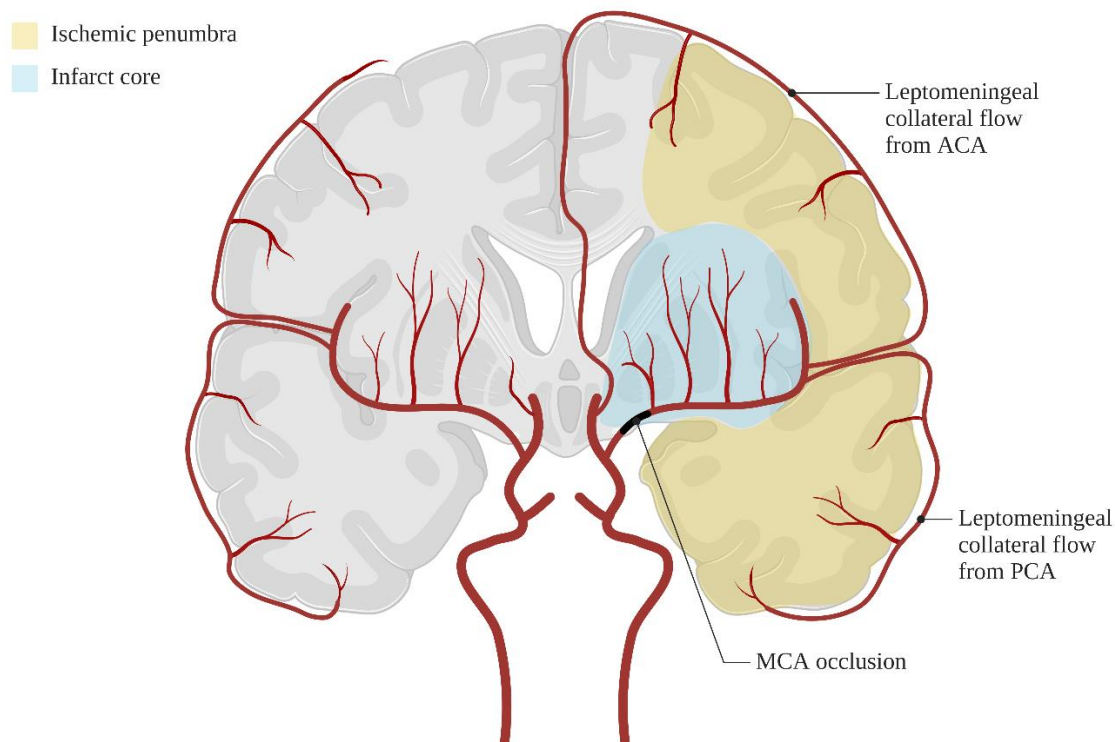


Figure 1-1. The concept of ischemic stroke. Large-vessel occlusion (LVO) due to thromboembolism or thrombus formation induces a restriction in cerebral blood flow (CBF). The most frequently affected arteries during ischemic stroke (IS) are the internal carotid artery and the middle cerebral artery (MCA) including its branches. In case of a MCA occlusion, the ischemic core is built by the striatum, which is most affected by inadequate CBF and will be irreversibly damaged after a short period of time. Brain tissue surrounding the ischemic core is referred to as ischemic penumbra. This potentially salvageable brain tissue is impaired in its functionality but is metabolically kept alive by retrograde blood flow. Collateral blood flow is thereby provided by leptomeningeal anastomoses of the anterior cerebral artery (ACA) and posterior cerebral artery (PCA) branches. Adapted by permission from Springer Nature: Nature, Nature Reviews Disease Primers, “Ischaemic stroke”, Campbell *et al.*, Copyright © 2019 [8].

1.2 Experimental models of ischemic stroke

Investigations of human brain biopsies are limited in excess and are often associated with time delays from insult onset to post-mortem brain tissue sampling, which mainly impedes examinations of the hyper-acute or early reperfusion phase. Only recently, though, local pial blood sampling within the ischemic vascular compartment of human stroke patients during MT enabled first intravascular insights into cellular and molecular mechanisms under occlusion [25]. This unique technique is at present the only and most appropriate option for the investigation of the human system during the ultra-early phase of IS. However, shortcomings of this methods are spatio-temporal and probing restrictions, which solely allow for the

sampling of blood within large arteries during vascular occlusion. This in turn, prohibits detailed insights on molecular and cellular interactions within different vascular beds including the microvascular system, which is first affected during early MCA occlusion [24]. Thus, animal models constitute an essential complementation for the investigation of pathomechanisms or for testing of potential pharmacologic agents within the early time periods post occlusion. The experimental induction of focal cerebral ischemia was established in various models that mirror distinct clinical conditions of human stroke patients [26]. Dependent on the scientific question the selection of the appropriate model is crucial while considering the advantages and disadvantages (see Table 1).

Table 1. List of common experimental ischemic stroke models in rodents (modified from Fluri *et al.*, 2015 [26] under the terms of the Creative Common Attribution License)

Model	Advantages	Disadvantages
Intraluminal suture	Mimics human ischemic stroke	Hyper-/hypothermia
MCAO model	Exhibits a penumbra Highly reproducible Reperfusion highly controllable No craniectomy	Increased hemorrhage with certain suture types Not suitable for thrombolysis studies
Craniotomy model	High long-term survival rates Visual confirmation of successful MCAO	Highly invasive Consecutive complications
Photothrombosis model	Enables well-defined localization of an ischemic lesion Highly reproducible Low invasiveness	Causes early vasogenic edema Not suitable for the investigation of neuroprotective agents
Endothelin-I model	Low invasiveness Low mortality	Duration of ischemia not controllable Induction of astrocytosis and axonal sprouting
Embolic stroke model	Mimics most closely the pathogenesis of human stroke Appropriate for studies of thrombolytic agents	Low reproducibility of infarcts Spontaneous recanalization High variability of lesion size

At present, the intraluminal suture transient middle cerebral artery occlusion (tMCAO) model is the most frequently used experimental stroke model in rodents, closely mimicking the current clinical treatment scenario of LVO by MT. In this model, a coated filament is inserted into the common carotid artery (CCA) and advanced to the origin of the MCA for occlusion. To enable reperfusion, the filament is removed and thereby reflects thrombus removal as performed by MT [27]. This model advantageously allows for the simulation of I/R injury, as infarcts are not fully developed after one hour of occlusion, but evolve upon recanalization [24]. However, by increasing the occlusion durations in a step-wise manner, the model of MCA occlusion is also suitable to mimic either the kinetics of prolonged LVO or permanent occlusion (pMCAO). Of note, this model has additionally proven to predict bleeding complications and unfavorable outcome in clinical studies [28, 29].

Independent of the used IS model, all enable a direct investigation of the immune, vascular and central nervous system (CNS), being involved in the pathogenesis of IS and representing target structures for pharmacologic treatments.

1.3 The blood-brain barrier in health and ischemic stroke

The cerebral vasculature exhibits a unique structural organization at the interface between blood and the brain – the blood-brain barrier (BBB). This physical barrier effectively separates the cerebral microenvironment from the peripheral circulation by the lack of fenestration and a tightly regulated entry of molecules into the brain [30]. These functional properties of the BBB are crucial for the maintenance of brain homeostasis, which is coordinated by its specialized multicellular structure, constituting endothelial cells (ECs), pericytes, astrocytes, and the basal lamina. ECs, lining the inner lumen of the vessels, thereby possess the most critical and complex function. Unlike peripheral vascular beds, ECs of the BBB are characterized by a flattened structure and a high transendothelial electrical resistance (TEER) [31]. This integral feature is mainly related to the continuous interconnection of adjacent ECs via junctional complexes. Thereby, adherens junctions (AJ), gap junctions, and tight junctions (TJ) collectively seal paracellular clefts to limit the free diffusion of solutes or pathogens while allowing intercellular communication [32]. This restrictive nature of the sealed endothelium also limits the transport of essential nutrients and molecules to the brain, requesting for a polarized exposure of ion

channels, transporters, and receptors. To ensure the proper functioning of these energy-intensive transport pathways, ECs contain high amounts of mitochondria [33]. Although ECs exert substantial properties of the BBB, formation, function, and integration into neuronal circuits of the CNS highly rely on pericytes and astrocytes. These cell types enable an association of the vasculature with the CNS network by the so-called neurovascular unit (NVU). Besides the cellular components of the BBB, the NVU consists of neurons, interneurons, microglia, smooth muscle cells, and the extracellular matrix [34]. The interplay among each of these components establishes a highly complex network that regulates CBF and maintains the BBB, as well as cerebral homeostasis.

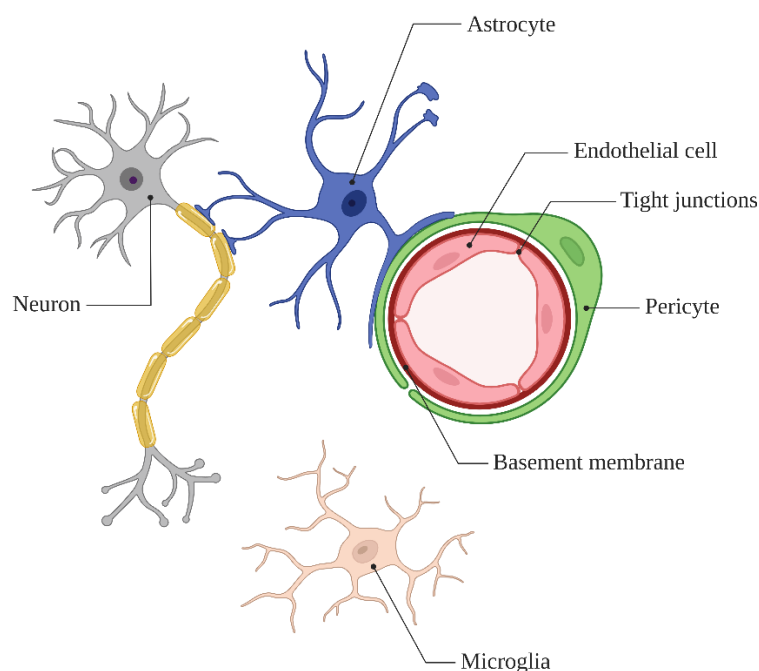


Figure 1-2. Schematic diagram of the Neurovascular Unit (NVU). The NVU is an interconnected network of different cell types that regulates cerebral blood flow (CBF) and maintains blood-brain barrier (BBB) function as well as cerebral haemostasis. At the level of brain capillaries, the NVU consists of vascular endothelial cells, pericytes, the basement membrane, astrocytes, microglia, and neurons. Adopted from Sweeney *et al.*, 2015 [35] under the terms of the Creative Common Attribution License.

Disruption of BBB integrity is a major pathological hallmark of IS and is evident within hours after ischemia onset [36]. Since pleiotropic mechanisms were traditionally made accountable

for a biphasic cycle of opening and refractory phases, estimations that are more recent propose a continuous opening of the BBB with peak phases of additional integrity loss [37, 38]. Within murine studies, the initial opening of the BBB could be designated to the first 30 to 120 min post recanalization (hyper-acute stroke) [36, 39]. The ischemic insult thereby elicits a hypoxia-induced ischemic cascade, including cytotoxic edema, cell death, and subtle cytoskeletal alterations of ECs, which are referred to as stress fibers. These morphological changes create tension on TJ complexes, loosening the connection of adjacent ECs and increasing the permeability of the affected vessels. During the following peak phase (acute stroke, 3 to 24 h) neuro-inflammatory processes executed by cells of the peripheral immune system and matrix metalloproteinases (MMP) further extend the damage to the BBB. This greater increase in BBB permeability could be observed in humans as well as in mice [38, 39]. Sustained vascular permeability in later stages of stroke (subacute/ chronic stroke, 48 h to several weeks), however, is most likely associated with regenerative rather than destructive processes [37].

Independent of the BBB-damaging mechanisms, extravasation of fluid and blood-borne cells into the brain parenchyma due to increased para- and transcellular permeability leads to vasogenic edema or even HT [40].

1.4 The role of platelets in cerebral ischemia

Platelets are cell fragments originating from their precursors – the megakaryocytes (MKs). These anucleated cells with a discoid shape have long been constrained to their role in thrombosis and haemostasis. During the last decades, however, platelets were augmentally recognized at sites of cerebral infarction, where they participate in inflammation and lesion development [41-43]. However, the exact molecular pathways that contribute to local accumulation and activation of platelets still remained to be elucidated. Today, it is well established that glycoprotein (GP) Ib, a surface receptor exclusively found on platelets and MKs, is utilized by platelets to guide inflammation [44]. GPIb facilitates the initial tethering of platelets to the pre-injured vasculature by the binding of von Willebrand factor (vWF) [45, 46]. Within experimental stroke studies, blockade of GPIb α decreased infarct growth under occlusion (pMCAO) and reduced I/R injury (tMCAO) independent of prophylactic or therapeutic treatment application [12, 47, 48]. Additionally, treatment of aged and comorbid

mice, resembling the common patient characteristics in the clinics, significantly reduced cerebral damage as well [49]. Likewise, the genetic deficiency in GPIIb/IIIa or vWF reduced infarct volumes and improved neurological outcomes, while reconstitution of vWF plasma levels restored susceptibility to I/R injury in vWF-deficient mice [50-52]. These experimental data establish the GPIIb/IIIa-vWF axis as an important mechanistic pathway in the pathophysiology of IS.

Since GPIIb/IIIa-vWF interactions are too transient and weak to firmly attach platelets to the vessel wall, further platelet activation is required through the platelet-specific activatory receptor – GPVI [53]. Upon ligand binding, particularly to collagen and fibrin, platelet activation is induced via an immunoreceptor tyrosine-based activation motif (ITAM) resulting in shape change of platelets and inside-out activation of $\beta 1$ and $\beta 3$ integrins [54]. Pharmacologic targeting of GPVI can be achieved by antibody-mediated depletion from the platelet surface (JAQ1 antibody) [28] or by competitive inhibition via a recombinant soluble dimeric GPIV-Fc fusion protein [55]. Both treatment settings substantially augmented stroke outcomes under permanent [56] and transient occlusion without inducing intracerebral haemorrhages (ICH) [28, 57]. These results are in line with experiments that targeted the ITAM inhibitory proteins Src-like adapter protein (SLAP) and SLAP2. Constitutive SLAP/SLAP2 knockout mice developed increased infarct volumes and revealed worsened functional outcomes after 30 minutes (min) of focal cerebral ischemia. These findings were accompanied by an increased occurrence of occluded vessels and an accumulation of fibrin within the infarcted areas. Moreover, adoptive transfer of SLAP/SLAP2-deficient platelets into wild-type (WT) mice confirmed that aggravated damage was attributable to platelet-specific absence of both adaptor proteins, underlining the critical role of GPVI-ITAM signalling in cerebral I/R injury [58]. This is further supported by the fact that patients suffering from transient ischemic attacks (TIA) or stroke presented elevated levels of GPVI on the platelet surface compared to controls [59]. With Revacept a humanized Fc fusion protein of the GPVI ectodomain was tested in a phase I clinical trial [55, 60]. Due to the high tolerability and the absence of altered platelet functions in healthy humans, blockage of GPVI-collagen interactions was further tested within a phase II clinical trial (NCT01645306) in the context of carotid artery stenosis, TIA, or stroke [61]. Thereby, high doses of Revacept significantly reduced the occurrence of combined safety and efficacy endpoints in comparison to placebo treatment within the patient cohort [62]. These findings argue for a potential treatment option of Revacept as an add-on therapy in acute IS patients and lay the foundation for future phase III clinical studies.

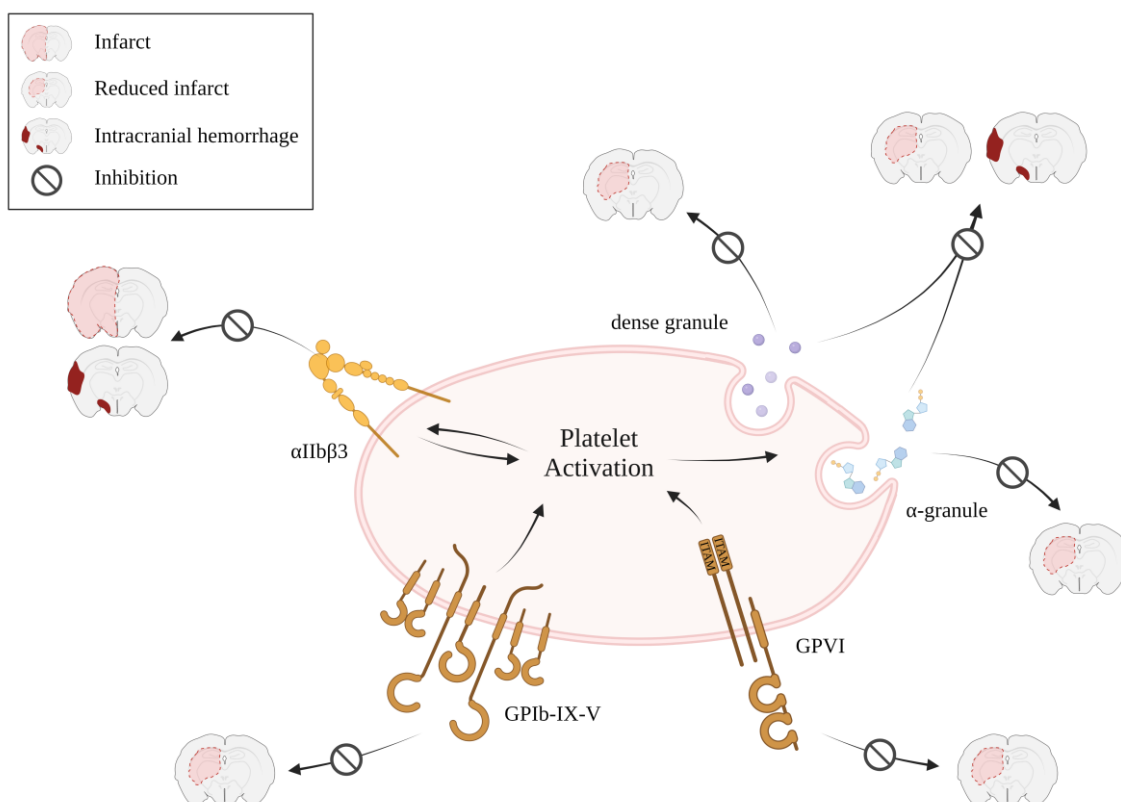


Figure 1-3. Platelets as determinants of stroke outcome in a murine experimental ischemic stroke model. Inhibition of platelet activation via GPIIb/IIIa or GPVI reduces infarct sizes following cerebral ischemia reperfusion. Similarly, single deficiency in one of the two major platelet granules, α - or dense granules, prevents from large infarcts. However, simultaneous loss of both granules as well as inhibition of platelet aggregation via GPIIb/IIIa increases mortality rates as a consequence of intracranial haemorrhages. Adopted from Stegner *et al.*, 2019 [63] under the terms of the Creative Common Attribution License.

GPVI-mediated signaling is also crucial for the release of stored granules, thereby contributing to platelet functions in hemostasis, thrombosis, and inflammation [64]. Three main secretory granules have been defined in platelets: α -granules, δ -granules (dense granules), and lysosomes [65]. Lysosomes are the least abundant granules in platelets (1-3 lysosomes/platelet) and contain diverse proteolytic enzymes and proteins with bactericidal activity. Their function in the pathology of IS, however, remains elusive. Dense granules are packed with biogenic amines like serotonin or histamine, adenine nucleotides (ADP, ATP), and cations (Ca^{2+} , Mg^{2+}) [66]. On account of their cargo, these granules appear as an electron-dense spot within electron microscopic analysis [67]. Upon release, dense granule content mainly acts as a second wave

mediator, promoting platelet activation and thrombus formation. Decisive for platelet dense granule exocytosis is the bridging of the granule with the plasma membrane or the open canalicular system by the effector protein Munc13-4 [68]. Mice deficient for Munc13-4 (*Unc13d*^{-/-}) are unable to secrete platelet dense granules and show a 60% reduction in α -granule secretion, translating into malfunctioning hemostasis and impaired thrombus formation [69, 70]. In the experimental model of tMCAO, *Unc13d*^{-/-} mice had an improved stroke outcome in comparison to control animals and showed no signs of ICH [71]. Platelet α -granules are the most prevalent granules (50-80 granules/platelet) and comprise roughly 10% of the total platelet volume [72]. These granules are unique to platelets and equipped with a plethora of bioactive proteins driving versatile processes like coagulation, platelet adhesion, hemostasis, wound healing, or inflammation [72]. Due to their ability to endocytose proteins from their surrounding and adding them to their existent pool of stored content, α -granule content is often heterogeneous [73]. During the maturation and biogenesis of α -granules, neurobeachin-like 2 (NBEAL2) regulates the retention of MK-synthesized and endocytosed proteins, thereby contributing to platelet α -granule development [74, 75]. Mutations within this gene could therefore be linked to defective biogenesis of platelets, which results in α -granules deficiency along with macrothrombocytopenia and bleeding symptoms [76, 77]. These characteristics apply to patients suffering from gray platelet syndrome, making *Nbeal2*^{-/-} mice a fitting model system for investigations [78]. Testing of *Nbeal2*^{-/-} mice in the setting of cerebral ischemia with subsequent reperfusion revealed significantly reduced infarct volumes, which translated into improved neurological and motor function [79]. These observations strongly argue for an involvement of platelet α -granule secretion in stroke development. Remarkably, single deficiency in either platelet granule type did not induce bleeding complications. This is in line with the fact, that a 95% reduction in platelet count is still sufficient to maintain vascular integrity after the induction of cerebral ischemia [80]. However, if deficiencies become too major like in the case of *Nbeal2/Unc13d*-double deficiency, a hemostatic phenotype with ICH and high mortality rates can be observed [81]. This also emphasizes the importance of platelet granule content in maintaining vascular integrity following cerebral ischemia.

For stable thrombus formation, platelet integrins have to shift from a low to a high affinity state to allow aggregation [46]. One of such integrins is the highly abundant GPIIb/IIIa (integrin α IIb β 3) [82]. By cross-linking adjacent platelets via its main ligand fibrinogen, GPIIb/IIIa mediates aggregation and thrombus formation [46]. In stroke pathophysiology, it is still controversially discussed, if re-thrombosis after recanalization drives further infarct

development within thrombo-inflammatory processes, as platelet aggregates were found to obstruct arterial vessels 2 days (d) post stroke [41]. However, this assumption is in distinct contrast to findings, showing that GPIIb/IIIa blockage in experimental stroke is highly lethal due to the occurrence of ICH. In the rare occasion of survival, anti-GPIIb/IIIa treatment did not show an improvement in stroke outcome [28, 49]. Similarly, the application of anti-GPIIb/IIIa treatment within a clinical trial was aborted, because of the drastic increase in ICH that was attributable to the treatment [29]. These findings demonstrate that platelet aggregation via GPIIb/IIIa is dispensable for infarct expansion in the context of IS, while other platelet functions like GPIb-mediated tethering, GPVI-mediated platelet activation and granule release are essential.

1.5 Immune responses following ischemic stroke

IS has been associated with an intense inflammatory response in rodents as well as men and is seen as a co-driver of infarct progression following reperfusion [83-85]. This response includes the innate immune system and involves the exposure of adhesion molecules, the upregulation of cytokines alongside the infiltration of lymphocytes, polymorphonuclear leukocytes (PMN), and monocytes/macrophages [83, 85]. Despite a divergent cellular composition of the murine and human immune system [86], temporal dynamics of immune cell infiltration into the ischemic brain territory are comparable [83]. In both organisms, neutrophils are the first immune cells that are recruited [83]. These immune cells could also be associated with stroke severity [87], infarct volume [88], and an unfavorable functional outcome [89, 90]. Just recently, human observational data disclosed the presence of an intravascular immune response during the hyper-acute, occlusive phase of IS. Here, neutrophils formed the predominant leukocyte population [25, 91]. Since immune cells normally circulate in the blood and are not resident in distinct vascular compartments, they likely infiltrated to the ischemic vasculature via collateral anastomoses [16, 92]. Data originating from murine experiments likewise observed a major restriction of neutrophils to the luminal surface and perivascular spaces rather than a transmigration to the brain parenchyma [93], pointing towards a detrimental luminal influence on the NVU. Such damaging effects are harbored by the formation of neutrophil extracellular traps (NETs) and degranulation of proteolytic enzymes like MMP-9 and myeloperoxidase (MPO) [94, 95]. The release of NETs, consisting of DNA lattices equipped

with bactericidal proteins, is commonly described in the setting of infection where NETs trap pathogens and exert anti-microbial activity. Only recently Denorme and colleagues showed that NETs also exert a pathological role in IS [96], demonstrating that NETosis is also instrumental in sterile inflammation. Based on their sticky nature, NETs built a scaffold for circulating blood cells and coagulation factors [97, 98], thus contributing to neutrophil stalling within the distal capillary segments during reperfusion and consequently to the no-flow phenomenon [18, 99]. Although these studies argue for a substantial role of neutrophils in stroke pathology, three clinical trials failed to report a beneficial effect of neutrophil inhibition on stroke outcome in humans [100-102].

Besides neutrophils, lymphocytes have been a focus in stroke research for a long time. This is at least partly based on experimental data, which made use of immunodeficient recombinant activating gene 1 (*Rag1*) mice. Here, the lack functional T and B cells significantly reduced infarct volumes under permanent and transient ischemia when compared to WT control mice [12, 103]. These studies were followed by further analysis that aimed to disclose the lymphocyte subpopulation, contributing to secondary tissue damage by the promotion of inflammation. It was shown that reconstitution of B cells in *Rag1*^{-/-} mice had no effect on stroke outcome [104], neither was the pharmacologic [105] nor genetic depletion [103] of B cells. In contrast, others reported a worse stroke phenotype in mice lacking B cells compared to WT controls [106], showing that the role of B cells in the setting of IS is not yet clear. This is different when considering T lymphocytes. Here, adoptive transfer of CD4⁺ T cells into *Rag1*^{-/-} mice completely restored stroke susceptibility under permanent and transient occlusion [12, 107]. Furthermore, it could be shown that CD4⁺ T cell-deficient mice developed smaller infarcts following tMCAO, which was accompanied by reduced neuro-inflammation and oxidative stress [108], arguing for a crucial contribution of CD4⁺ T cells in secondary tissue damage. Interestingly, forkhead box P3 (FOXP3)-positive regulatory T cells (T_{reg}), a unique T cell subpopulation prototypic for their anti-inflammatory properties, were also identified to facilitate secondary brain damage in the acute phase of experimental IS [109]. Based on these data, a subsequent study investigated the superagonistic anti-CD28 antibody (CD28 SA), which induces the expansion and release of T_{regs} from lymphoid organs, with regard to its effect on acute stroke [110]. Administration of the CD28 SA antibody increased ischemic brain damage and translated into a worsened functional outcome. Together, these findings demonstrate that CD4⁺ T and T_{reg} cells participate in lesion growth following cerebral ischemia under experimental conditions. Due to the robust effects of T cells in stroke pathology,

pharmacological approaches for clinical use strived. Inspired by the positive effects of fingolimod (FTY720) in the treatment of multiple sclerosis (MS), first tests were performed in animal models of IS. Blocking the egress of lymphocytes from lymphoid organs by the sphingosine-1-phosphate receptor modulator FTY720 came along with a 60% reduction in circulating leukocyte numbers within 3 h post treatment, which resulted in an ameliorated stroke outcome [111]. These beneficial effects could also be preserved in a clinical setting [112, 113], providing preliminary evidence for the potential association of a beneficial outcome due to the elimination of detrimental T cells from the vascular system. Of note, natalizumab, another approved therapeutic of MS, inhibiting the transmigration of leukocytes across the BBB, was shown to be neither beneficial in a murine, randomized control trial nor under clinical use [114, 115].

Importantly platelet depletion in *Rag1*^{-/-} mice before tMCAO and reconstitution of CD4⁺ T/T_{reg} cells, protect from tissue-damaging effects exerted by T lymphocytes [109]. These experimental data point towards a platelet-dependent effect on T cells in the process of thrombo-inflammation during stroke. Recently, with CD84, a homophilic cell adhesion molecule, first mechanistic insights into how platelets and leukocytes interact have been provided [107]. Under physiologic conditions, CD84 is present on both cell types, platelets as well as T cells. In T lymphocytes, CD84 mediates immune cell activation [116], while its role in platelets is poorly understood. However, platelet activation was shown to induce CD84 shedding from the platelet surface, resulting in soluble CD84 (sCD84) [117]. The shed CD84 in turn binds to CD84 on CD4⁺ T cells, promoting T cell motility due to costimulatory effects, which results in a worsened stroke outcome [107]. This is supported by human data that showed a reduction of CD84 on the platelets surface in ischemic blood samples aspirated from the secluded vasculature of stroke patients, establishing CD84 as potential therapeutic target in IS treatment.

1.6 Aim of the study

Considerable progress has been made in stroke research and clinical treatment over the last years. Nonetheless, successful recanalization still remains futile in more than half of the treated patients. These modest success rates are highly dependent on the progression of infarcts under occlusion (penumbral tissue loss) and during reperfusion (I/R injury). Previous investigations, addressing the pathomechanisms underlying the perpetuation of structural brain damage, enclosed a participation of platelets, immune cells, and the vascular endothelium in a process referred to as thrombo-inflammation. However, molecular and mechanistic linkages between these central mediators and their spatio-temporal interaction during infarct expansion remain to a large extent elusive. Therefore, this study intended to resolve deeper insights into the process of infarct progression in the setting of IS.

The initial obstruction of a cerebral vessel in IS pathology involves the aggregation of platelets. Thus, the observation of obstructive platelet aggregates within the cerebral vasculature after recanalization fueled the idea that these newly formed platelet aggregates contribute to infarct progression. On the contrary to this assumption, however, other studies reported non beneficial effects by the blockage of platelet aggregation via GPIIb/IIIa. Since the question of cause or consequence of cerebral microthrombi in the process of infarct expansion was still not yet clarified, the aim of the thesis was to address this issue.

The second part of the thesis aimed to investigate the disruption of the BBB as a potential contributor of infarct expansion. Since cerebral ischemia has been proven to induce platelet activation, resulting in platelet granule release, the impact of platelet-derived soluble molecules on cerebral ECs and vascular patency was centrally addressed. Therefore, an *in vitro* approach, consisting of a simplified model of the BBB, was combined with a murine tMCAO model.

In humans, the local intracerebral analysis of ultra-early stroke pathophysiology has only recently become accessible by pial blood sampling during MT. This technique allows for the identification of the cellular composition, as well as the mapping of cellular interactions within the occluded ischemic vascular compartment. However, until now the hyper-acute phase during LVO remained largely unexplored. Taking advantage of this novel technique, the third part of the thesis aimed to contribute to the elucidation of ultra-early processes under occlusion and to verify main experimental findings in the human system. Therefore, the recruitment of immune

cell subpopulations and the interaction of leukocytes and platelets within the human secluded vasculature were assessed using a flow cytometric approach.

2 Material and Methods

2.1 Material

Detailed itemisation of the used devices, consumables, chemicals, buffers and solutions, antibodies or software is provided in the appendix.

2.2 Methods

2.2.1 Murine experiments

2.2.1.1 Preparation of murine brain tissue

Following tMCAO surgery with distinct reperfusion times, mice were sacrificed under deep anaesthesia. Brains were taken out and cut into 2 mm thick coronal consecutive sections with the help of a brain slice matrix. Until further processing, slices were stored in PBS.

Surgery and preparation of brain tissue was either performed by Vanessa Göb, Department of Experimental Biomedicine I, University Hospital Würzburg or members of the working group of Michael Schuhmann, Department of Neurology, University Hospital Würzburg.

2.2.1.2 Brain tissue lysates

The rostral brain section was processed by the centric division into the ipsilateral (i) and contralateral (c) hemisphere with further separation into cortex and basal ganglia, respectively. Samples were snap frozen in liquid nitrogen and stored at -20 °C until usage.

For further processing, brain tissue was homogenized in ice-cold lysis buffer by pre-mincing with a mortar followed by 25 seconds (s) of sonification. To remove cell debris, samples were centrifuged at 16,000 rounds per minute (rpm) for 30 min at 4 °C. The clear supernatant was transferred into a new Eppendorf tube and protein concentration was determined using a

bicinchoninic acid (BCA) protein assay. Before western blot analysis, samples were adjusted to 200 µg/50 µl by adding the respective amount of 2x loading buffer.

2.2.1.3 Endothelial cell lysates

For the generation of cell lysates, MBMECs were cultured in collagen type IV (16 µg/ml)/fibronectin (10 µg/ml) coated 24 well plates at a cell density of 2×10^4 /200 µl. Cultivation and treatment resembled the ones described in 2.2.1.7. Following 18 h of treatment, culture medium was removed and cultivated cells were washed twice with warm PBS. Ice-cold cell lysis buffer was added and cells were scraped from the cell culture plates. Lysates were transferred to 1.5 ml Eppendorf tubes and subsequently incubated on a horizontal shaker for 30 min at 4 °C. Afterwards samples were centrifuged at 14,000 rpm for 30 min at 4 °C to remove residual cell fragments. Clear supernatant was again transferred to new Eppendorf tubes and protein concentration was determined using a BCA protein assay. Before western blot analysis, samples were adjusted to 2 µg/20 µl by adding the respective amount of 4x laemmli buffer containing 3% β-mercaptoethanol (ME).

2.2.1.4 Western blot analysis

For western blot analysis, prepared brain lysates (see 2.2.1.2 and 2.2.1.3) were boiled for 10 min at 95 °C to denature the proteins. Cell lysates were loaded onto the gel and separated by molecular weight during SDS-polyacrylamide gel electrophoresis (SDS-PAGE). Proteins were transferred onto a nitrocellulose membrane by wet immunoblotting and unspecific binding sites were blocked by 5% fat-free milk powder dissolved in 1x washing buffer (blocking solution) for 1 h at RT under gentle shaking. Afterwards, membranes were incubated on a shaking platform with the respective primary antibodies, diluted in blocking solution, over night (o/n) at 4 °C. The next day, membranes were washed three times for 10 min with 1x washing buffer. Respective secondary horseradish peroxidase (HRP)-conjugated antibodies were added at a concentration of 1:10,000 for 1 h at RT under gentle shaking. After repeated washing, proteins were visualized with Enhance Chemiluminescence (ECL) at a ChemiDoc™ Touch Imaging System (Bio-Rad). Actin served as an internal loading control. Densitometric quantification of protein bands was performed using Fiji.

2.2.1.5 Platelet isolation, washing, and generation of platelet releasate

Blood from mice with different genetic backgrounds (WT, *Nbeal2*^{-/-}, *Unc13d*^{-/-}, *Nbeal2*^{-/-}/*Unc13d*^{-/-}) was collected from the retroorbital plexus under isoflurane anaesthesia and gathered in an Eppendorf reaction tube containing 300 µl heparin solution (20 Units(U)/ml in TBS, pH 7.3). After centrifugation at 800 rpm for 6 min (Eppendorf Centrifuge 5415C), plasma and buffy coat were transferred into a new reaction tube with 200 µl of heparin solution and centrifuged again. Afterwards, platelet rich plasma (PRP) was transferred into a new tube and platelets were pelleted by centrifugation at 2,800 rpm for 5 min. The pellet was resuspended in calcium-free Tyrode's buffer with apyrase (0.02 U/ml) and prostacyclin (PGI₂, 0.1 µg/ml). Platelets were washed two more times by centrifugation and resuspension with Tyrode's buffer containing apyrase and PGI₂. Platelet count was determined using a Sysmex KX-21N Hematology Analyzer.

Washed platelets were adjusted to a concentration of 500,000 platelets/µl in Tyrode's buffer containing Ca²⁺ and allowed to rest for 30 min at 37 °C. In order to generate platelet releasate, platelets were stimulated with 10 µg/ml collagen-related peptide (CRP) for 15 min at 37 °C. Afterwards, samples were centrifuged at 2,800 rpm for 5 min at RT to remove cellular debris. Platelet releasate was collected, filtered (pore size 0.22 µm) and aliquoted before storage at -80 °C.

Preparation was performed by Vanessa Göb, Department of Experimental Biomedicine I, University Hospital Würzburg.

For protein denaturation, platelet releasate was boiled at 95 °C for 10 min. Before cell treatment, platelet releasate was cooled down for 10 min at RT. For the neutralization of PDGF, 1 µg/ml anti-PDGF antibody (PDGF-NAb) was incubated with WT platelet releasate 10 min prior to treatment. The same procedure was followed for the incubation of *Nbeal2*^{-/-} platelet releasate with recombinant PDGF-AB. For experimental use platelet releasate was not thawed and frozen more than four times.

2.2.1.6 Isolation of primary brain microvascular endothelial cells (MBMECs)

For the isolation of primary murine brain microvascular ECs (MBMECs) [118], brains from ten WT mice were harvested and stored in Dulbeccos's modified eagle's medium (DMEM) on ice. Further, bulbi olfactori, brain stems, cerebella and thalami were mechanically removed with forceps. Remaining meninges and larger vessels were detached by carefully rolling the brains over sterile Whatman paper. After homogenization of the tissue, the first enzymatic digestion was performed by the addition of 900 μ l collagenase type 2 (CLS2) and 225 μ l DNase I. The mixture was then incubated at 37 °C for 1 h on a Bio RS-24 rotator. The reaction was stopped by the addition of 10 ml of DMEM. Tissue was spun down at 2,300 rpm for 10 min at 4 °C and thoroughly resuspended in DMEM containing 20% BSA (25 ml) for the removal of remaining myelin. After centrifugation at 2,300 rpm for 20 min at 4 °C, myelin and the BSA layer were carefully removed. For the second enzymatic digestion, collagenase/dispase (600 μ l) and DNase I (100 μ l) were added to the resuspended pellet and incubated for 1 h at 37 °C on a Bio RS-24 rotator. During digestion, the percoll density gradient was prepared by centrifugation at 15,000 rpm for 1 h at 4 °C, in an ultracentrifuge without deceleration. Further, a 25 cm² cell culture flask was coated with collagen type IV (16 μ g/ml)/fibronectin (10 μ g/ml) coating solution for 1 h at 37 °C. To stop the digestion, 10 ml of DMEM was added and the suspension was spun down at 2,300 rpm for 10 min at 4 °C. The cell pellet was resuspended in 2 ml of DMEM, carefully loaded onto the percoll gradient and centrifuged at 2,300 rpm for 10 min at 4 °C without deceleration. Microvascular capillaries appeared as an opaque cloud in the interphase. Using a long sterile needle, this fraction was generously aspirated and transferred to a 50 ml Falcon tube containing DMEM (5 ml). The Falcon tube was centrifuged at 1,700 rpm for 10 min at 4 °C, the pellet was resuspended in puromycin-containing cell culture medium and seeded into the cell culture flask, from which the coating medium was removed. Cell cultures were kept at 5% CO₂, 95% humidity, 21% O₂ and 37 °C with regular medium changes. Before freezing, cells were kept on puromycin-free medium for at least one day. At a confluence of 90%, cells were detached with Trypsin-EDTA (0.25%) solution, resuspended in freezing medium, aliquoted, gradually frozen and stored in liquid nitrogen.

2.2.1.7 Transendothelial electrical resistance (TEER) measurements of MBMECs

Impedance spectroscopy is an electrochemical technique used for the quantitative evaluation of the integrity of barrier-forming tissue. Cerebral ECs for instance, that line the cerebral vasculature, are commonly used as a simplified *in vitro* model of the BBB. Thereby, the automated surveillance of EC layer resistance yields reliable information about the cell layer properties (integrity, permeability, expression of membrane extrusions) under physiological or pathological treatment conditions. The measurement of the cellular resistance (transendothelial electrical resistance, TEER) is performed by applying small alternating currents with different frequencies to established cell layers on a permeable membrane. Ionic conductance is though limited by the presence of the cell layer and allows for a direct correlation between the measured resistance and cell layer integrity. Consequently, high electrical resistance is an indicator for a well-established and tight cell layer, whereas lower resistance indicates leakiness. This setup not merely enables non-invasive surveillance of cell layers as interfacial tissue, but also allows simulation of pathological conditions and synchronous monitoring in real time [119].

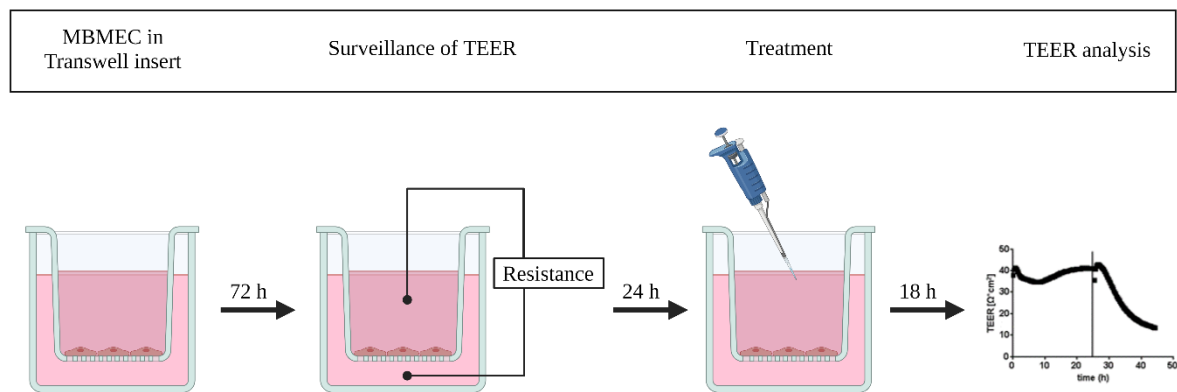


Figure 2-1. Experimental design of MBMEC culture. MBMECs were seeded onto the permeable membrane of the transwell insert. After 72 h, transendothelial electrical resistance (TEER) was constantly monitored. When resistance reached its maximum (approx. 24 h), MBMECs were treated with the respective stimulants and TEER was monitored for another 18 h.

For the measurement of TEER in MBMEC cultures, transwell inserts with a pore size of $0.4 \mu\text{m}$ were coated with collagen type IV ($16 \mu\text{g/ml}$) and fibronectin ($10 \mu\text{g/ml}$) for 1 h at 37°C . Afterwards, the coating solution was carefully removed and the inserts were allowed to dry. Cells were thawed and seeded at a density of $2 \times 10^4/100 \mu\text{l}$ per well onto the semipermeable

membrane. A total volume of 100 μ l in the apical insert and 600 μ l of puromycin-free medium in the basolateral well was used for cultivation. Cells were incubated for 1 d in a Hera incubator at 5% CO₂, 95% humidity, 21% O₂ and 37 °C. The next day, medium was exchanged and cells were treated with 1 μ Mol (μ M) hydrocortisone in both compartments. After another 48 h, cells were transferred into a prewarmed measuring chamber and incubated with RPMI medium supplemented with B27 (2%) and Penicillin/Streptomycin (Pen/Strep, 1%) for automatic surveillance of MBMEC integrity. Once the cells reached confluence (= maximal resistance) the treatment regime was performed. MBMECs were either treated with platelet releasate generated from the indicated genotypes (see 2.2.1.5), control buffer (Tyrode's buffer + Ca²⁺) containing 10 μ g/ml CRP, ADP, thrombin, different recombinant proteins, PDGF neutralizing antibody or culture medium (control). During 18 h of treatment, MBMEC were cultivated under normoxic/ glycemic (5% CO₂, 95% humidity, 21% O₂, 37 °C, 2 g/l glucose) or hypoxic/ aglycemic conditions (5% CO₂, 95% humidity, 1% O₂, 37 °C, 0 g/l glucose), depending on the experimental setup.

2.2.1.8 Isolation of lymphocytes from murine lymph nodes

For the isolation of murine lymphocytes, cervical, axillary and inguinal lymph nodes from WT mice were harvested and stored in splenocyte complete medium on ice. To obtain a single cell suspension, lymph nodes were mashed through a cell strainer (40 μ m) using a 2 ml syringe piston. To avoid cell loss, the cell strainer and the syringe piston were washed with a total of 30 ml of splenocyte washing medium. The cell suspension was centrifuged at 1,500 rpm for 5 min at 4 °C and the cell pellet was resuspended in RPMI medium supplemented with B27 (2%) and Pen/Strep (1%). Remaining connective tissue was removed by passing the cell suspension through a fresh cell strainer (40 μ m). After counting, lymphocytes were adjusted to a final concentration of 1×10^6 cells/100 μ l prior to use.

2.2.1.9 Transmigration of lymphocytes over MBMEC monolayers

For the transmigration of lymphocytes across MBMEC monolayers, a Boyden chamber setup was used. MBMECs were seeded onto collagen type IV (16 μ g/ml)/fibronectin (10 μ g/ml) coated transwell inserts with a pore size of 3.0 μ m. Seeding density and cultivation resembled

the ones described in 2.2.1.7. At day five of cultivation, medium was changed to RPMI medium supplemented with 10% fetal calf serum (FCS), 2% B27 and 1% Pen/Strep in the basolateral compartment, while in the apical compartment a mixture of serum-free RPMI medium containing B27 (2%) and Pen/Strep (1%), 1×10^6 lymphocytes/100 μ l and the different treatments were applied (Fig. 2-1). Treatments consisted of platelet releasate from different genotypes (see 2.2.1.5) or control buffer (10 μ g/ml CRP in Tyrode's buffer + Ca^{2+}). After 18 h of incubation under normoxic/ glycemic conditions, fluids of the basolateral compartment were transferred into separate Eppendorf tubes. Washing of this compartment was performed twice and pooled with the existing medium. Additionally, the MBMEC layer was detached by trypsinization (0.25% trypsin, 10 min, 37 °C) and transferred into another tube. Again, the medium of the two washing steps was added to the existing tube.

To determine the number of lymphocytes in each compartment (MBMEC layer, basolateral), cells were counted using a Neubauer counting chamber.

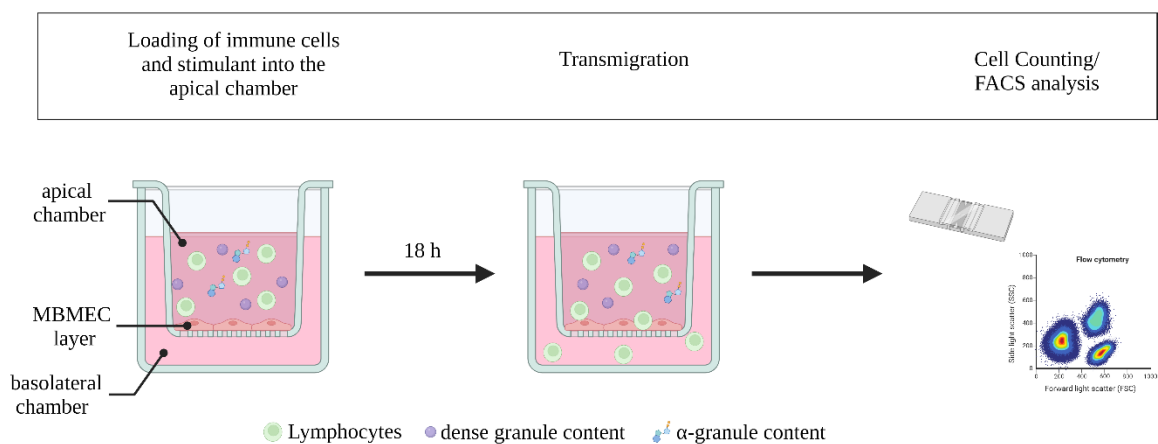


Figure 2-2. Schematic Boyden chamber approach. MBMECs were seeded onto the permeable membrane of transwell inserts. After reaching confluence, isolated lymphocytes and the respective treatment was applied to the apical chamber, while FCS was added to the basolateral chamber as chemoattractant. Lymphocytes were allowed to transmigrate for 18 h. Cells from the basolateral compartment and the MBMEC layer were collected, counted and analysed by FACS.

2.2.1.10 Flow cytometric analysis of lymphocytes after transmigration

To determine the proportion of CD3⁺ T lymphocyte in samples generated within 2.2.1.9, immune cells were pelleted by centrifugation and resuspended in 100 µl fluorescence activated cell sorting (FACS) buffer. Blocking was performed using Fc-blocking solution for 10 min on ice and cells were subsequently stained with respective fluorescence antibodies (30 min, 4 °C, in the dark). After centrifugation at 1,500 rpm for 6 min at RT a Life/Dead stain was applied for another 30 min at 4 °C in the dark. Excess antibody was removed by centrifugation and the pellet was resuspended in 400 µl FACS buffer. Analysis was immediately performed using a BD FACSLyric and FlowJo.

2.2.1.11 Staining and quantification of gaps in MBMEC monolayers

For immunofluorescence staining, MBMECs were seeded in collagen type IV (16 µg/ml)/fibronectin (10 µg/ml) coated 18-Well-Chamber Ibidi slides as described in 2.2.1.7. After 18 h of treatment with the indicated platelet releasates or controls (see 2.2.1.5), cells were washed with PBS and fixed using a glyoxal fixation solution (20 min, RT). Unspecific binding sites were blocked with 0.5% bovine serum albumin (BSA) and 0.2% Triton dissolved in PBS for 1 h at RT. Epitopes of interest were stained with primary antibodies o/n at 4 °C in the dark. The following day, cells were repeatedly washed and incubated with the respective fluorescently-labelled secondary antibodies for 1 h at RT in the dark. After three washing steps with PBS, cells were mounted with Prolong Gold containing DAPI to stain the cell nuclei.

Tile scans were acquired using a SP8 confocal microscope (Leica) equipped with a HC PL APO CS2 40x/1.30 OIL objective. Upon recommendation of Ibidi, Immersol 518F immersion oil was utilized during imaging. For gap quantification, a newly developed analysis pipeline from Dr. Katherina Hemmen was followed (for detailed information see Dissertation from Vanessa Göb “Pathomechanisms underlying ischemic stroke”).

Image acquisition and analysis was performed by Vanessa Göb (Department of Experimental Biomedicine I, University Hospital Würzburg) with assistance from Dr. Katherina Hemmen (Core Unit Fluorescence Imaging, Rudolf-Virchow-Center for Integrative and Translational Bioimaging, University of Würzburg).

2.2.1.12 Measurement of intracellular Ca^{2+} in MBMECs

For the determination of intracellular Ca^{2+} in MBMECs, Fura-2-AM, a ratiometric calcium indicator, was used. The ability of Fura-2 to intercalate with calcium ions at its negatively charged carboxyl groups influences its spectral properties, which allows for a determination of calcium bound Fura-2 at an excitation of 340 nano meters (nm) and calcium free Fura-2 at an excitation of 380 nm. Using a comparison of the fluorescence intensities after excitation at the previously named wavelengths, calcium concentration can be calculated.

$$[\text{Ca}^{2+}] = K_d * \left(\frac{R - R_{min}}{R_{max} - R} \right) * B$$

Figure 2-2. Equation for the calculation of intracellular Ca^{2+} concentrations. Intracellular Ca^{2+} concentration consist of the dissociation constant of Ca^{2+} (K_d), the ratio of fluorescence intensity of Fura-2 at both measured wavelengths (R) during treatment conditions, R in the absence of Ca^{2+} (R_{min}), R in the presence of a saturated Ca^{2+} concentrations (R_{max}), and the ratio of fluorescence intensity of Fura-2 at the excitation wavelength of 380 nm in the absence of Ca^{2+} and in the presence of saturated Ca^{2+} concentrations (B).

However, based on the permanent negative charge of the aliphatic carboxylic acids of Fura-2 under physiological conditions, it is not able to cross the cell membrane. Therefore, the mechanism of prodrugs was exploited, which is commonly utilized to make pharmaceuticals biologically available. Esterification of the five carboxylic acids generate an uncharged, calcium insensitive Fura-2 derivative, which is freely cell membrane permeable. Application of pluronic acid (F-127) was used to fruther increase the uptake of the drug into the cell. Once inside the cell, the previously built esters are hydrolysed by unspecific esterases, which restore the ability of Fura-2 to complex calcium.

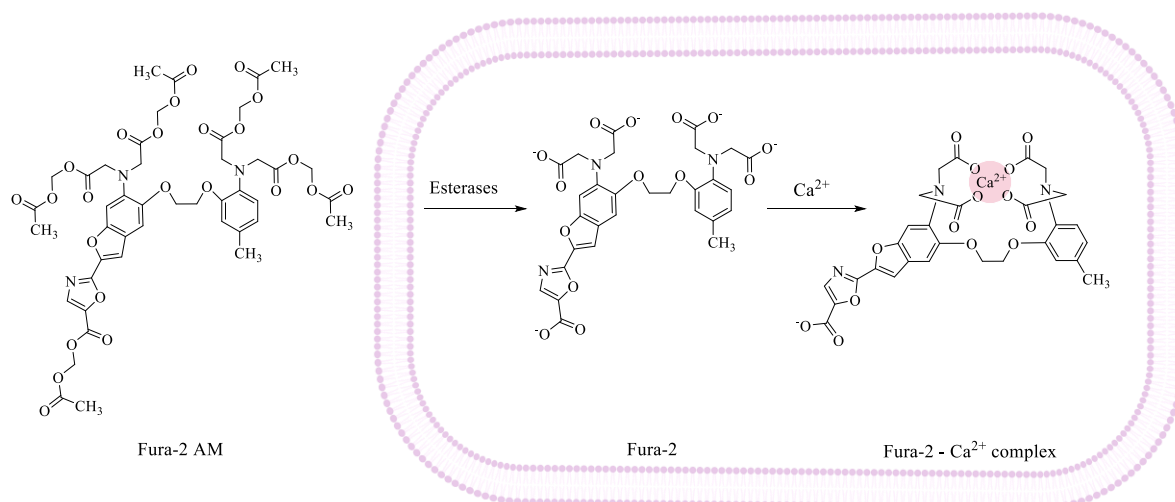


Figure 2-3. Intracellular complex formation of Ca²⁺ and Fura-2 after hydroxylation of the previously built prodrug. Chemical structure of Fura-2-AM (left), Fura-2 (middle), and Fura-2-Ca²⁺ complex (right). The uncharged Fura-2 derivative (Fura-2 AM) is able to pass the cell membrane due to the esterification of its five carboxylic acids with acetoxymethyl groups. Inside the cell, unspecific esterases hydrolyse the acetoxymethyl groups and thereby restore the Ca²⁺ sensitivity of Fura-2. Upon Ca²⁺ complexation at its negatively charged carboxylic acids, the spectral properties of Fura-2 changes and Ca²⁺ bound Fura-2 can be detected at an excitation of 340nm.

For the experiment, MBMECs were seeded at a density of 2×10^4 /100 μ l in black-walled 96 well plates and cultured as described in 2.2.1.7. Cells were loaded with Fura-2-AM (5 μ M) in the presence of Pluronic acid F-127 (0.2 μ g/ml) for 20 min at 37 °C. For the removal of residual Fura-2, cells were washed twice with 100 μ l warm PBS and suspended in serum-free RPMI medium supplemented with B27 (2%) and Pen/Strep (1%). Respective treatments were applied and recorded for 300 s after a 60 s baseline measurement. Treatment consisted either of platelet releasate generated from WT mice (see 2.2.1.5) or CRP as a control. Calibration was performed using Ionomycin (1 μ M) and EDTA (0.5 M) to determine maximal and minimal emission values, allowing for the calculation of absolute values. Emitted fluorescence was measured at 509 nm with alternating excitations waves between 340 and 380 nm. Plates were read with an Infinite M200PRO fluorimeter equipped with an i-control software. Calculations of absolute calcium concentrations were performed in Excel.

2.2.1.13 Murine PDGF-AB ELISA

Quantification of PDGF-AB concentrations within platelet releasate generated from WT and *Nbeal2^{-/-}* mice (see 2.2.1.5) was conducted using an enzyme linked immune sorbent assay (ELISA) specific for mouse PDGF-AB following the manufacturers' instructions. Briefly, all materials and reagents were equilibrated to RT prior to use. Standards were prepared using a dilution series of PDGF-AB Stock. Calibrator Diluent RD5-3 served as the zero standard (0 pg/ml). 50 µl of standard or sample were added to the appropriate wells containing 50 µl of Assay Diluent. After 2 h at RT under gentle shaking, 100 µl of conjugate was added and incubated for another 2 h at RT under gentle shaking. Washing of the samples was performed five times and the ELISA was developed using substrate solution (100 µl) for 30 min protected from light. To stop the reaction 100 µl of Stop Solution was added and the plate was read at 450 nm with a TECAN Infinite M200PRO fluorimeter.

2.2.2 Human experiments

2.2.2.1 Analysis of leukocyte subpopulations in human ischemic stroke patients by flow cytometry

From July 2020 to May 2021 citrate-phosphate-dextrose-adenine 1 (CPDA1) anticoagulated whole blood from patients meeting all *a priori* defined inclusion criteria [25] was used for the determination of leukocyte subpopulations [120]. Local microcatheter blood aspiration enabled the collection of cerebral-ischemic blood under occlusive conditions (D) and intraindividual control blood under physiological blood flow in the cervical internal cerebral artery (ICA, C). Shortly after individual, local blood collection, 50 µl well mixed, anticoagulated whole blood from each vascular region (D and C) was incubated with 20 µl of the BD Multitest 6-color TBNK reagent in BD Trucount Tubes for 15 min at RT in the dark. Epitopes included within the BD Multitest 6-color TBNK reagent were the following: fluorescein-5-isothiocyanate (FITC)-labeled CD3, phycoerythrin (PE)-labeled CD16, PE-labeled CD56, peridinin-chlorophyll-protein (PerCP)-cyanine (Cy)5.5-labeled CD45, PE-Cy7-labeled CD4, allophycocyanin (APC)-labeled CD19, and APC-Cy7-labeled CD8. Erythrocyte lysis and fixation was performed by the addition of 450 µl BD FACS Lysing solution (previously diluted

1:10 with distilled water). After 15 min of incubation at RT in the dark, samples were analysed using a BD FACSLyric and the BD FACSSuite Software.

2.2.2.2 Determination of platelet-leukocyte-aggregates in ischemic blood using flow cytometry

Analysis of platelet-leukocyte aggregates (PLAs) was performed with citrate anticoagulated whole blood following the protocol described in 2.2.2.1 with the addition of a Brilliant Violet (BV) 421-conjugated CD41a antibody. Samples analysis was performed with the BD FACSLyric and the BD FACSSuite Software.

2.2.2.3 Immunofluorescence staining of platelet-neutrophil aggregates in human blood smears of the ischemic brain territory

Blood smears from ischemic and systemic blood samples were generated by spreading a droplet of blood over a glass slide. After drying at RT, slides were stored at 4 °C until further usage. For immunofluorescence staining, ice-cold methanol was used to fix the samples for 10 min at 4 °C. The slides were allowed to dry and a region with a thin coverage of blood was selected for staining. This region was framed using a Pap-Pen and unspecific binding sites were blocked with 5% BSA, 0.2% Triton X diluted in 1x PBS for 1 h at RT. Afterwards, samples were incubated with the primary antibodies directed against CD42b and neutrophil elastase (diluted in 5% BSA in 1x PBS) o/n at 4 °C. The following day, samples were washed three times with 1x PBS and incubated with the respective secondary antibodies for 1 h at RT in the dark. After another three washing steps with PBS, samples were mounted with ProlongGold containing DAPI to stain the cell nuclei.

Images were acquired using a Leica DMI8 microscope (DMC 2900 camera control) equipped with a HC PL FUOTARL 40x/0.60 DRY objective.

2.3 Graphical illustrations

Graphical illustrations were either created with BioRender.com, ChemDraw, FlowJo, or GraphPad.

2.4 Statistics

Data is given as mean \pm standard deviation (SD) or as percentage of leukocyte population. The applied statistical test for each graph is indicated in the figure legend. Statistical significance was considered for p-values <0.05 (*), $p<0.01$ (**), and $p<0.001$ (***). GraphPad Prism 9 was used to perform all statistical analyses.

3 Results

This thesis was conducted within the DGF-funded Collaborative Research Centre/Transregio 240 (CRC/TR240) ‘Platelets – Molecular, cellular and systemic functions in health and disease’. Murine experiments were part of the B06 (Heinze/Schuhmann/Stegner) project and comprised a close collaboration with Vanessa Göb from the Department of Experimental Biomedicine I of the Rudolf-Virchow-Center in Würzburg. Human experiments were conducted within the B02 (Stoll/Pham) project and comprised a close collaboration with the clinicians of the Department of Neuroradiology and the Department of Neurology at the University Hospital Würzburg.

3.1 Characterization of the temporal dynamics of secondary microthrombosis following recanalization in an experimental stroke model

Microthrombosis after successful re-opening of a secluded cerebral vessel is still being made accountable for infarct expansion. However, studies performed in mice and patients found no beneficial effects of inhibiting platelet aggregation *via* anti-GPIIb/IIIa treatment, suggesting other mechanisms as cause for further tissue death [28]. To clarify the ongoing controversial debate on the contribution of secondary microthrombosis on infarct expansion, six- to eight-week-old C57BL/6J mice were subjected to 1 h right-sided MCA occlusion followed by different time periods of reperfusion. The determination of infarct volumes by 2,3,5-triphenyltetrazolium chloride (TTC), which is commonly used to distinguish metabolically active (dark red) from ischemic tissue (white) [121], revealed full-grown infarcts already after 8 h of reperfusion ($122.4 \pm 29.65 \text{ mm}^3$; Figure 3-1 A) [122]. To investigate whether thrombus formation, indicated by the accumulation of platelets in the ischemic brain, occurs prior to maximal tissue damage, temporal dynamics of this process were assessed. Therefore, western blot analysis with cortical brain lysates of the ipsi- (i) and contralateral (c) hemispheres was performed using an antibody directed against platelet specific GPIIb β (22 kDa). Evaluation of the respective protein bands showed that relative GPIIb β protein content was comparable in sham-operated mice (1.25 ± 0.46), 4 h (1.21 ± 0.80) and 8 h (1.28 ± 0.32) reperfused mice, while a significant 4-fold increase could be observed 24 h post recanalization (4.51 ± 2.22 , Figure 3-1 B).

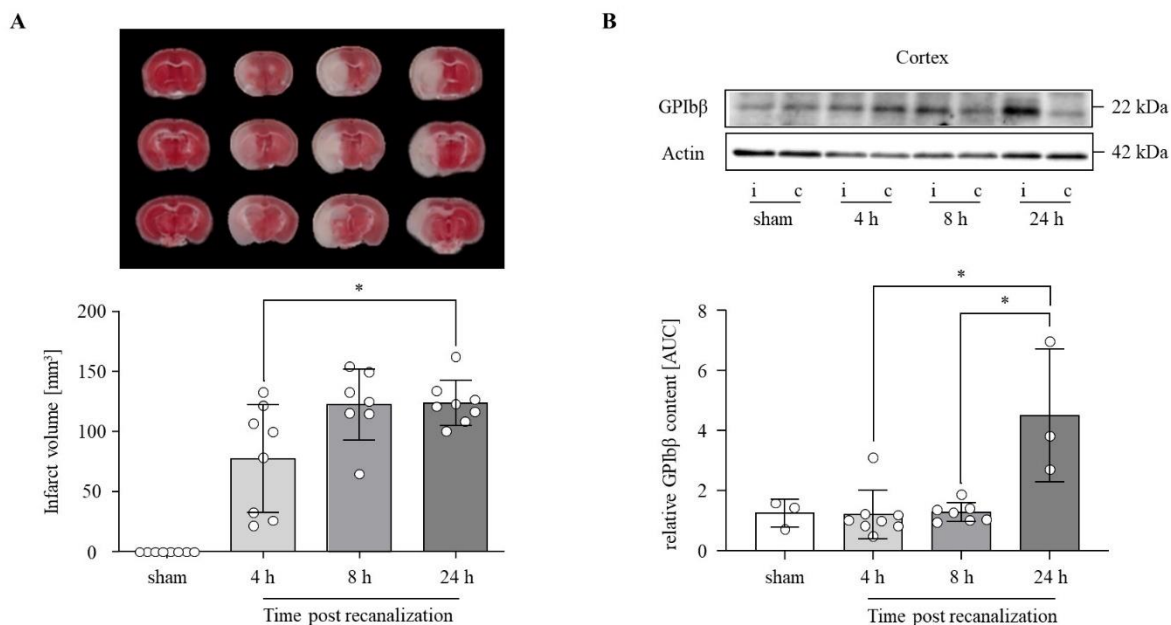


Figure 3-1. Thrombus formation occurs after infarct development. (A) Infarct quantification of TTC-stained brain section from WT mice after tMCAO followed by 4 h, 8 h and 24 h of reperfusion or sham surgery. Representative images of three consecutive brain sections from one mouse per group (upper panel). Edema corrected infarct volumes after respective reperfusion times (lower panel). Data are shown as mean \pm SD of 7 to 8 mice per group. Each data point represents one mouse per time point. P-values were calculated by two-tailed Mann Whitney U test and considered statistically significant with * $P < 0.05$. (B) Western blot analysis of platelet GPIIb (22 kDa) in cortices of WT mice after tMCAO following 4 h, 8 h, and 24 h of reperfusion or sham surgery. Relative GPIIb content was calculated by the normalization of GPIIb protein content to the Actin (42 kDa) loading control and additional normalization to the contralateral hemisphere. Representative immunoblots are shown above the densitometric quantification. Data are shown as mean \pm SD of 3 to 8 mice per group. Each data point represents one mouse per time point. i = ipsilateral, c = contralateral. P-values were calculated by two-tailed Mann Whitney U test and considered statistically significant with * $P < 0.05$. Adopted from Göb *et al.*, *Scientific Reports* 2021 [122] under the terms of the Creative Common Attribution License.

These results were in line with imaging-based quantifications [122], demonstrating that thrombus formation within the vasculature occurs after maximal infarct development. This in turn also provides evidence that the pathomechanisms underlying progressive infarct growth have to take place within the first 8 h post recanalization.

3.2 Blood-brain barrier breakdown as potential pathomechanism underlying progressive infarct growth

3.2.1 Early blood-brain barrier disruption after vessel recanalization

To elucidate further potential mechanisms underlying secondary infarct development following recanalization, the analysis of BBB breakdown was focused due to its early appearance in human and murine stroke pathogenesis [36, 123]. Therefore, 2-photon intravital microscopy (2-PM) was applied in WT mice subsequently after filament removal to observe the brain vasculature during early reperfusion. In order to get access to the brain vasculature, an open cranial window was installed on the murine skull above the territory of the MCA 14 d prior to tMCAO surgery. After 1 h of right-sided MCA occlusion, the filament was removed and the fluorescently labelled antibodies for the visualization of platelets (anti-GPIX-Alexa Fluor 488) and the vasculature (anti-BSA-Alexa Fluor 546, anti-CD105-Alexa Fluor 546) were injected. Already shortly after vessel recanalization, extravasation of fluorescently labelled BSA (magenta) out of the ipsilateral vessel lumen into the brain parenchyma was observed, indicating BBB integrity loss. This extravasation was immediately followed by platelet adhesion (green) at the site of vascular impairment (Figure 3-2, upper panels), which suggests that platelets seal the damaged vasculature to prevent passive bleedings. In contrast, vessel integrity was maintained within the contralateral hemisphere throughout the entire time of recording (Figure 3-2, lower panels).

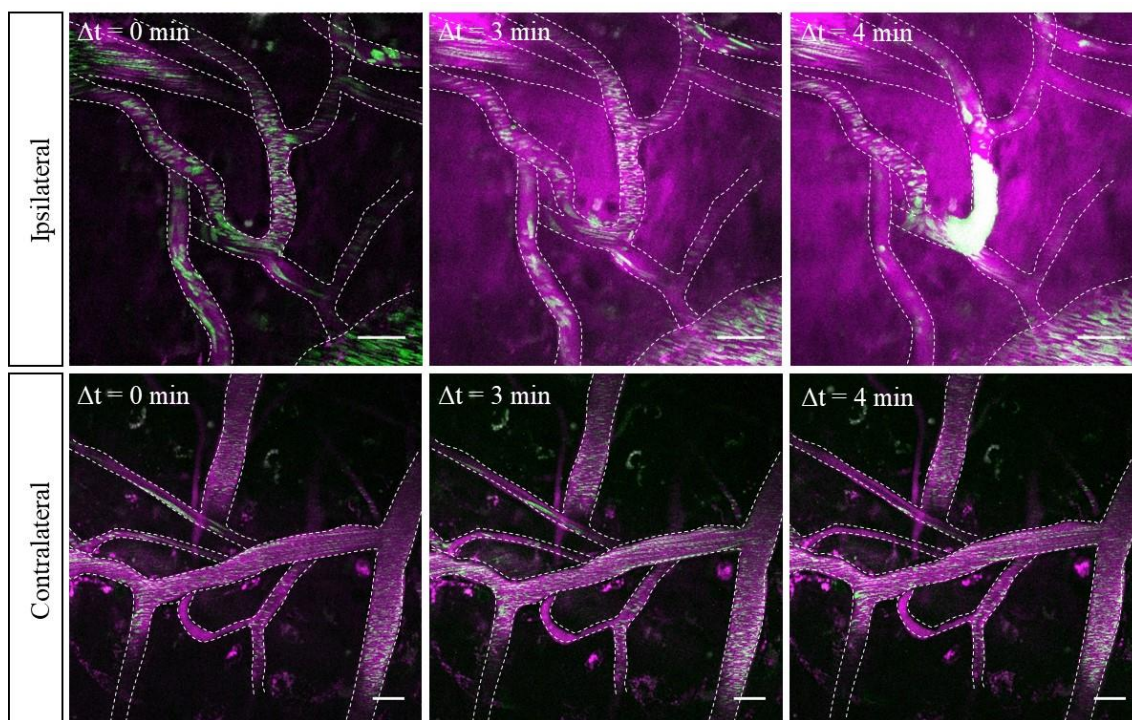


Figure 3-2. Disruption of the blood-brain barrier is initiated early during reperfusion within the ipsilateral hemisphere. Representative intravital 2-photon microscopy (2-PM) images of the brain vasculature of WT mice in the early phase of reperfusion following tMCAO. Vasculature of the ipsilateral hemisphere is depicted in the upper panels, vasculature of the contralateral hemisphere in the lower panels. Platelets (green) are labeled by anti-GPIX-Alexa Fluor 488. Vessels and vessel lumen are labeled by anti-BSA-Alexa Fluor 546 and anti-CD105-Alexa Fluor 546. Time between separate images is indicated as Δt . Scale bar, 20 μm . Intravital microscopy was performed by Vanessa G6b.

Since 2-PM is not suitable for the quantification of vascular leakage due to its limited field of view, relative Albumin protein content was quantified using western blot analysis. The quantification of vascular leakage, a measure of BBB integrity loss, was thereby based on the amount of Albumin signal within the ipsilateral hemisphere. While sham-operated mice revealed no leakage, significantly increased Albumin content was observed after 4 h, 8 h and 24 h of reperfusion in both investigated brain regions, the cortex and the basal ganglia (Cortex: 4 h i 0.99 ± 0.46 vs c 0.63 ± 0.26 ; 8 h i 1.38 ± 0.52 vs c 0.51 ± 0.19 ; 24 h i 1.58 ± 0.66 vs c 0.47 ± 0.18 ; Basal ganglia: 4 h i 0.73 ± 0.26 vs c 0.42 ± 0.07 , 8 h i 1.24 ± 0.35 vs c 0.44 ± 0.08 ; 24 h i 1.69 ± 0.44 vs c 0.58 ± 0.17 ; Figure 3-3 A). Additional imaging dependent immunofluorescent staining for Albumin in brain cryosections, originating from mice that underwent variable reperfusion times, was achieved by the classification of leakage severity by the means of a 5-point scoring system (no (0), mild (1), moderate (2), major (3) to severe

leakage (4)). The analysis of the stained coronal brain sections yielded almost similar results, with the exception of mild leakage after 4 h of reperfusion (sham 0 ± 0 vs 8 h 2.71 ± 0.49 ; sham 0 ± 0 vs 24 h 3.0 ± 0.76 ; Figure 3-3 B).

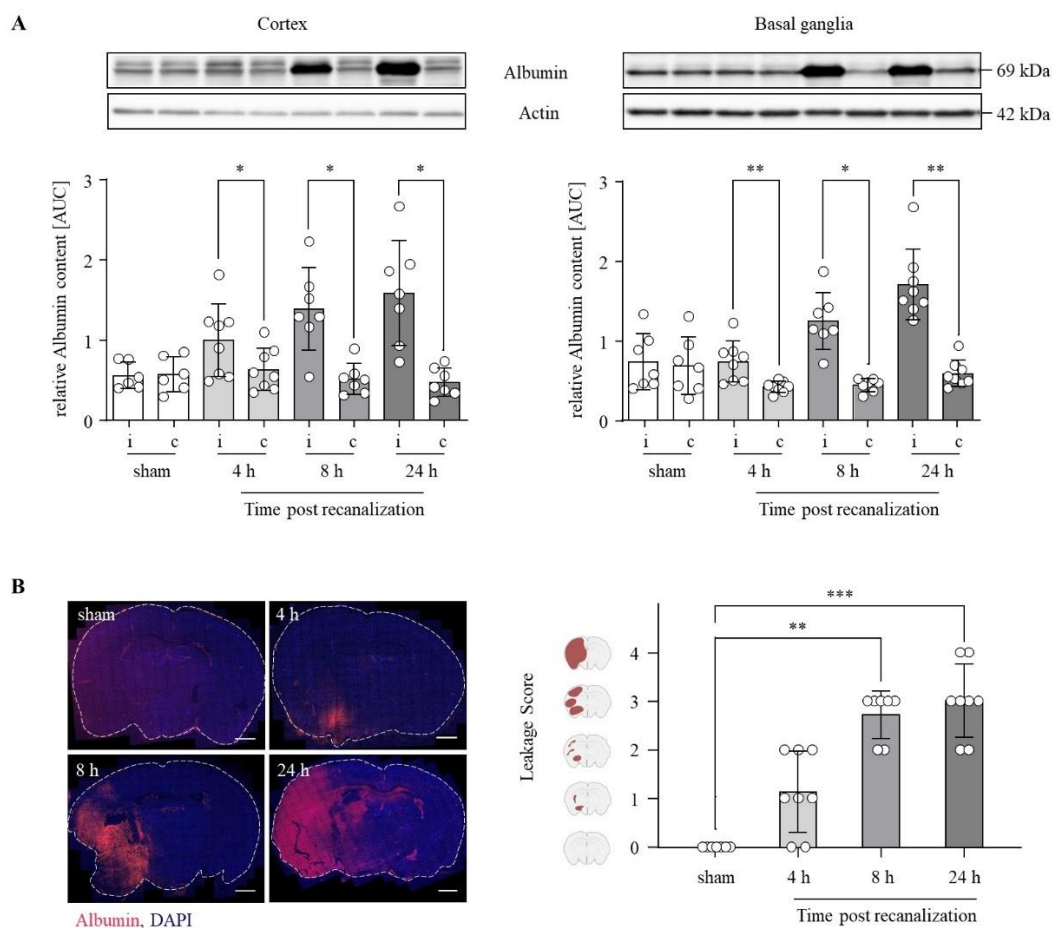


Figure 3-3. Vascular leakage is an early event post recanalization. (A) Western blot analysis of endogenous Albumin (69 kDa) in cortices (left) and basal ganglia (right) of WT mice that underwent 4 h, 8 h, and 24 h of reperfusion after tMCAO. Relative Albumin content calculated by the normalization of Albumin protein content to the Actin (42 kDa) loading control. Representative immunoblots are shown above the densitometric quantification. Data are shown as mean \pm SD of 6 to 8 mice per group. Each data point represents one mouse per time point. i = ipsilateral, c = contralateral. P-values were calculated by Wilcoxon mated-pairs signed rank test or paired Student's t-test and considered statistically significant with * $P < 0.05$; ** $P < 0.01$. (B) Representative coronal brain sections from mice that underwent 4 h, 8 h, 24 h of reperfusion after tMCAO. Cryosections were stained for endogenous Albumin (red) and cell nuclei (DAPI, blue). Scale bar, 1 mm. (left panels). Quantification of vascular leakage within brain sections by a 5-point leakage score. The degree of vascular leakage was estimated by the means of Albumin signal within the ipsilateral hemisphere: 0 = no leakage, 1 = minor leakage, 2 = moderate leakage, 3 = major leakage, 4 = severe leakage. (To be continued on the following page)

Data are shown as mean \pm SD of 8 mice per group. Each data point represents one mouse. The mean of each mouse was calculated from at least 3 sections. P-values were calculated by Kruskal-Wallis test followed by a Dunn's multiple comparison test and considered statistically significant with ** $P < 0.01$; *** $P < 0.001$ (right). Confocal microscopy and leakage score analysis were performed by Vanessa G6b.

Overall, these results clearly demonstrate an integer BBB under sham conditions, while BBB breakdown is induced within the first 4 h of vessel recanalization.

3.2.2 Elevated MMP9 levels after vessel recanalization

Disruption of the BBB is closely related to MMP activity [124]. Therefore, we addressed the temporal regulation of MMP9 protein content within the ipsilateral and contralateral hemisphere after an ischemic insult followed by reperfusion. Comparable to the breakdown of vascular integrity (see 3.2 and 3.3), relative MMP9 protein content significantly increased after 4 h of reperfusion in the ipsilateral cortices and basal ganglia and remained elevated until 24 h post recanalization (Cortex: 4 h i 0.45 ± 0.34 vs c 0.13 ± 0.04 ; 8 h i 0.5 ± 0.23 vs c 0.13 ± 0.04 ; 24 h i 0.85 ± 0.27 vs c 0.09 ± 0.01 ; Basal ganglia: 4 h i 0.3 ± 0.15 vs c 0.13 ± 0.06 , 8 h i 0.69 ± 0.46 vs c 0.33 ± 0.4 ; 24 h i 1.1 ± 0.78 vs c 0.2 ± 0.12 ; Figure 3-4).

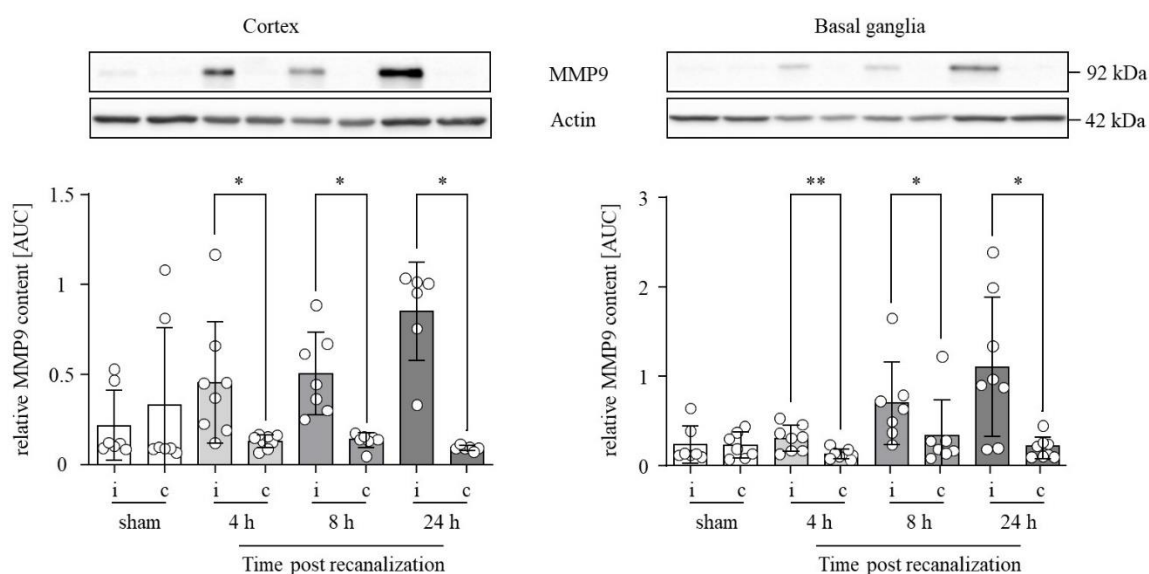


Figure legend on the following page

Figure 3-4. MMP9 protein levels are elevated within the first 4 h of reperfusion in the ipsilateral hemisphere after tMCAO. Western blot analysis of MMP9 (92 kDa) in cortices (left) and basal ganglia (right) of mice that underwent 4 h, 8 h, and 24 h of reperfusion after tMCAO. Relative MMP9 content was calculated by the normalization of MMP9 protein content to the Actin (42 kDa) loading control. Representative immunoblots are shown above the densitometric quantification. Data are shown as mean \pm SD of 7 to 8 mice per group. Each data point represents one mouse per time point. i = ipsilateral, c = contralateral. P-values were calculated by Wilcoxon matched-pairs signed rank test or paired Student's t-test and considered statistically significant with * $P < 0.05$; ** $P < 0.01$.

These results show that MMP9 is elevated in the ipsilateral hemisphere within 4 h post recanalization, representing the same time window in which BBB disruption after vessel recanalization was observed.

3.3 The role of platelets in blood-brain barrier disruption

3.3.1 Platelet GPVI-deficiency sustains vascular integrity following tMCAO

In the first place, platelets are known to maintain haemostasis and to safeguard vascular integrity. In the setting of thrombo-inflammation, however, they seem to exert opposing functions by mechanisms that still remain elusive. Experiments in model systems of rheumatic arthritis [125] or myocardial ischemia and reperfusion [126] could in fact reveal a contribution of platelets in enhancing vascular permeability. Since the activatory platelet receptor GPVI was already shown to critically contribute to cerebral ischemia [28, 58], the participation of this platelet receptor in the disturbance of vascular integrity was investigated. Therefore, mice were injected with the anti-GPVI antibody (JAQ1) four and five d prior tMCAO surgery, which causes shedding of GPVI from the platelet surface [127]. Remarkably, GPVI-deficiency prevented from Albumin extravasation into the ipsilateral hemisphere (1.84 ± 1.18), which could not be observed in control IgG treated mice (0.53 ± 0.27 , Figure 3-5). Additionally, these mice developed smaller infarct sizes 24 h post reperfusion [28], demonstrating an elementary role of GPVI-activated platelets in I/R injury after cerebral ischemia.

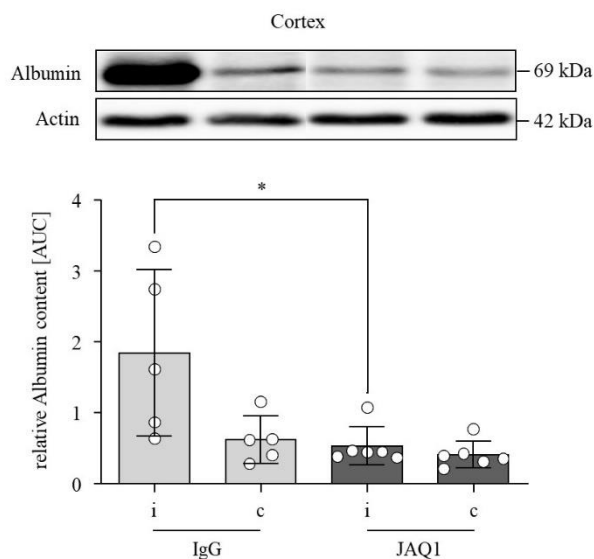


Figure 3-5. Vascular integrity is sustained in GPVI depleted mice after tMCAO. Western blot analysis of endogenous Albumin (69 kDa) in cortices of WT mice treated with control IgG or GPVI antibody 4 and 5 days prior to surgery. Relative Albumin content calculated by the normalization of Albumin protein content to the Actin (42 kDa) loading control. Representative immunoblots are shown above the densitometric quantification. Data are shown as mean \pm SD of 5 to 6 mice per group. Each data point represents one mouse per time point. i = ipsilateral, c = contralateral. P-values were calculated by two-tailed Mann Whitney U test and considered statistically significant with * $P < 0.05$.

3.3.2 Platelet α -granules induce the loss of endothelial cell monolayer integrity

Engagement of platelet GPVI, by collagen binding, triggers platelet activation via the phosphorylation of downstream ITAM and the mobilization of Ca^{2+} from intracellular stores [128, 129]. Once activated, platelets secrete their stored granular cargo and thereby contribute to the pathophysiology of cerebral ischemia [81, 128]. This prompted us to investigate the effect of platelet granule content on the patency of the BBB. Therefore, a simplified *in vitro* BBB model was established, in which primary MBMECs were seeded onto a permeable membrane. Upon confluence, the cell layer was treated with the soluble components released from platelet granules upon activation (platelet releasate) and EC layer integrity was continuously monitored for 18 h post treatment using an impedance-based measurement setup. This method allows for the recording of TEER, a measure for the barrier integrity. Cell layers treated with platelet releasate generated from WT mice strikingly reduced TEER values within the first 6 h of treatment, corroborating an integral role of platelet-derived soluble molecules in the disruption of EC layer integrity. Next, the pathologic relevance of the different granules contained by

platelets were distinguished by the usage of three knock-out mouse lines: *Nbeal2*^{-/-} (lack of α -granules), *Unc13d*^{-/-} (defective dense granule secretion), and *Nbeal2/Unc13d* double deficient mice (lack of α -granules and defective dense granule secretion). Within each experiment, additional control treatments were applied as a reference, which consisted of a treatment with culture medium (control) or collagen related peptide (CRP). CRP was used in a concentration of 10 μ g/ml in Tyrode's buffer with Ca²⁺ to generate platelet releasate and served to exclude side effects of this stimulant on MBMECs. While endothelial integrity was significantly impaired by the application of *Unc13d*^{-/-} releasate, barrier function was maintained at control levels when treated with releasate from *Nbeal2*^{-/-}/*Unc13d*^{-/-} and *Nbeal2*^{-/-} mice (WT 26.7 \pm 4.04% vs *Nbeal2*^{-/-}/*Unc13d*^{-/-} 58.97 \pm 10.09%; WT 26.7 \pm 4.04% vs *Nbeal2*^{-/-} 68.91 \pm 6.97%; *Nbeal2*^{-/-}/*Unc13d*^{-/-} 58.97 \pm 10.09% vs *Unc13d*^{-/-} 31.89 \pm 8.33%; *Nbeal2*^{-/-} 68.91 \pm 6.97% vs *Unc13d*^{-/-} 31.89 \pm 8.33%; Figure 3-6 A). These observations showed that platelet α -granule content is responsible for the induction of barrier disintegration. Next, the influence of platelet releasate on MBMEC morphology was investigated by histological analysis. Here, 18 h treated MBMEC monolayers were stained for CD31 and examined using confocal microscopy. In line with decreased TEER values, MBMECs treated with WT or *Unc13d*^{-/-} platelet releasate showed morphological changes, which manifested in an unequal, squeezed appearance (Figure 3-6 B). Furthermore, a remarkable number of cell layer disruptions in form of holes (black arrows, Figure 3-6 B, C) were found within these cell cultures. Control treatment and treatment with either releasate of *Nbeal2*^{-/-} or double deficient platelets, however, resulted in uniform cell layers whereby ECs exhibited their typical spindle-like morphology. For the quantification of the observed barrier disruptions, entropy images were generated and the percentage of area covered by endothelial holes was calculated for each treatment. Entropy-based hole quantification revealed only marginal defects in cell layers treated with control substances (control, CRP), double deficient and *Nbeal2*^{-/-} platelet releasate, while WT and *Unc13d*^{-/-} releasate treatment disclosed a significant increase in hole formation related to the total surface coverage (WT 0.78 \pm 0.85% vs *Nbeal2*^{-/-}/*Unc13d*^{-/-} 0.12 \pm 0.28%; WT 0.78 \pm 0.85% vs *Nbeal2*^{-/-} 0.2 \pm 0.5%; *Nbeal2*^{-/-}/*Unc13d*^{-/-} 0.12 \pm 0.28% vs *Unc13d*^{-/-} 1.49 \pm 1.45%; *Nbeal2*^{-/-} 0.2 \pm 0.5% vs *Unc13d*^{-/-} 1.49 \pm 1.45%; Figure 3-6 B, C). These data indicate an exclusive endothelial-damaging phenotype of platelet α -granules. In line with these observations, treatment of EC monolayers with different concentrations of adenosine diphosphate (ADP), a major constituent of dense granules, did not induce integrity loss. In comparison to thrombin, which served as positive control for the induction of barrier disruption,

both concentrations of ADP did not induce integrity loss of the cultured ECs (control $69.19 \pm 18.50\%$ vs thrombin $20.86 \pm 10.89\%$; Figure 3-6 D).

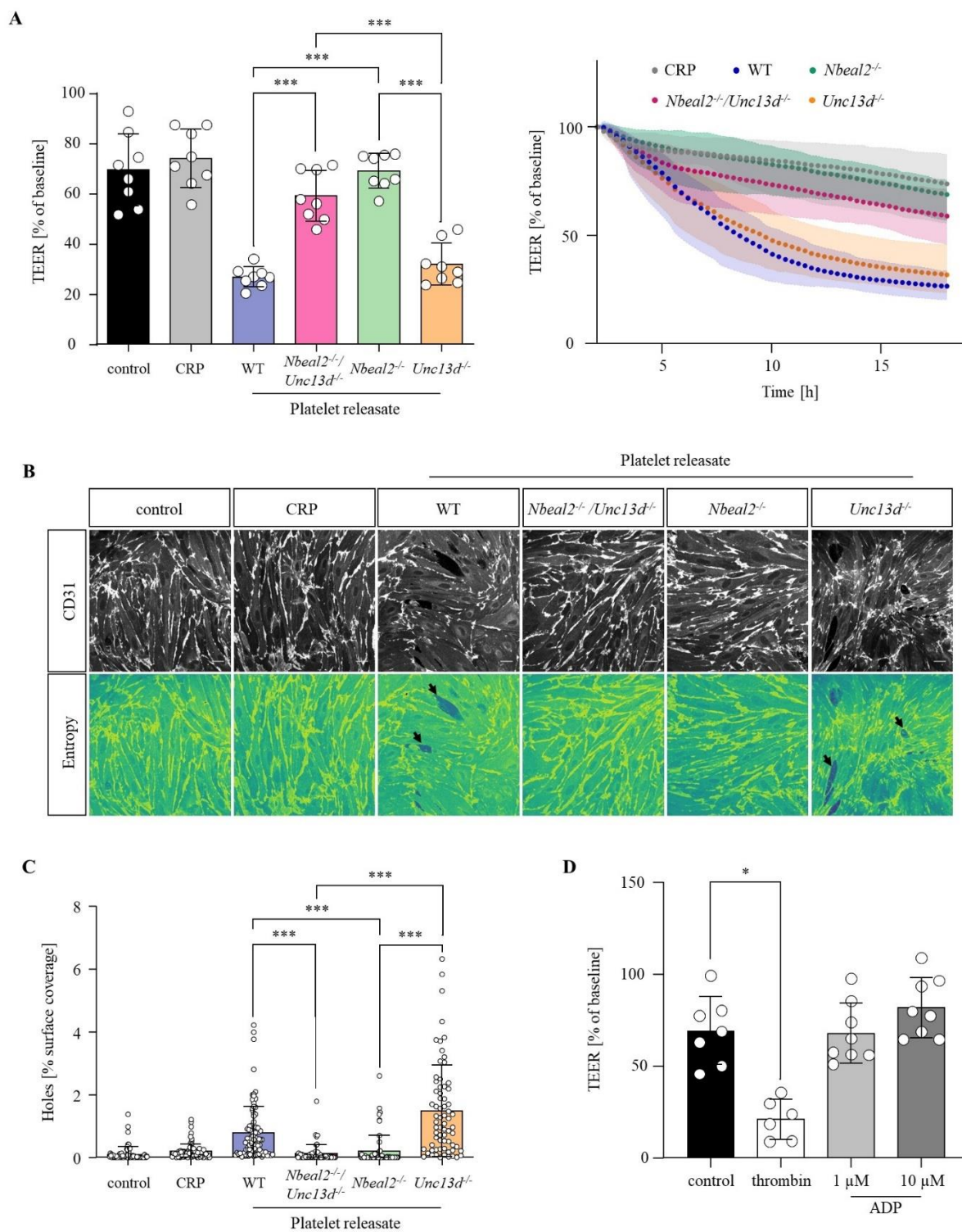


Figure legend on the following page

Figure 3-6. Platelet α -granules, but not dense granules induce integrity loss of MBMEC monolayers. Transendothelial electrical resistance (TEER) of primary mouse brain microvascular endothelial cell (MBMEC) monolayers after 18 h of treatment and simultaneous recording. **(A)** TEER values of MBMEC monolayers treated with platelet releasate of wild-type (WT), *Nbeal2/Munc13-4* double-deficient (*Nbeal2^{-/-}/Unc13d^{-/-}*), *Nbeal2* deficient (*Nbeal2^{-/-}*), and *Munc13-4* deficient (*Unc13d^{-/-}*) mice. Controls were treated with culture medium. Collagen related peptide (CRP) was used in a concentration of 10 $\mu\text{g/ml}$ in Tyrode's buffer with Ca^{2+} and served as control to exclude side effects of the stimulant on MBMEC, as it was used to generate platelet releasate. Data are shown as mean \pm SD. Each data point represents one transwell insert. Data was collected within 4 independent experiments. P-values were calculated by Ordinary one-way ANOVA followed by a Tukey's multiple comparison post-hoc test and considered statistically significant with *** $P < 0.001$ (left). Trajectory course of TEER after treatment with platelet releasate. Data are shown as mean \pm upper/lower limit. Each data point represents the mean of 8 transwell inserts at a distinct time point during measurement. TEER was measured every 10 minutes for at least 18 h post-treatment. Data was collected within 4 independent experiments. Shown is the percentual change of TEER to baseline (100%) (right). **(B)** Representative confocal images of MBMEC monolayers after treatment with platelet releasate for 18 h. Upper panels show anti-CD31 labeled cell monolayers grown in 18-well chamber Ibbidi slides. Lower panels show entropy images generated for the quantification of holes in the cell layer. Scale bar, 25 μm . **(C)** Quantification of holes within MBMEC layers after respective treatments is shown as percentage of surface coverage. Data was collected within 3 independent experiments. P-values were calculated by Kurskal-Wallis test followed by a Dunn's multiple comparison post-hoc test and considered statistically significant with *** $P < 0.001$. **(D)** TEER values of MBMEC monolayers treated with human thrombin (0.1U/260 μl) or adenosine diphosphate (ADP, 1 or 10 μM). Controls were treated with culture medium. Data are shown as mean \pm SD. Each data point represents one transwell insert. Data was collected within 4 independent experiments. P-values were calculated by Kruskal-Wallis test followed by a Dunn's multiple comparison test and considered statistically significant with * $P < 0.05$. Confocal microscopy and entropy-based hole quantification was performed by Vanessa G6b.

These data indicate that platelet α -granule content, but not dense granule content contribute to the disruption of endothelial barrier integrity.

3.3.3 Platelet releasate does not affect tight junction protein levels in endothelial cells

Since BBB patency is to a large extent based on the formation of TJs and AJs between adjacent ECs, western blot analysis of treated cell cultures was performed 18 h post treatment to investigate if platelet granule content influences TJ and AJ protein levels. Interestingly, protein content of the AJ protein VE-Cadherin and the TJ proteins Occludin and Claudin-5 were not affected by granule content (Figure 3-7 A). This emphasizes that the disruption of the EC monolayers cannot be accounted to the degradation of TJ and AJ proteins.

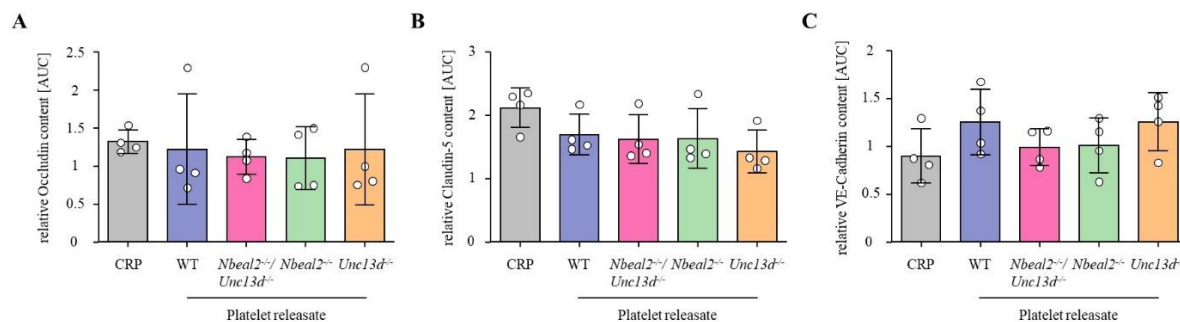


Figure 3-7. Platelet releasate does not alter TJ protein content in MBMEC monolayers. Western Blot analysis of the tight and adherens junction proteins occludin (A), claudin-5 (B), and VE-cadherin (C) in MBMEC lysates after platelet releasate treatment. Relative protein content was calculated by the normalization of the respective junctional proteins to the Actin loading control. Data are shown as mean \pm SD of 4 independent experiments. Each data point represents one well. P-values were calculated by Kruskal-Wallis test followed by a Dunn's multiple comparison test.

3.3.4 Lack of platelet α -granules, but not dense granules protect from blood-brain barrier breakdown after tMCAO

To test whether the findings of an α -granule dependent barrier disruption can be validated *in vivo*, NBEAL2-deficient mice and their WT littermates, which served as control animals, were subjected to 1 h of tMCAO followed by 4 h of reperfusion. In accordance with the *in vitro* results, 2-PM revealed vascular leakage within the ipsilateral hemisphere of WT but not NBEAL2 knockout mice (Figure 3-8 A). Furthermore, endogenous Albumin content remained unaltered between the ipsilateral and contralateral hemisphere of *Nbeal2*^{-/-} mice 8 h post reperfusion (Cortex: *Nbeal2*^{+/+} i 0.79 ± 0.34 vs c 0.28 ± 0.08 ; *Nbeal2*^{-/-} i 0.55 ± 0.22 vs c 0.4 ± 0.18 ; Basal ganglia: *Nbeal2*^{+/+} i 0.73 ± 0.43 vs c 0.25 ± 0.09 ; *Nbeal2*^{-/-} i 0.46 ± 0.35 vs c 0.29 ± 0.21) (Figure 3-8 B). Together, these findings implicate a protective effect of α -granule deficiency on barrier integrity that additionally correlated with infarct development [79].

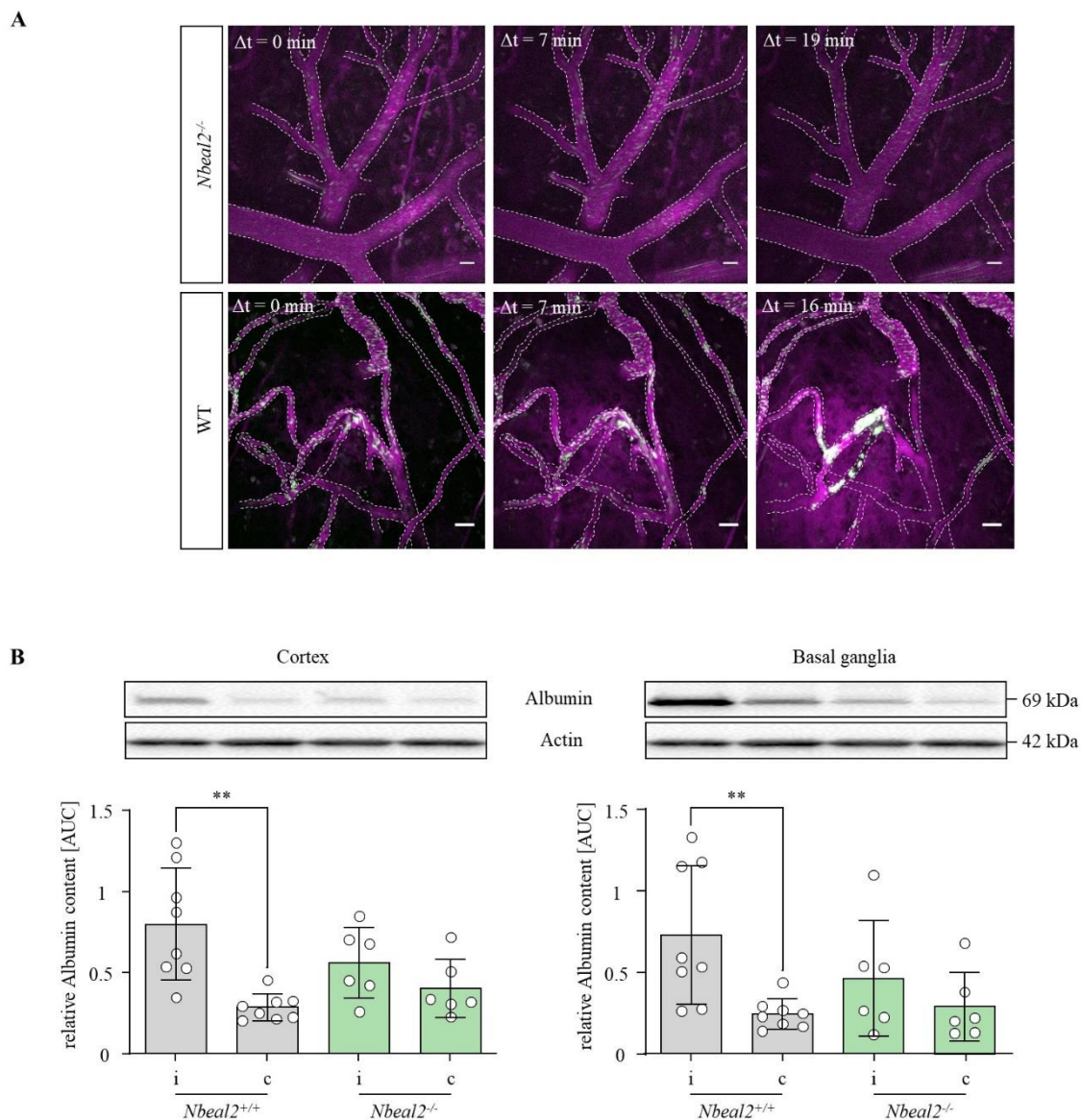


Figure 3-8. Lack of platelet α -granules protects from blood-brain barrier breakdown after tMCAO. (A) Representative intravital 2-photon microscopy (2-PM) images of the brain vasculature of *Nbeal2*^{-/-} (upper panels) and WT (lower panels) mice in the early phase of reperfusion following tMCAO. Platelets (green) are labeled by anti-GPIX-Alexa Fluor 488. Vessels and vessel lumen are labeled by anti-BSA-Alexa Fluor 546 and anti-CD105-Alexa Fluor 546. Time between separate images is indicated as Δt . Scale bar, 20 μ m. (B) Western blot analysis of endogenous Albumin (69 kDa) in cortices (left) and basal ganglia (right) of *Nbeal2*^{+/+} and *Nbeal2*^{-/-} mice 8 h after tMCAO. Relative Albumin content calculated by the normalization of Albumin protein content to the Actin (42 kDa) loading control. Representative immunoblots are shown above the densitometric quantification. Data are shown as mean \pm SD of 6 to 8 mice per group. Each data point represents one mouse. i = ipsilateral, c = contralateral. P-values were calculated by Wilcoxon signed-rank test or paired Student's t-test and considered statistically significant with ** $P < 0.01$. Intravital microscopy was performed by Vanessa G**ö**b.

Furthermore, *Unc13d*^{-/-} mice were investigated to assess the effect of dense granule deficiency on barrier integrity *in vivo*. In contrast to *Nbeal2*^{-/-} mice, western blot analysis revealed increased Albumin content in the ipsilateral hemisphere of *Unc13d*^{-/-} as well as *Unc13d*^{+/+} (WT littermates) mice (Cortex: *Unc13d*^{+/+} i 0.83 ± 0.3 vs c 0.52 ± 0.21; *Unc13d*^{-/-} i 0.79 ± 0.38 vs c 0.48 ± 0.15; Basal ganglia: *Unc13d*^{+/+} i 1.31 ± 0.18 vs c 0.78 ± 0.12; *Unc13d*^{-/-} i 0.98 ± 0.24 vs c 0.69 ± 0.14; Figure 3-9), confirming the hypothesized concept of a platelet α-granule mediated barrier disruption.

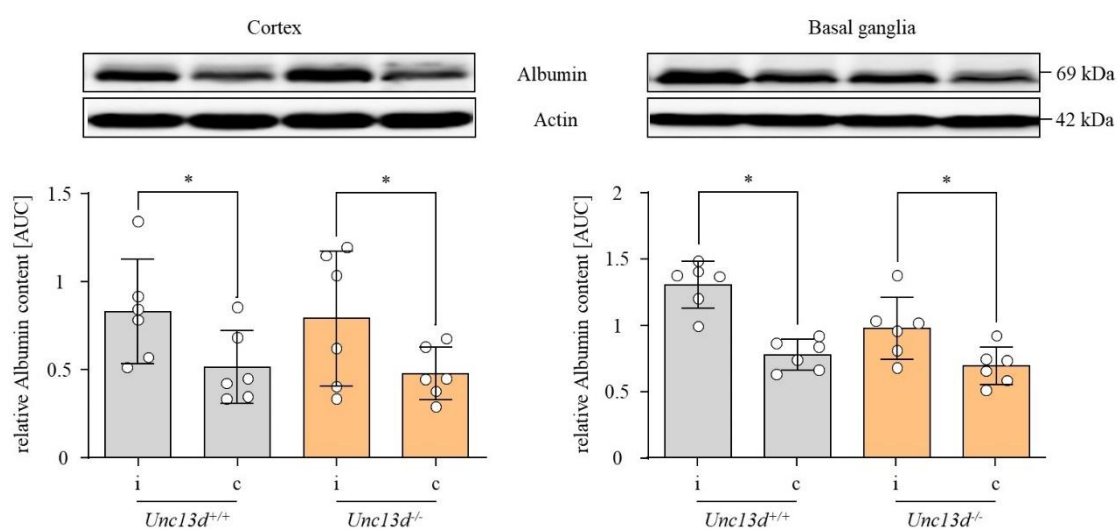


Figure 3-9. *Unc13d*^{-/-} mice are not protected from blood-brain barrier breakdown after tMCAO. Western blot analysis of endogenous Albumin (69 kDa) in cortices (left) and basal ganglia (right) of *Unc13d*^{+/+} and *Unc13d*^{-/-} mice 24 h after tMCAO. Relative Albumin content calculated by the normalization of Albumin protein content to the Actin (42 kDa) loading control. Representative immunoblots are shown above the densitometric quantification. Data are shown as mean ± SD of 6 mice per group. Each data point represents one mouse. i = ipsilateral, c = contralateral. P-values were calculated by Wilcoxon signed-rank test and considered statistically significant with * P<0.05.

3.3.5 Screening for an endothelial harming α-granule component

In a next step, the damage-inducing constituent of platelet granules should be identified. By the denaturation of proteins within WT platelet releasate prior to EC monolayer application, it was proven that the harmful component is indeed of proteinaceous origin. Denaturation of proteins within WT releasate rescued from the perturbation of vascular integrity, but did not reach control levels. However, the boiled platelet releasate constituted TEER values to *Nbeal2*^{-/-}

treatment niveau, while unconditioned WT releasate was destructive again (CRP $83.96 \pm 9.82\%$ vs WT $24.02 \pm 3.44\%$; Figure 3-10). Thus, it could be shown that EC barrier loss is provoked by a proteinaceous platelet granule component. Since platelet α -granules predominantly contain a plethora of vasoactive proteins and the lack of these granules protects from EC barrier disruption (Figure 3-6), these data suggest that the barrier disrupting protein originates from platelet α -granules.

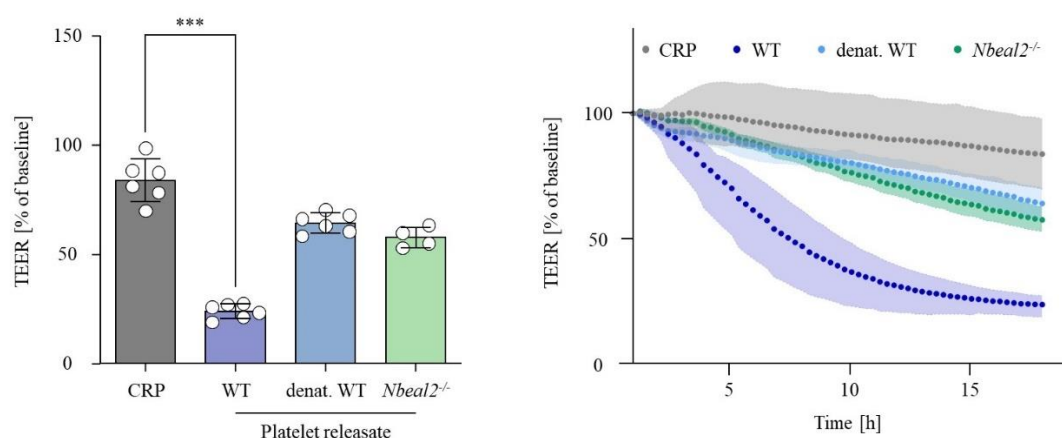


Figure 3-10. Protein denaturation sustains cell layer integrity. Transendothelial electrical resistance (TEER) of primary mouse brain microvascular endothelial cell (MBMEC) monolayers after 18 h of treatment and simultaneous recording. TEER values of MBMEC monolayers treated with platelet releasate of wild-type (WT) and *Nbeal2*^{-/-} mice. Denatured WT platelet releasate (denat. WT) was boiled for 5 min at 95 °C and was allowed to cool down before usage. Collagen related peptide (CRP) was used in a concentration of 10 $\mu\text{g}/\text{ml}$ in Tyrode's buffer with Ca^{2+} and served as control to exclude side effects of the stimulant on MBMEC, as it was used to generate platelet releasate. Data are shown as mean \pm SD. Each data point represents one Transwell insert. Data was collected within 3 independent experiments. P-values were calculated by Kruskal-Wallis test followed by a Dunn's multiple comparison test and considered statistically significant with *** $P < 0.001$ (left panel). Trajectory course of TEER after treatment with platelet releasate. Data are shown as mean \pm upper/lower limit. Each data point represents the mean of 4 to 6 Transwell inserts at a distinct time point during measurement. TEER was measured every 10 min for at least 18 h post-treatment. Data was collected within 2 to 3 independent experiments. Shown is the percentual change of TEER to baseline (100%) (right panel).

Based on this knowledge, screening of promising proteinaceous α -granule candidates, that might exert barrier-disrupting properties, was performed. Among others, the chemokines CXCL7, CXCL12, and CXCL5 were selected due their increased appearance in human IS patients [25, 130] or their barrier-harming roles in other neurological diseases [131]. However, all of the examined chemokines were unable to induce a reduction in TEER (control

$88.06 \pm 11.66\%$ vs thrombin $45.39 \pm 6.38\%$; Figure 3-11 A). Screening of growth factors, on the contrary, was successful. Among the investigated growth factors, the PDGF isoform AB significantly induced loss of barrier integrity when compared to control-treated cell layers (control $90.47 \pm 11.04\%$ vs PDGF-AB $68.86 \pm 8.905\%$; Figure 3-11 B), making PDGF-AB a promising candidate for further investigations.

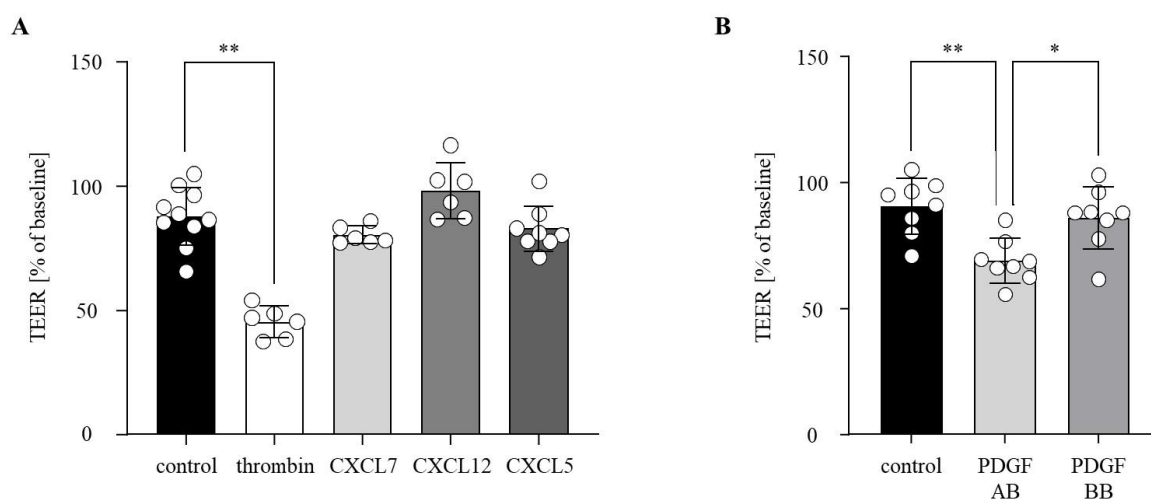


Figure 3-11. Recombinant PDGF-AB induces brain endothelial cell layer disruption. Transendothelial electrical resistance (TEER) of primary mouse brain microvascular endothelial cell (MBMEC) monolayers after 18 h of treatment and simultaneous recording. **(A)** TEER values of MBMEC monolayers treated with human thrombin (0.38 U/ml) or recombinant CXCL7 (6.92 $\mu\text{g/ml}$), CXCL12 (1 $\mu\text{g/ml}$), and CXCL5 (1 $\mu\text{g/ml}$). Controls were treated with culture medium. Thrombin served as positive control. **(B)** TEER values of MBMEC monolayers treated with culture medium (control), recombinant PDGF-AB (10 $\mu\text{g/ml}$), or PDGF-BB (10 $\mu\text{g/ml}$). Data are shown as mean \pm SD. Each data point represents one Transwell insert. Data was collected within 4 **(A)** or 3 **(B)** independent experiments. P-values were calculated by Ordinary one-way ANOVA followed by a Tukey's post-hoc test **(B)** or Kruskal-Wallis test **(A)** and considered statistically significant with ** $P < 0.01$.

Since screening was performed using recombinant proteins, it was assessed whether PDGF-AB is present in the releasate of platelets. Therefore, PDGF-AB concentrations in platelet releasate of WT and *Nbeal2*^{-/-} mice were estimated. Enzyme-linked immunosorbent analysis revealed 4-times higher PDGF-AB concentrations in releasate of WT platelets compared to releasate of *Nbeal2*^{-/-} platelets, confirming the presence and release of PDGF-AB from WT platelets.

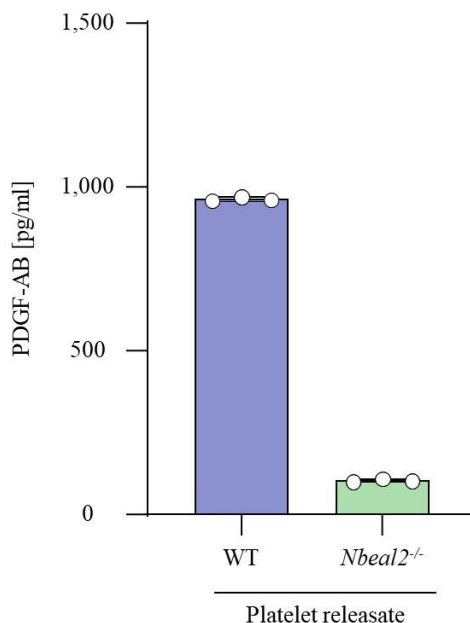


Figure 3-12. PDGF-AB is a component of platelet α -granules. Quantitative analysis of PDGF-AB concentrations in platelet releasate of wild-type (WT) and *Nbeal2*^{-/-} mice by ELISA. Data are shown as mean \pm SD. Each data point represents one batch of platelet releasate.

Finally, the role of platelet derived PDGF-AB in the disruption of EC barrier integrity was reviewed by the neutralization of PDGF within WT releasate. While incubation of ECs with WT releasate or *Nbeal2*^{-/-} releasate supplemented with recombinant PDGF-AB significantly reduced TEER, neutralization of PDGF in WT platelet releasate restored barrier function of MBMECs (CRP $64.94 \pm 10.06\%$ vs WT $29.77 \pm 8.84\%$; CRP $64.94 \pm 10.06\%$ vs *Nbeal2*^{-/-} + PDGF-AB $31.76 \pm 6.72\%$; Figure 3-13). The PDGF neutralization antibody (PDGF-NAb) itself, however, did not affect barrier integrity at all.

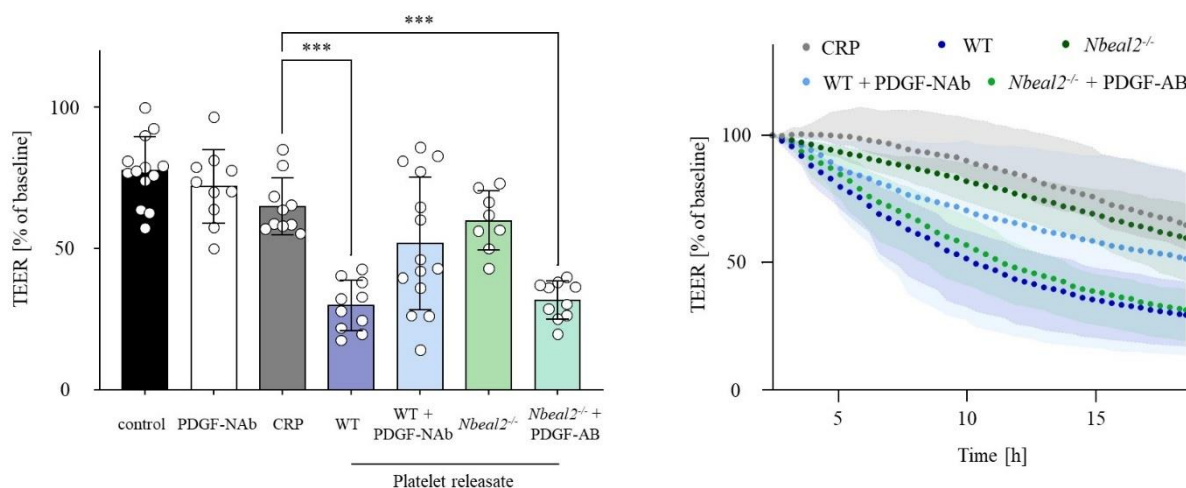


Figure 3-13. Antibody-mediated neutralization of PDGF rescues barrier integrity of MBMEC monolayers. Transendothelial electrical resistance (TEER) of primary mouse brain microvascular endothelial cell (MBMEC) monolayers after 18 h of treatment and simultaneous recording. TEER values of MBMEC monolayers treated with platelet releasate of wild-type (WT) and *Nbeal2*^{-/-} mice. *Nbeal2*^{-/-} and WT platelet releasate were either preincubated with recombinant PDGF-AB (PDGF, 10 μ g/ml) or PDGF neutralization antibody (PDGF-NAb, 1 μ g/ml) for 10 min prior to treatment. Controls were treated with culture medium. PDGF neutralization antibody treatment of MBMEC without additional platelet releasate treatment served as control to exclude side effects of the antibody. Collagen related peptide (CRP) was used in a concentration of 10 μ g/ml in Tyrode's buffer with Ca²⁺ and served as control to exclude side effects of the stimulant on MBMEC, as it was used to generate platelet releasate. Data are shown as mean \pm SD. Each data point represents one Transwell insert. Data was collected within 4 independent experiments. P-values were calculated by One-Way ANOVA followed by a Dunn's multiple comparison test and considered statistically significant with *** P<0.001 (left panel). Trajectory course of TEER after treatment with platelet releasate and PDGF neutralization antibody. Data are shown as mean \pm upper/lower limit. Each data point represents the mean of 8 Transwell inserts at a distinct time point during measurement. TEER was measured every 10 min for at least 18 h post-treatment. Data was collected within 4 independent experiments. Shown is the percentual change of TEER to baseline (100%) (right panel).

Together, the presented results are indicative for a participation of platelet α -granule secretion in the breakdown of the BBB and therefore in the pathomechanism of I/R injury following IS. This mechanism seems to involve platelet α -granule derived PDGF-AB.

3.3.6 Platelet secretion mediates Ca²⁺ signalling in cultured endothelial cells

Calcium is a well described second messenger, involved in several cellular processes [132, 133]. Among other functions, increased intracellular Ca²⁺ concentrations in ECs have been described to affect endothelial integrity [134]. In order to identify mechanistic signalling pathways underlying platelet-dependent barrier perturbation, calcium mobilization from the endoplasmatic reticulum or extracellular space was analysed in cultured ECs in response to platelet releasate. Therefore, Fura-2 loaded primary ECs were stimulated with either platelet releasate or control treatment (10 µg/ml CRP) for 5 min in the presence of extracellular calcium. Basal calcium levels did not differ between both treatment groups. However, upon stimulation with WT releasate an immediate calcium influx could be detected, which was absent in CRP-treated cells (Figure 3-14 A, left). This response was mirrored by dramatically increased intracellular calcium concentrations (CRP 168 ± 73.67 mM vs WT platelet releasate 345.4 ± 245.1 mM; Figure 3-14 A, right), demonstrating a platelet granule content-induced calcium response in ECs. These findings prompted for further analyses of signal transduction pathways triggered by Ca²⁺, which might relate to EC barrier dysfunction. Therefore, one well established downstream pathway was investigated – the mitogen-activated protein kinase/extracellular signal-regulated protein kinase (MAPK/ERK) pathway. Western blot analysis of cortical and basal ganglia brain lysates from mice that underwent 1 h of tMCAO and various reperfusion periods revealed a phosphorylation of ERK within the ipsilateral hemisphere at all investigated time points (Cortex: 4 h i 0.61 ± 0.3 vs c 0.24 ± 0.09 ; 8 h i 0.73 ± 0.3 vs c 0.25 ± 0.1 ; 24 h i 0.47 ± 0.24 vs c 0.36 ± 0.23 ; Basal ganglia: 4 h i 0.58 ± 0.31 vs c 0.26 ± 0.11 , 8 h i 0.68 ± 0.26 vs c 0.3 ± 0.04 ; 24 h i 0.47 ± 0.18 vs c 0.33 ± 0.15 ; Figure 3-14 B), being indicative for an activation of the MAPK/ERK signalling pathway.

These data demonstrate on the one hand that platelet granule content from WT mice can evoke an increase in intracellular Ca²⁺ in MBMECs *in vitro*. On the other hand, it could be shown that the activation of the MAPK/ERK pathway is induced early after reperfusion *in vivo*, displaying remarkable similarities with the temporal kinetics of BBB disruption.

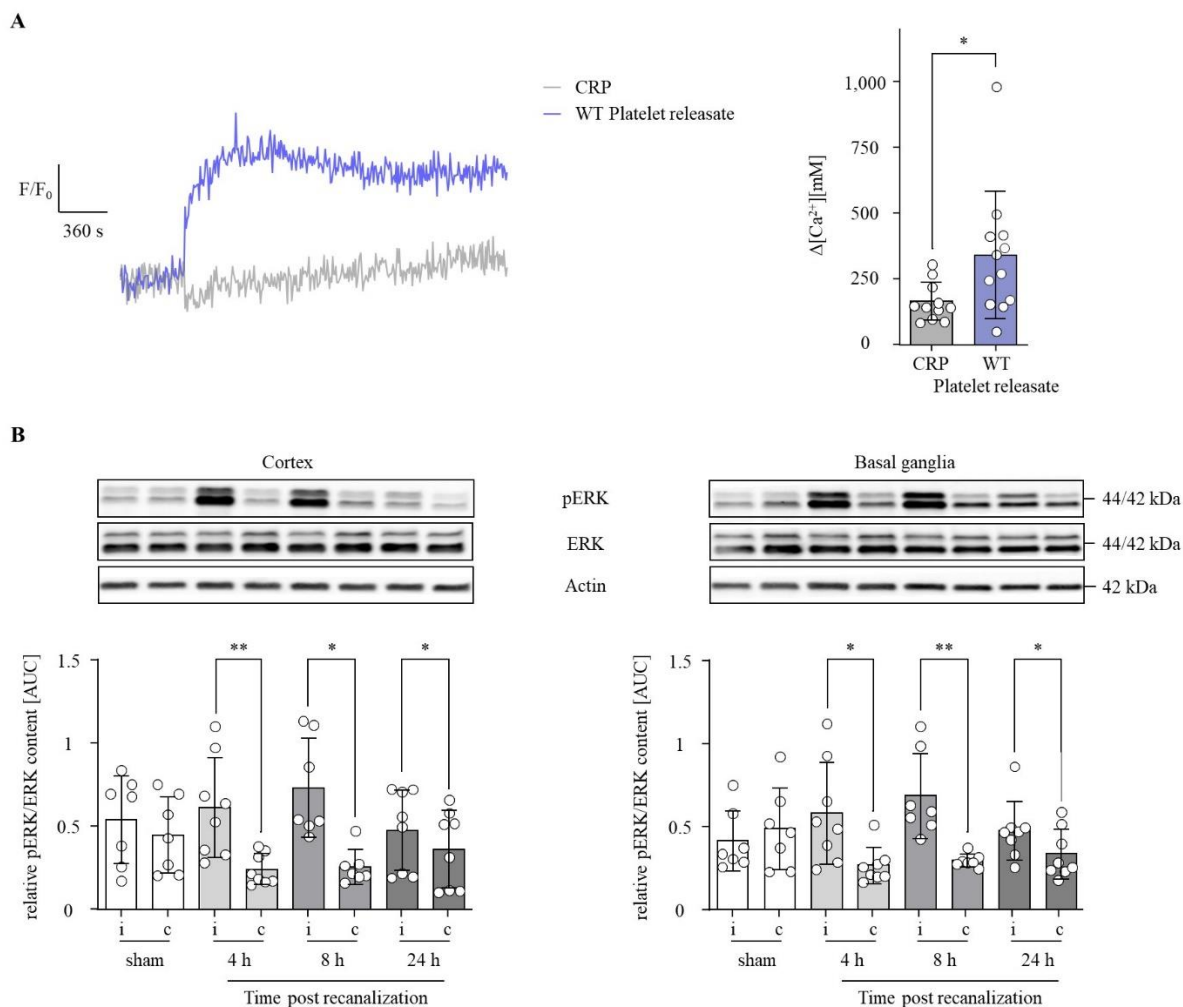


Figure 3-14. Platelet releasate induced intracellular Ca^{2+} signaling *in vitro* and activation of the ERK pathway after tMCAO with different reperfusion periods *in vivo*. (A) Representative curves of Ca^{2+} responses after treatment of cultures EC with WT platelet releasate (blue) or CRP (control, gray) (left). Maximal Ca^{2+} concentrations in MBMECs after treatment with the indicated agonists (right). Each dot represents one measurement and were acquired in 4 independent experiments. P-values were calculated by Mann Whitney test and considered statistically significant with $* < 0.05$. (B) Western blot analysis of extracellular signal-regulated kinases (ERK, 44 kDa, 42 kDa) in cortices (left) and basal ganglia (right) of WT mice that underwent 4 h, 8 h, and 24 h of reperfusion after tMCAO. Protein phosphorylation was expressed as relative amount of phosphorylated protein to total protein. Actin served as loading control. Representative immunoblots are shown above the densitometric quantification. Data are shown as mean \pm SD of 6 to 8 mice per group. Each data point represents one mouse. i = ipsilateral, c = contralateral. P-values were calculated by Wilcoxon matched-pairs signed rank test or paired Student's t-test and considered statistically significant with $* P < 0.05$; $** P < 0.01$.

3.3.7 Platelet releasate affects lymphocyte distribution in an *in vitro* blood-brain barrier model

Due to the proposed interaction of platelets, immune cells and ECs during thrombo-inflammation and the fact that WT platelet releasate promotes T cell motility in a 2-dimensional *in vitro* setup [107], the influence of platelet releasate on the transmigratory ability of lymphocytes was assessed in a Boyden chamber approach (see 2.2.1.9). Therefore, MBMECs were seeded and cultivated on 3 μm pore size transwell inserts, lymph node cells were isolated from WT mice and platelet releasate of WT and *Nbeal2*^{-/-} mice was utilized for stimulation. In order to induce migration across the MBMEC layer to the basolateral compartment, serum was added as a chemotactic agent. After 18 h of incubation, cell numbers were unaltered upon respective treatment within the distinct compartments (Figure 3-15 A). Consequently, it was investigated if platelet granule content, in particularly α -granule content, influences CD3⁺ lymphocyte distribution within the respective Boyden chamber compartments. Remarkably, treatment with WT platelet releasate induced an increase in CD3⁺ cells in the MBMEC layer when compared with *Nbeal2*^{-/-} platelet releasate treatment (WT 76.2% vs *Nbeal2*^{-/-} 60.3%). In the basolateral compartment, WT releasate increase the amount of CD3⁺ lymphocytes by 15.4% (compared to CRP control; CRP 57.09% vs WT 72.48%), whereas *Nbeal2*^{-/-} platelet releasate treatment was comparable to CRP treatment (CRP 57.1% vs. *Nbeal2*^{-/-} 49.7%).

Collectively, these data demonstrate that platelet releasate modulates the distribution of CD3⁺ T lymphocytes within an *in vitro* Boyden chamber approach, leading to an accumulation within the MBMEC monolayer.

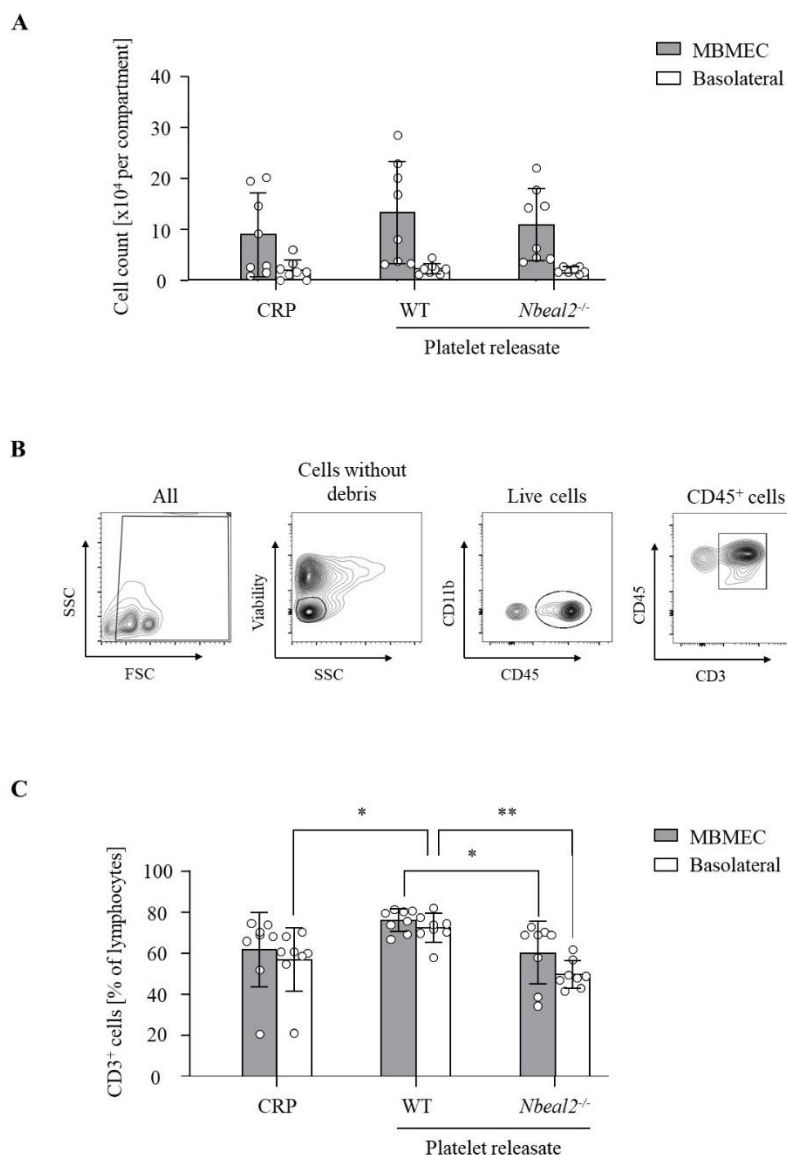


Figure 3-15. Platelet releasate influences CD3⁺ T lymphocyte distribution in an *in vitro* Boyden chamber assay. Flow cytometric analysis of lymph node cells in a Boyden chamber setup after treatment with platelet releasate of wild-type (WT) or *Nbeal2* deficient (*Nbeal2*^{-/-}) mice, and collagen related peptide (CRP). CRP was used in a concentration of 10 $\mu\text{g/ml}$ in Tyrode's buffer with Ca^{2+} and served as control to exclude side effects of the stimulant on the migratory behavior, as it was used to generate platelet releasate. **(A)** Absolute cell number of the respective treatment groups in the MBMEC monolayer (grey) and the basolateral compartment (white). **(B)** Representative flow cytometric gating strategy of murine lymph node cells after 18 h of treatment. **(C)** Percentual distribution of CD3⁺ lymph node cells within the respective compartments after treatment with platelet releasate or CRP. All graphs show data as mean \pm SD. Each data point represents one Transwell insert. Data was collected within 4 independent experiments. P-values were calculated by Two-way ANOVA followed by a Tukey's multiple comparison test and considered statistically significant with * $P < 0.05$; ** $P < 0.01$, *** $P < 0.001$.

3.4 Unravelling intravascular processes in patients with hyper-acute stroke

3.4.1 Large vessel occlusion is accompanied by an immediate immune response, mainly consisting of granulocytes and CD4⁺ T cells

Based on the observations made in 3.3.7 and other experimental studies, showing that immune cells infiltrate the ischemic brain [135, 136], we were interested whether an early immune response could also be found in the human system. Since information of human patients especially under occlusive conditions are largely missing, we made use of a novel technique, allowing for local pial blood sampling during MT and thus investigation of the intravascular pathophysiology during hyper-acute human stroke. In total, 36 human IS patients were analysed to determine the local leukocyte composition within the secluded vasculature. Using flow cytometric analysis (Figure 3-17 A, B), a significant increase in absolute granulocyte numbers was observed in blood samples aspirated under ischemia when compared to intraindividual systemic controls (systemic 5394 ± 2540 cells/ μ l vs ischemic 5901 ± 2706 cells/ μ l). Monocyte and lymphocyte numbers, instead, revealed no differences between the sampling locations (Figure 3-17 C). Further, detailed phenotyping of lymphocytes, presented as percentage of gated lymphocytes, revealed an overrepresentation of CD3⁺ T cells (systemic $69.56 \pm 12.00\%$ vs ischemic $72.45 \pm 11.12\%$) with an additional shift towards the CD4-positive population (systemic $46.99 \pm 12.03\%$ vs ischemic $50.96 \pm 12.81\%$) at costs of CD8⁺ T cells in the ischemic blood samples. B and NK cells, on the contrary, were overrepresented within the systemic control sample (Figure 3-17 D).

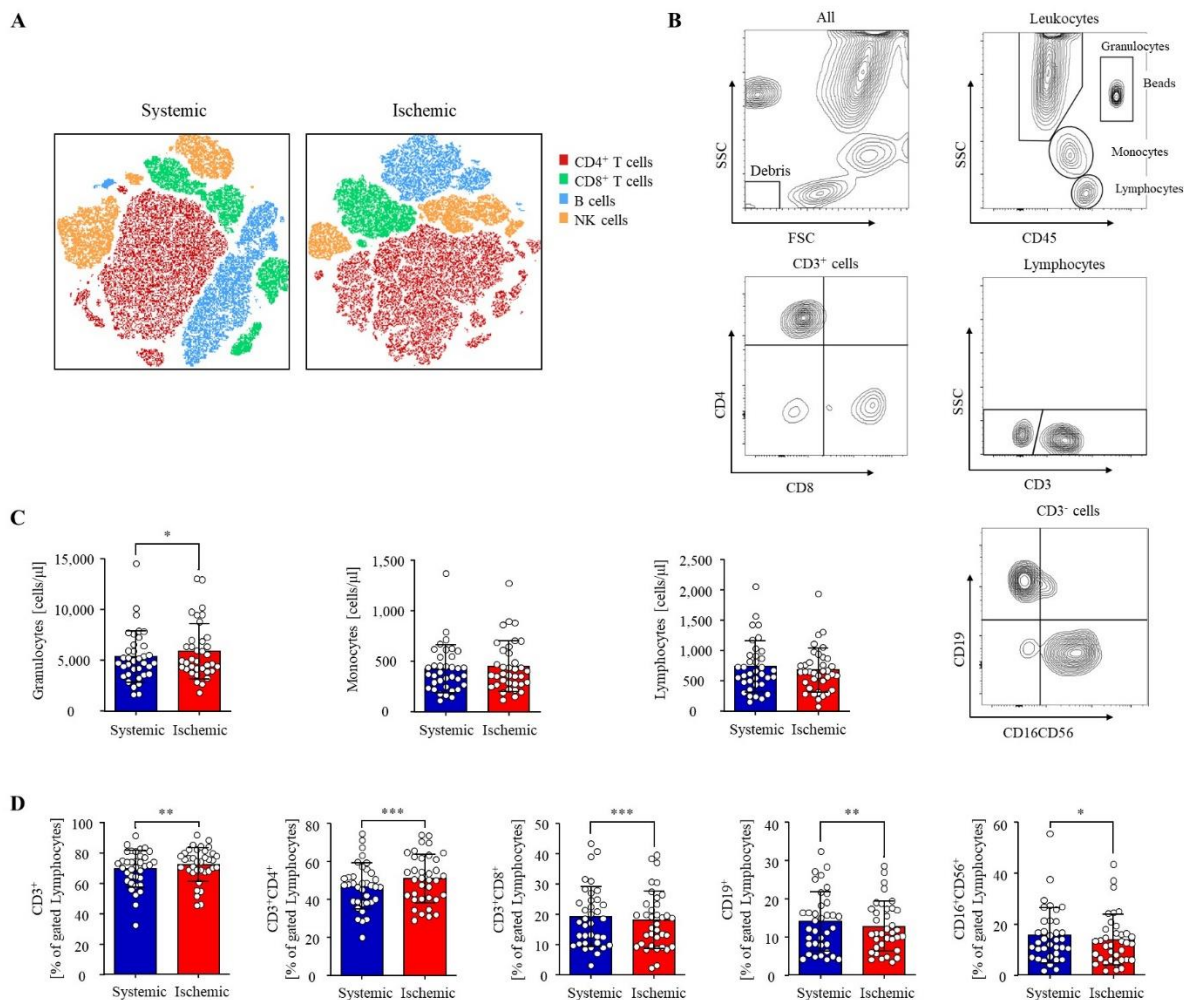


Figure 3-17. Local ischemic leukocyte composition is shifted towards granulocytes and CD4⁺ T cells in patients with hyperacute stroke. (A) Distribution of t-SNE identified leukocyte populations. (B) Representative flow cytometric gating strategy of human whole blood to analyze leukocyte subpopulations. (C) Absolute cell numbers of leukocyte subpopulations within ischemic (red) and systemic (blue) blood samples. (D) Percentual distribution of CD3⁺, CD3⁺CD4⁺, CD3⁺CD8⁺, CD19⁺, and CD16⁺CD56⁺ lymphocyte subpopulations, shown as percent of gated lymphocytes. Data are shown as mean \pm SD of 36 patients. Each data point represents one patient. P-values were calculated by Wilcoxon signed-rank test or paired Student's t-test and considered statistically significant with * P<0.05; ** P<0.01; *** P<0.001. Adopted from Zimmermann*, Pham* *et al.*, *JCBFM* 2022 [120] under the terms of the Creative Common Attribution License.

These findings are in line with results from independently investigated cohorts, which show a predominance of granulocytes/neutrophils within the secluded, ischemic vasculature. Additional immune phenotyping of the lymphocyte subpopulation, however, disclosed a novel finding – an increase in CD4⁺ T cells.

Overall, these results emphasize an immediate immune response within the secluded vasculature.

3.4.2 Increased numbers of platelet-leukocyte aggregates in the ischemic vasculature of stroke patients

Immune cell functions can potentially be modulated by platelets via direct engagement with leukocytes. Such interactions between platelets and leukocytes are referred to as platelet-leukocyte aggregates (PLAs). At sites of inflammation, levels of circulating PLAs are significantly increased and thus represent a highly sensitive marker for thrombo-inflammation and platelet activation [137]. Since the activation of platelets has been recently shown by increased plasma levels of CXCL4 and CXCL7 within the cerebral ischemic vasculature of IS patients [130], this thesis aimed to bring these findings together by the analysis of circulating PLAs in human ischemic pial blood. Platelets predominantly formed aggregates with monocytes and granulocytes within the ischemic vasculature, whereas binding to lymphocytes occurred to the same extent in distally and systemically aspirated blood (platelet-granulocyte aggregates: systemic $16.91 \pm 12.08\%$ vs ischemic $22.97 \pm 14.52\%$; platelet-monocyte aggregates: systemic $45.69 \pm 18.80\%$ vs ischemic $64.06 \pm 17.02\%$; platelet-leukocyte aggregates: systemic $10.81 \pm 6.93\%$ vs ischemic $11.93 \pm 6.45\%$; Figure 3-18 A, B). To confirm PLA formation by immunohistochemistry, blood smears of one representative patient were prepared and stained for platelets (CD42b, magenta) and neutrophils (neutrophil elastase, green; Figure 3-18 C). In line with the flow cytometric data, histology revealed PLAs predominantly in the ischemic sample. Taken together, these findings clearly confirm the local activation of platelets within the human ischemic compartment, as shown by the presence of PLAs.

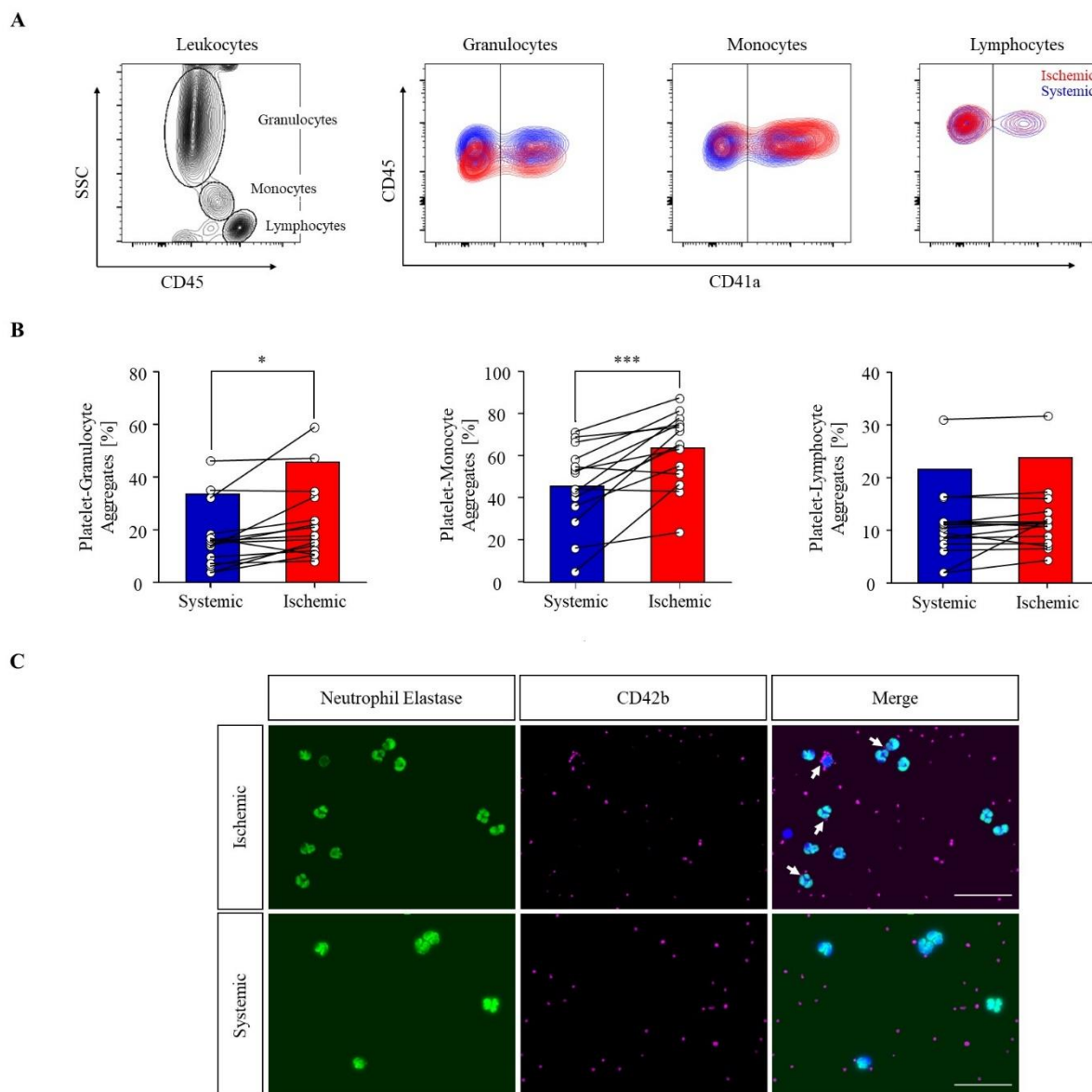


Figure 3-18. Increased platelet-monocyte and platelet-granulocyte aggregates within the occluded cerebral-ischemic vasculature during hyper-acute stroke. (A) Representative gating strategy of flow cytometric analysis to quantify circulating platelet leukocyte aggregates (PLAs) in human hyper-acute stroke patients. (B) Percentual numbers of platelet-granulocyte, platelet-monocyte, and platelet-lymphocyte aggregates within intraindividual systemic (blue) and ischemic (red) blood samples. Data are shown as percentage of the respective leukocyte population. In total 15 patients were evaluated by FACS analysis. Each data point represents one patient. Systemic and ischemic blood samples originating from the same patient are interconnected *via* a line. P-values were calculated by paired Student's t-test and considered statistically significant with * P<0.05; *** P<0.001. (C) Representative blood smear staining of platelet-neutrophil-aggregates (PNAs). Blood smears were stained with neutrophil elastase (neutrophils, green), CD42b (platelets, magenta) and DAPI (cell nuclei, blue). White errors indicate PNAs. Scale bar, 50 μ m.

4 Discussion

IS is one of the most frequent cardiovascular diseases worldwide and accounts for 40% of premature deaths annually [138]. The obstruction of cerebral vessels is not only related to primary brain damage but also accounts for life-long disabilities or the loss of disability-adjusted life years [139, 140]. Rapid restoration of anterograde blood flow is the ultimate aim of acute IS therapy. To date, the standard treatment consists of chemical thrombolysis via alteplase (rt-PA) and/or MT. These therapeutic options, however, are temporarily constrained in their clinical application [141]. Of note, despite recanalization only 26.1 to 36.7% of the treated patients benefit [7]. These modest success rates are mainly attributable to factors like stroke severity at admission, infarct size before therapy and the duration from stroke onset to blood flow restoration [142], reinforcing the need for a detailed understanding of cellular and molecular mechanisms within stroke pathogenesis in order to identify new targetable structures for therapy.

4.1 Secondary microthrombosis is not causative for infarct development

Recanalization of the secluded cerebral vasculature is the mainstay of acute IS treatment and indispensable to salvage the ischemic penumbra. The paradoxical phenomenon of ongoing infarct growth during reperfusion of previously ischemic brain areas, however, is most likely attributable to the detrimental interactions of platelets, immune cells and the endothelium within the process of thrombo-inflammation. Rationales, trying to explain the progression of infarct expansion despite successful recanalization are ample [18, 143]. Among them is the hypothesis that perfusion failure is caused by thrombi or small platelet aggregates distal to the primary occlusion site [41, 144]. Such occlusions are discussed to originate from the initial thrombus as embolic fragments during clot retrieval or are newly formed upon recanalization and dislocate at remote cerebral vascular sites [145-147]. Another report suggests that hypoperfusion itself limits the clearance of present thrombi from the cerebral circulation as the reduced blood flow is insufficient to flush these microvascular thrombi out and thereby contribute to infarct expansion [148]. Previous experimental and clinical studies, however, clearly demonstrated non-beneficial effects of the absence or blockade of platelet aggregation *via* GPIIb/IIIa in the setting of IS. Instead, the prevention of platelet aggregate formation induced severe bleeding

complications that were often fatal [28, 29, 49], indicating that thrombus formation is not causative for infarct expansion after recanalization. Nonetheless, most experimental studies that tried to elucidate the mechanisms underlying infarct expansion, applied tMCAO in mice with an average occlusion time of 1 h followed by 23 h of reperfusion. Recent evidence, though, revealed fully developed infarcts already after 8 h post recanalization [122], indicating that these end-point-analysis (24 h after stroke onset) miss the critical time window causative for infarct progression. Therefore, it is necessary to enquire the first 8 h after recanalization to resolve the mechanisms underlying infarct maturation. By doing so, this thesis could provide evidence that thrombus formation within the ischemic brain occurs after maximal tissue damage and is therefore not causative for successive infarct development [122] (Fig. 3-1), corroborating the findings of GPIIb/IIIa blockade or its genetic deletion. Another line of evidence, supporting the findings of this thesis are post-mortem neuropathological examinations of IS patients that revealed thrombi in the ipsi- as well as the contralateral hemisphere [144]. Accordingly, if the hypothesis of microthrombi causing infarct progression would hold true, this would mean that upon the occurrence of thrombi, infarcts should also be present within the contralateral hemisphere. However, such observations have not been made so far. This leads to the conclusion that these thrombi are rather the consequence and not the cause of perpetuating tissue death. Nonetheless, even if secondary cerebral thrombi after an ischemic insult do not contribute to infarct progression, their presence is undeniable. Considering that the occurrence of secondary thrombi might be largely independent from thrombosis in its original context, but is rather of thrombo-inflammatory nature – neutrophils appeared as promising actors. Just recently, stalling dynamics of neutrophils could be identified as cause of vascular obstructions during reperfusion by imaging cerebral vessels within the ischemic core and penumbra using 2-PM [99]. These obstructions could be prevented by the specific targeting of neutrophils through an anti-Ly6G antibody, which restored vascular perfusion and translated into decreased cellular damage. Furthermore, the interference with NET formation also ameliorated stroke outcome in a murine model of tMCAO [96]. Consequently, neutrophils in form of NETs might act as scaffold to trap circulating platelets and increase hypercoagulability by the activation of the complement system [149], which together might facilitate the formation of cerebral thrombi in the later stages of reperfusion. Despite neutrophil stalling or NET formation, which might contribute to secondary thrombus formation, the activation of neutrophils and the concomitant degranulation of MMP9 could be linked to the modulation and deterioration of the BBB [95].

4.2 Early blood-brain barrier breakdown during reperfusion is associated with the secretion of platelet α -granules

Postischemic BBB disruption is an intensive studied pathophysiological hallmark of IS [150]. Nevertheless, underlying molecular mechanisms and key cellular contributors of this process still remain largely elusive. On a cellular level, the loss of BBB integrity is associated with the extravasation of water and small blood borne molecules into the ischemic brain parenchyma, which is provoked by an increased permeability in trans- and paracellular pathways [151]. This in turn enhances the risk of stroke-related complications like oedema formation and HT, which further aggravate initial ischemic damage [152-154]. However, due to the different peak phases during BBB disruption and their distinct functions, it is essential to consider the timing of these events. In this work, the dynamics of BBB disruption were investigated, combining the surveillance of TEER *in vitro* with the tMCAO model *in vivo*, to gain a better understanding of the temporal sequence underlying this pathomechanism. Histological and biochemical analysis revealed a commencing BBB disruption already after 4 h post reperfusion, indicating that BBB integrity loss occurs early after recanalization (Fig. 3.3). This was further validated by 2-PM analysis of the cerebral vasculature (Fig. 3-2). Setting these findings in the context of time-related infarct development, it becomes apparent that BBB perturbation precedes infarct growth and thus represents a potential mechanism underlying infarct expansion following reperfusion. This is in accordance with previous studies, which attribute BBB loss severity a predictive value on final ischemic lesion size [36, 155, 156].

However, beyond these observations, 2-PM additionally showed the subsequent adherence of platelets at the site of vascular leakage. Hereby, platelets most likely seal vascular breaches to prevent cerebral bleedings and massive extravasation of blood-borne molecules into the ischemic brain parenchyma [80, 81], like they do during leukocyte extravasation [157]. This mechanism might suppress initial vascular integrity loss after recanalization, but seems not to be able to cope with multifocal BBB impairment at later stages of reperfusion [36], explaining the commencing BBB disruption 4 h post reperfusion.

Platelets do not only seal vascular breaches in the setting of IS, but also critically contribute to infarct growth by their tethering/adhesion to the vascular endothelium *via* the platelet receptors GPIb α and GPVI [28]. GPVI-dependent platelet activation, furthermore, induces the release of

platelet granules. Previous studies, demonstrating that the lack of these granules translates into a protection from I/R injury [71, 79, 81], were thus used as point of reference to clarify if this protection might be a consequence of an improved microvascular patency. By measuring the electrical resistance of a simplified *in vitro* BBB model, it could be shown that platelet α -granule content is able to disrupt EC monolayer integrity by the induction of intercellular gaps (Figure 3-6). In line with this, absence of α -granules (*Nbeal2*^{-/-}) did not disrupt BBB integrity (Figure 3-8) and reduced infarct sizes after experimental stroke [79], suggesting a direct correlation of vascular leakage and infarct progression due to platelet derived α -granule components. Unlike the compliant results of platelet α -granules, findings involving dense granules are more complex. Here, the absence of dense granules (*Unc13d*^{-/-}) resulted in a protection of IS within the tMCAO model [71], but did not prevent from barrier disruption within the ipsilateral hemisphere (Figure 3-9). *In vitro* experiments, however, did not reveal any direct effects of platelet dense granules on microvascular endothelial integrity (Figure 3-6). This observation is in line with the fact that mechanisms underlying infarct progression are multifactorial and does not solely include the release of platelet granule content, but also involve the action of immune cells for example. The protection of *Unc13d*^{-/-} mice in the setting of I/R injury, therefore, might be related to the fact that the genetic deficiency of the Munc13-4 gene is not restricted to platelets. Munc13-4 is also present in several hematopoietic cells, like cytotoxic T lymphocytes, natural killer (NK) cells or neutrophils, obeying similar functions in the fusion of cytosolic granules with the plasma membrane as in platelets [158, 159]. Accordingly, Munc13-4-deficiency might also abolish detrimental functions of the above-mentioned immune cells under ischemic conditions and thus prevent ongoing tissue damage. However, to understand the exact mode of action of dense granule content on endothelial barrier function and infarct expansion, more studies are needed.

Following the promising finding of a platelet α -granule mediated EC barrier disruption, it was of great interest to identify the amenable trigger molecule. However, these highly prevalent platelet granules contain over 300 bioactive molecules with versatile functions [72]. Among them are membrane bound integrins, like GPVI, PECAM or α_{IIb} , and soluble molecules that are released into the extracellular space upon degranulation. The latter were focused in this thesis and comprise hemostatic factors (coagulation factors, vWF, fibrinogen), angiogenic factors (VEGF), anti-angiogenic factors (PF4), growth factors (PDGF, bFGF), proteases (MMP9, MMP2), necrotic factors (TNF α) and chemokines (CXCL4, CXCL5, CXCL7, CXCL8, CXCL12). The experiments of this thesis pinpointed the assortment of platelet α -granules to a

proteinaceous component that is responsible for the induction of endothelial barrier loss (Fig. 3-10). Based on observations of previous reports showing that chemokines are nearly instantaneously released upon platelet activation [160] and that elevated quantities of CXCL4 and CXCL12 were found in IS patients [130, 161], further experimental approaches were confined to the functional group of chemokines. However, neither pathological concentrations of CXCL7 nor CXCL12 impacted EC barrier integrity (Figure 3-11). The most likely explanation for these findings might lie in their functions as neutrophil attractants and regulators of leukocyte trafficking under inflammatory conditions. Hence, these chemokines might rather propagate vascular inflammation *via* neutrophils than acting on barrier function themselves. This fact also appears to hold true for the chemokine CXCL4, which is also elevated within the ischemic vasculature of IS patients. Indeed, previous studies demonstrated CXCL7-mediated leukocyte migration to sites of vascular injury [162] and CXCL4-dependent NET formation in anti-neutrophil cytoplasmic antibody (ANCA)-associated vasculitis [163]. Their importance in the setting of IS is further underpinned by logistic regression and random forest analysis using artificial intelligence, which revealed an association of CXCL4 and CXCL7 with cerebral small vessel disease that make up 25% of IS [164]. Another chemokine, selected because of its increased appearance within the cerebrospinal fluid after stroke [165] and its reported function on microvascular permeability [131, 166], was CXCL5. However, a compromising effect on EC integrity could not be validated in the BBB model of this thesis. Since the role of chemokines on BBB integrity might rather be indirect *via* the recruitment and activation of immune cells, another functional group of platelet α -granules was considered – PDGFs (Figure 3-12). This growth factor family comprises four PDGF isoforms PDGF-A, -B, -C, and -D, which only occur as biologically active homo- (PDGF-AA, PDGF-BB, PDGF-CC, PDGF-DD) or heterodimer (PDGF-AB). These dimers act *via* two receptor tyrosine kinases, PDGFR- α and PDGFR- β . Both receptors thereby bind merely distinct PDGF isoforms. While PDGF-A, -B and -C bind to PDGFR- α , PDGF-B and -D bind to PDGFR- β . Regardless of the isoform or receptor, upon ligand binding the receptor subunits dimerize and launch signalling via the phosphorylation of the downstream protein kinases [167, 168]. This in turn lays the foundation of its involvement in BBB function and angiogenesis [72, 169]. The results of this thesis revealed barrier-damaging properties of recombinant PDGF-AB on MBMECs (Figure 3-11), reinforcing the hypothesis of an involvement in BBB function. Since PDGF-AB binds the PDGFR- α , these findings are in line with previous studies, which showed that the inhibition of PDGFR- α prevented from BBB impairment in a mouse model of ICH [170]. A recent study of Grosse and colleagues, moreover, could link peripheral plasma levels of PDGF-AB to MT

treatment success following LVO [171], implying a role of PDGF-AB and/or PDGFR- α in stroke dependent BBB disruption and stroke pathology in general. In contrast to PDGF-AB, barrier-damaging properties were absent in recombinant PDGF-BB treated cell cultures (Figure 3-11). These findings are supported by a study, in which PDGFR- β deficiency in a model of pMCAO translated into severe neurological deficits and brain oedema formation [172]. Together these findings indicate that PDGFR- β and/or PDGF-BB rather preserves vascular integrity. However, since PDGF is not only secreted by platelets but also by ECs, macrophages or pericytes, PDGF-mediated induction of BBB disruption cannot be clearly ascribed to platelets at this time point. Therefore, future experiments are needed to clarify, if the here presented *in vitro* findings can be reproduced in the experimental model of tMCAO using platelet-specific PDGF knock out mice. Furthermore, it is of importance to mention that it is unlikely that platelet-derived PDGF-AB is the sole α -granule derived factor, which induces endothelial integrity loss. This is in accordance with the observation, which showed that neutralization of PDGF in platelet releasate could not completely restore TEER to control levels (Fig. 3-13). Therefore, the process of barrier disruption is rather of multifactorial nature and includes further components of platelet α -granules or even additional cellular sources. Hence, if a therapeutic approach would be considered on the basis of the current data situation, it might be more applicable to generally target platelet α -granule release than inhibiting single factors that do not encompass the whole assortment of barrier-harming components. Nonetheless, the identification of single players within the context of infarct maturation and BBB disruption are of utmost importance to find new targetable structures for future treatments.

Even though several contributors of BBB disruption could already be identified, it is still incompletely understood how they temporally and mechanistically integrate into the pathogenesis of IS. Hence, this thesis aimed to disclose mechanistic principles underlying α -granule-mediated barrier perturbation. First, calcium, a crucial, ubiquitous second messenger involved in a variety of signalling cascades [132], was investigated due to the well-known disruption of calcium homeostasis during acute IS [173, 174]. Besides the failure of $\text{Na}^+/\text{Ca}^{2+}$ pumps, which is linked to neuronal cell death, the release of inflammatory mediators, such as thrombin, serotonin, bradykinin, prostaglandins, or PDGF, was identified to trigger receptor-mediated calcium signaling in ECs and affect endothelial barrier permeability [133, 175]. To assess whether the latter process might also be induced by platelets, the effect of platelet-

derived factors on EC barrier function was determined. Indeed, WT platelet releasate increased intracellular calcium concentrations in ECs within seconds after treatment, demonstrating that a rise in endothelial Ca^{2+} can be induced by platelet granule components and thus might contribute to barrier disruption (Figure 3-14). However, when it comes to the question how calcium flux alters BBB functions and which downstream signaling transduction pathways are involved, one has to differentiate between rapid and slow events. Slow events involve changes in gene expression [133, 176], which can be modulated by mitogen-activated protein kinases like ERK1/2 or protein kinase C [177, 178]. Just recently, a study interrelated these findings in the setting of IS by demonstrating that the overexpression of ERK2 exacerbated tissue damage and induced BBB disruption following tMCAO [179]. These findings along with the data of this thesis, which show a phosphorylation of ERK after 4 h of reperfusion, therefore suggest that the induction of the Ras-Raf-MEK-ERK transduction pathway is pestilent during IS and might possibly be induced by increased intracellular Ca^{2+} levels. On the contrary, the calcium-dependent disassembly of the AJ protein VE-cadherin is categorized as a rapid event, since calcium seem to modulate the existing proteins rather than regulate gene transcription of VE-cadherin [180, 181]. Nonetheless, investigations within the early phase after tMCAO showed only minimal modifications in TJ morphology, which changed after 48-58 h post stroke, whereupon ultrastructural alterations in form of junctional protrusions became visible [151]. These deviations from the typical linear, continuous morphology of TJs, however, are most likely independent of rapid calcium signalling, but might rather be the consequence of slow events following calcium signalling, since these alterations occur at an advanced time point. In accordance with these findings are the data of this thesis, showing no alterations in TJ and AJ protein content in ECs after treatment with platelet releasate (Figure 3-7). Thus, early BBB disruption most likely involves alternate pathways that are independent of TJs and AJs alterations. One of such pathways may include a group of versatile endopeptidases, that is able to modulate or even degrade components of the extracellular matrix - MMPs [182]. As shown in the data depicted here, MMP9 activity could be assigned to the early reperfusion phase after tMCAO and thus strongly suggest an interrelation with the breakdown of the BBB (Figure 3-3, Figure 3-4). Nonetheless, uncertainties remain about the cellular source of MMPs. However, following the recent idea of a neutrophil-dominated intravascular immune response during LVO and considering neutrophils as a cellular source of MMP9, it is tempting to assume neutrophil-derived MMP9 as an effector molecule of BBB breakdown and infarct growth [25, 92]. This assumption is further supported by several clinical and experimental studies, and therefore appears to be a promising target for future treatment strategies [183-186].

The participation of immune cells in the pathology of IS and especially following reperfusion is well established [83]. Now, experimental data could show that the blockade of both platelet-specific receptors, GPIb α and GPVI, efficiently retarded primary infarct growth already under occlusion and additionally decelerated immune cell infiltration into the ischemic brain [12, 56]. These findings suggest (I) that platelets somehow influence immune cells during tissue damage in the setting of IS and (II) that thrombo-inflammatory processes not only drive infarct expansion during I/R injury, but also account for progressive tissue death under occlusion (penumbral tissue loss). Apart from this knowledge, only rudimental understanding exists about the molecular interactions and mechanistic consequences of these cellular co-operations. Since recent research revealed that immune cells have to be activated to exacerbate BBB disruption and that platelet releasate promoted migratory behaviour [107, 187], this part of the thesis determined the impact of platelet granule cargo on lymphocytes within a Boyden chamber approach. Of note, platelet releasate did not stimulate transmigratory behaviour of lymphocytes over an EC monolayer, but instead increased the abundance of CD3⁺ lymphocytes within the endothelium (Figure 3-15), indicating a platelet-dependent detrimental crosstalk of immune cells with the endothelium rather than a damaging transmigration into the brain parenchyma. This is in line with clinical studies showing that the depletion of lymphocytes from the blood stream (FTY720) was protective in the setting of IS, while the inhibition of lymphocyte transmigration (natalizumab) did not alter stroke outcome [112-114]. Together, with the findings of an α -granule dependent impairment of the endothelium (Figure 3-6) and an immediate immune response under occlusion, these results emphasize that IS pathology is of multifactorial nature, however, the underlying mechanisms seem to act from an intravascular perspective, rather than from the brain parenchyma [16, 25, 130]. Nonetheless, further studies are required to resolve deeper, mechanistically insights into the platelet granule dependent modulation of immune cells and their contribution to the pathomechanisms underlying IS.

4.3 Local immune cell invasion and formation of platelet-leukocyte aggregates during occlusion in human hyper-acute stroke

Animal models are essential tools for the investigation of molecular and cellular mechanisms in response to cerebral ischemia. However, the acquired knowledge cannot be directly extrapolated to the human system. This is, on the one hand, based on the fact that the murine and human immune system substantially differ in their composition [188]. On the other hand, mice are more susceptible to hypoxia and represent a time lapse of the human situation. This reinforces the need for investigations within the human system. But so far, human studies were restricted to remote sites from acute cerebral ischemia, which include investigations of peripheral blood samples or the cerebrospinal fluid. The advent of MT combined with a novel method of local cerebral blood aspiration, however, opened up new possibilities to investigate cellular and molecular responses directly within the secluded vasculature of IS patients. Making use of this method, it was possible to reveal an immediate intravascular immune response distal to the occluding thrombus [25, 91, 120, 189]. Immune phenotyping, furthermore, identified granulocytes as the dominant leukocyte population and disclosed a yet unknown shift within the lymphocyte population towards CD4⁺ T cells [120] (Fig. 3-17). However, at present uncertainties exist how leukocytes infiltrate the occluded vascular compartment, since these immune cells do not reside within this vascular bed under physiologic conditions [16, 190]. The finding of Essig *et al.*, who showed that rt-PA entered the occluded MCA territory in equal concentrations as intravenously administered, only recently indicated a possible infiltration route through collateral anastomoses [92]. These findings together with the locally enriched plasma concentrations of the potent neutrophil attractant CXCL7 (NAP-2) within the ischemic compartment [130], which is almost exclusively released from platelet α -granules upon platelet activation [191, 192], suggest that this platelet component might guide leukocytes/neutrophils to the site of vascular occlusion. Additionally, increased concentrations of the neutrophil-activating chemokine CXCL4 and the danger associated molecular pattern (DAMP) high-mobility-group box protein 1 (HMGB1) were found in IS patients under occlusion, further emphasizing the concept of an immediate activation of the infiltrated neutrophils within the secluded vasculature by platelet released α -granule content [130, 193]. This in turn might lead to the release of MMP9 and MPO from infiltrating neutrophils, which either ensure the disruption of the BBB or induce the formation of detrimental NETs [194, 195] (Figure 4-1). Together these findings suggest a relation between early platelet activation and neutrophil responses within the ischemic compartment during hyper-acute stroke.

With regard to lymphocytes, experimental studies in mice provide compelling evidence that lymphocytes and especially CD4⁺ T cells are involved in the process of infarct development [12, 104]. These findings were proven to hold true in the human system, since a pilot trial with 22 IS patients could show that oral application of the immunosuppressive fingolimod decreased microvascular permeability and limited secondary tissue damage [113]. Thus, overrepresentation of CD4⁺ T cells within the secluded vasculature during hyper-acute stroke might modulate microvascular permeability and therefore contribute to infarct development in humans. Moreover, a study of Li *et al.* provided evidence for systemic alterations of CD4⁺ T_{reg} cells in patients with acute IS, which correlated with infarct volume and neurological outcome. Consequently, CD4⁺ T_{reg} cells were suggested as biomarker for stroke outcome [196]. However, it remains to be determined how systemic and intracerebral T cell responses interrelate.

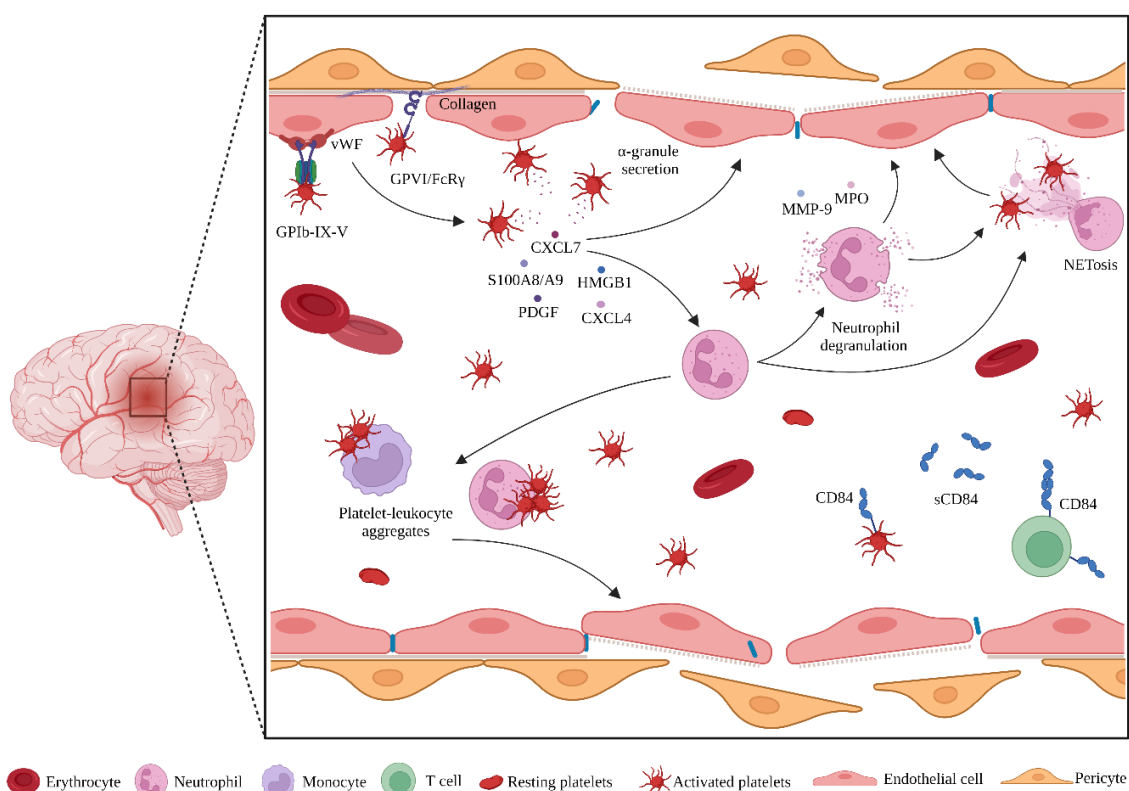


Figure 4-1. Schematic overview of human and experimental stroke data and their implication in blood-brain barrier breakdown. During cerebral ischemia, platelets adhere to the preactivated endothelium via GPIb-IX-V complex binding to vWF and GPVI/FcR γ binding to collagen. GPVI engagement thereby induces platelet activation, which results in the release of platelet granules. This in turn, enforces a local enrichment of platelet α -granule derived CXCL7, CXCL4, HMGB1, PDGF and S100A8/A9. The potent neutrophil chemoattractant CXCL7 then launches an immediate intravascular immune response dominated by neutrophils and CD4⁺ T cells. Adopted from Stoll *et al.* [16] under the terms of the Creative Common Attribution License.

As mentioned before, it could already be shown that platelets interact with immune cells to aggravate cerebral brain damage following IS. During these interactions, platelets seem to actively modulate immune cells in a direct and/or indirect way [107, 137] (Figure 4-1). Indirect engagement is mediated *via* platelet released cargo (see above) or the homophilic cell adhesion molecule CD84, which is highly abundant on various immune cell populations and platelets [107, 197, 198]. Soluble (s)CD84, which is shed from the platelet surface upon activation, thereby interacts with CD84 on the surface of CD4⁺ T cells and promotes their migratory ability. Since CD84-deficiency on each of these cell types protected from I/R injury, these findings suggest that platelets and immune cells interact within the ischemic brain and aggravate brain damage through CD84. This assumption was further validated within the human system by showing that reduced CD84 levels on platelets were independently associated with poor outcome in patients suffering from IS [107].

Direct engagement of immune cells through platelets, on the contrary, include receptor-receptor or receptor-integrin interactions [137, 199]. Receptors/integrins most commonly involved in these interactions are platelet P-selectin, GPIb, $\alpha_{IIb}\beta_3$, and CD40L, as well as leukocyte PSGL-1, $\alpha_M\beta_2$ and CD40 [199-202]. Several studies could already associate such interactions between platelets and leukocytes, referred to as PLAs, to a variety of thrombo-inflammatory diseases [203, 204]. However, this thesis provides first-time evidence for the increased appearance of PLAs within the occluded vasculature during human hyper-acute stroke (Fig. 3-18). These findings are in accordance with the study of Marquardt *et al.*, who found increased platelet-granulocyte aggregates and platelet-monocyte aggregates in the systemic blood of IS patients, while platelet-lymphocyte aggregate formation was unaltered [205]. However, apart from the assumed predictive value of PLAs for platelet activation, less is known about their mechanistic contribution to IS pathogenesis. Nonetheless, there are indications that the interplay between platelets and leukocytes increases the recruitment and activation of both cell types, thus, fostering inflammation and accelerating tissue damage [206]. This notion is at least indirectly supported by an experimental model of transient focal ischemia, in which the deficiency of two receptors that are critical for PLA formation (CD40, CD40L), diminished leukocyte as well as platelet recruitment to cerebral venules and concomitantly reduced vascular leakage and infarct sizes [207]. The relative importance of CD40L within a clinical setting was likewise shown by correlating the increased appearance of this platelet surface receptor with a worse clinical outcome [208]. Together, these results strongly argue for a PLA-modulated inflammation,

which contributes to perpetuating tissue damage. Therefore, the interference with platelet-leukocyte interactions appears as a potential attractive target for future treatment strategies.

4.4 Concluding remarks and future perspectives

This thesis provides new insights into thrombo-inflammatory processes under occlusive conditions in human IS patients and early murine reperfusion. It was shown that platelet-mediated BBB disruption but not secondary thrombus formation is causative for infarct expansion during ischemia reperfusion. However, when considering the *in vitro* results that addressed the role of platelets in BBB breakdown, one has to take into account that these investigations exclusively focused on ECs. This cell type does certainly not reflect the acutal multicellular structure of the BBB. Therefore, additional experiments are needed to validate the impact of platelet α -granules in a more complex BBB model, consisting of pericytes, astrocytes, and ECs. Furthermore, this thesis provided first mechanistically insights into BBB disrupting processes. However, detailed molecular investigations of how platelets and/or platelet-derived components induce endothelial damage remain to be determined. To this end, the assessment of additional outcome parameters, like the formation of ROS or Ca^{2+} signalling in response to platelet-EC and/or immune cell-EC interactions, might help to unravel some of these processes. Another issue that has not received adequate attention within the *in vitro* experiments presented here, is the imitation of LVO by a pre-injured endothelium due to tissue hypoxia. Future studies determining platelet granule-dependent effects on ECs under occlusive and ‘real’ reperfusion conditions should therefore include shear flow and a former deprivation of oxygen and glucose. This experimental approach might help to identify additional hypoxia-driven effects on the endothelium. First preliminary results addressing this issue revealed that platelet releasate maintains endothelial integrity under hypoxic/aglycemic conditions, contrasting the results generated under normoxic/glycemic conditions (Figure 4-2). These findings, however, clearly demonstrate a context dependent modulation of ECs and a barrier preserving effect of platelet-derived components under hypoxia and glucose deprivation. To elucidate further differences between these two conditions, proteome analysis of ECs after exposure to hypoxic/aglycemic

or normoxic/glycemic conditions and platelet releasate treatment could provide further insights into pathomechanisms underlying IS. In addition, the translation and validation of the murine results in a human *in vitro* BBB model would reinforce their clinical relevance and would provide an appropriate screening tool of potential pharmacological drugs.

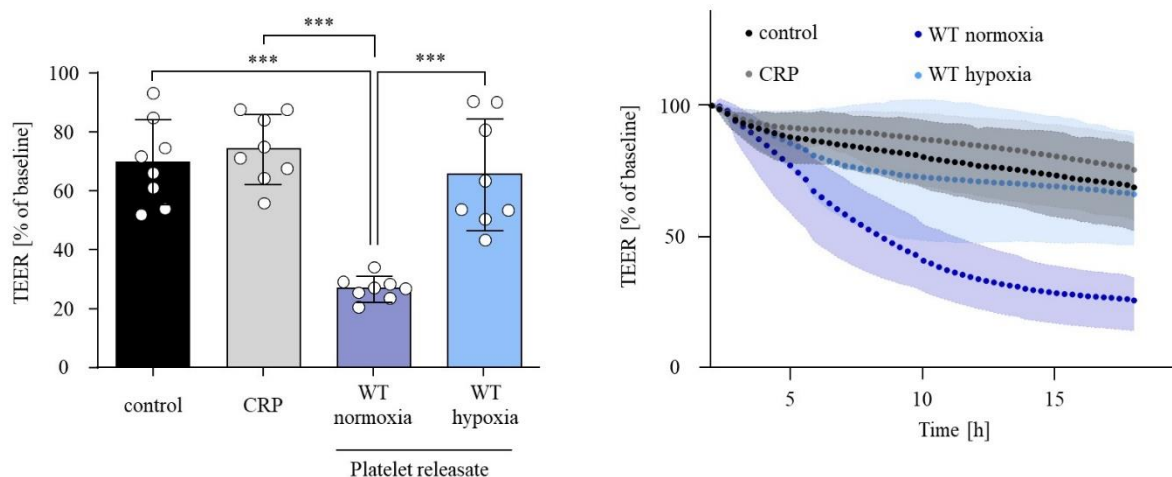


Figure 4-2. Platelet releasate from wild-type mice conducts different physiological effects on endothelial cells under normoxic or hypoxic conditions. Transendothelial electrical resistance (TEER) of primary mouse brain microvascular endothelial cell (MBMEC) monolayers after 18 h of treatment and simultaneous recording. TEER values of MBMEC monolayers treated with platelet releasate of wild-type (WT) mice and simultaneous incubation under normoxic/glycemic (5 % CO₂, 95 % humidity, 21 % O₂, 37 °C, 2 g/l glucose; WT normoxia) or hypoxic/aglycemic conditions (5 % CO₂, 95 % humidity, 1 % O₂, 37°C, 0 g/l glucose; WT hypoxia). Controls were treated with culture medium. Collagen related peptide (CRP) was used in a concentration of 10 µg/ml in Tyrode's buffer with Ca²⁺ and served as control to exclude side effects of the stimulant on MBMEC, as it was used to generate platelet releasate. Data are shown as mean ± SD. Each data point represents one transwell insert. Data was collected within 4 independent experiments. P-values were calculated by Ordinary one-way ANOVA followed by a Tukey's multiple comparison post-hoc test and considered statistically significant with *** P<0.001 (left panel). Trajectory course of TEER after treatment. Data are shown as mean ± upper/lower limit. Each data point represents the mean of 8 transwell inserts at a distinct time point during measurement. TEER was measured every 10 min for at least 18 h post-treatment. Data was collected within 4 independent experiments. Shown is the percentual change of TEER to baseline (100%) (right panel).

Built upon the hypothesis of an intertwined continuum between inflammatory and thrombotic events already during occlusion and thereafter [56, 57], *in vivo* imaging under occlusive conditions might help to unravel spatio-temporal dynamics between platelets, immune cells and the endothelium that possibly harbour information about the underlying mechanism of infarct expansion. The here presented experimental studies were furthermore complemented by studies

in hyper-acute stroke patients that underwent MT. These investigations could corroborate previous findings of an immediate intravascular immune response and revealed increased numbers of PLAs within the secluded vasculature. Based on the fact that neutrophils were among the predominating immune cells under cerebral occlusion and that investigations in the setting of myocardial infarction revealed a high neutrophil heterogeneity, research efforts within the human system should pursue to assess neutrophil heterogeneity and its functional relevance on penumbral tissue.

5 References

1. Organization, W.S. *World Stroke Organization Annual Report 2021*. 2021.
2. Global Burden of Disease Study, C., *Global, regional, and national incidence, prevalence, and years lived with disability for 301 acute and chronic diseases and injuries in 188 countries, 1990-2013: a systematic analysis for the Global Burden of Disease Study 2013*. *Lancet*, 2015. **386**(9995): p. 743-800.
3. Powers, W.J., et al., *2015 American Heart Association/American Stroke Association Focused Update of the 2013 Guidelines for the Early Management of Patients With Acute Ischemic Stroke Regarding Endovascular Treatment: A Guideline for Healthcare Professionals From the American Heart Association/American Stroke Association*. *Stroke*, 2015. **46**(10): p. 3020-35.
4. Goyal, M., et al., *Endovascular thrombectomy after large-vessel ischaemic stroke: a meta-analysis of individual patient data from five randomised trials*. *Lancet*, 2016. **387**(10029): p. 1723-31.
5. Stoll, G. and M. Pham, *Beyond recanalization - a call for action in acute stroke*. *Nat Rev Neurol*, 2020. **16**(11): p. 591-592.
6. Neurologie, D.G.f. *Leitlinie: Akuttherapie des ischämischen Schlaganfalls*. 2021.
7. Mueller-Kronast, N.H., et al., *Systematic Evaluation of Patients Treated With Neurothrombectomy Devices for Acute Ischemic Stroke: Primary Results of the STRATIS Registry*. *Stroke*, 2017. **48**(10): p. 2760-2768.
8. Campbell, B.C.V., et al., *Ischaemic stroke*. *Nat Rev Dis Primers*, 2019. **5**(1): p. 70.
9. Endres, M., U. Dirnagl, and M.A. Moskowitz, *The ischemic cascade and mediators of ischemic injury*. *Handb Clin Neurol*, 2009. **92**: p. 31-41.
10. Hammer, M.D., et al., *Safety and feasibility of NeuroFlo use in eight- to 24-hour ischemic stroke patients*. *Int J Stroke*, 2012. **7**(8): p. 655-61.
11. Goyal, M., et al., *Randomized assessment of rapid endovascular treatment of ischemic stroke*. *N Engl J Med*, 2015. **372**(11): p. 1019-30.
12. Schuhmann, M.K., et al., *Platelets and lymphocytes drive progressive penumbral tissue loss during middle cerebral artery occlusion in mice*. *J Neuroinflammation*, 2021. **18**(1): p. 46.
13. Sobesky, J., et al., *Which time-to-peak threshold best identifies penumbral flow? A comparison of perfusion-weighted magnetic resonance imaging and positron emission tomography in acute ischemic stroke*. *Stroke*, 2004. **35**(12): p. 2843-7.
14. Baron, J.C., *Mapping the ischaemic penumbra with PET: implications for acute stroke treatment*. *Cerebrovasc Dis*, 1999. **9**(4): p. 193-201.
15. Nour, M., F. Scalzo, and D.S. Liebeskind, *Ischemia-reperfusion injury in stroke*. *Interv Neurol*, 2013. **1**(3-4): p. 185-99.
16. Stoll, G., et al., *An intravascular perspective on hyper-acute neutrophil, T-cell and platelet responses: Similarities between human and experimental stroke*. *J Cereb Blood Flow Metab*, 2022. **42**(9): p. 1561-1567.
17. Campbell, B.C., et al., *Failure of collateral blood flow is associated with infarct growth in ischemic stroke*. *J Cereb Blood Flow Metab*, 2013. **33**(8): p. 1168-72.
18. Amki, M.E. and S. Wegener, *Reperfusion failure despite recanalization in stroke: New translational evidence*. *Clinical and Translational Neuroscience*, 2021. **5**(1): p. 2514183X211007137.
19. Ter Schiphorst, A., et al., *Tissue no-reflow despite full recanalization following thrombectomy for anterior circulation stroke with proximal occlusion: A clinical study*. *J Cereb Blood Flow Metab*, 2021. **41**(2): p. 253-266.

20. Cherian, P., et al., *Endothelial and platelet activation in acute ischemic stroke and its etiological subtypes*. Stroke, 2003. **34**(9): p. 2132-7.
21. Iadecola, C., M.S. Buckwalter, and J. Anrather, *Immune responses to stroke: mechanisms, modulation, and therapeutic potential*. J Clin Invest, 2020. **130**(6): p. 2777-2788.
22. Jung, S., et al., *Factors that determine penumbral tissue loss in acute ischaemic stroke*. Brain, 2013. **136**(Pt 12): p. 3554-60.
23. Bai, J. and P.D. Lyden, *Revisiting cerebral postischemic reperfusion injury: new insights in understanding reperfusion failure, hemorrhage, and edema*. Int J Stroke, 2015. **10**(2): p. 143-52.
24. Stoll, G. and B. Nieswandt, *Thrombo-inflammation in acute ischaemic stroke - implications for treatment*. Nat Rev Neurol, 2019. **15**(8): p. 473-481.
25. Kollikowski, A.M., et al., *Local Leukocyte Invasion during Hyperacute Human Ischemic Stroke*. Ann Neurol, 2020. **87**(3): p. 466-479.
26. Fluri, F., M.K. Schuhmann, and C. Kleinschnitz, *Animal models of ischemic stroke and their application in clinical research*. Drug Des Devel Ther, 2015. **9**: p. 3445-54.
27. Braeuninger, S., Kleinschnitz, C., Nieswandt, B., Stoll, G., *Focal cerebral ischemia*, in *Methods Mol. Biol.* 2012. p. 29-42.
28. Kleinschnitz, C., et al., *Targeting platelets in acute experimental stroke: impact of glycoprotein Ib, VI, and IIb/IIIa blockade on infarct size, functional outcome, and intracranial bleeding*. Circulation, 2007. **115**(17): p. 2323-30.
29. Adams, H.P., Jr., et al., *Emergency administration of abciximab for treatment of patients with acute ischemic stroke: results of an international phase III trial: Abciximab in Emergency Treatment of Stroke Trial (AbESTT-II)*. Stroke, 2008. **39**(1): p. 87-99.
30. Liebner, S., et al., *Functional morphology of the blood-brain barrier in health and disease*. Acta Neuropathol, 2018. **135**(3): p. 311-336.
31. Butt, A.M., H.C. Jones, and N.J. Abbott, *Electrical resistance across the blood-brain barrier in anaesthetized rats: a developmental study*. J Physiol, 1990. **429**: p. 47-62.
32. Castro Dias, M., et al., *Structure and Junctional Complexes of Endothelial, Epithelial and Glial Brain Barriers*. Int J Mol Sci, 2019. **20**(21).
33. Oldendorf, W.H. and W.J. Brown, *Greater number of capillary endothelial cell mitochondria in brain than in muscle*. Proc Soc Exp Biol Med, 1975. **149**(3): p. 736-8.
34. Muoio, V., P.B. Persson, and M.M. Sendeski, *The neurovascular unit - concept review*. Acta Physiol (Oxf), 2014. **210**(4): p. 790-8.
35. Sweeney, M.D., A.P. Sagare, and B.V. Zlokovic, *Cerebrospinal fluid biomarkers of neurovascular dysfunction in mild dementia and Alzheimer's disease*. J Cereb Blood Flow Metab, 2015. **35**(7): p. 1055-68.
36. Hoffmann, A., et al., *Early Blood-Brain Barrier Disruption in Ischemic Stroke Initiates Multifocally Around Capillaries/Venules*. Stroke, 2018. **49**(6): p. 1479-1487.
37. Bernardo-Castro, S., et al., *Pathophysiology of Blood-Brain Barrier Permeability Throughout the Different Stages of Ischemic Stroke and Its Implication on Hemorrhagic Transformation and Recovery*. Front Neurol, 2020. **11**: p. 594672.
38. Merali, Z., et al., *Evolution of blood-brain-barrier permeability after acute ischemic stroke*. PLoS One, 2017. **12**(2): p. e0171558.
39. Shi, Y., et al., *Rapid endothelial cytoskeletal reorganization enables early blood-brain barrier disruption and long-term ischaemic reperfusion brain injury*. Nat Commun, 2016. **7**: p. 10523.
40. Hong, J.M., D.S. Kim, and M. Kim, *Hemorrhagic Transformation After Ischemic Stroke: Mechanisms and Management*. Front Neurol, 2021. **12**: p. 703258.
41. Garcia, J.H., et al., *Influx of leukocytes and platelets in an evolving brain infarct (Wistar rat)*. Am J Pathol, 1994. **144**(1): p. 188-99.

42. Obrenovitch, T.P. and J.M. Hallenbeck, *Platelet accumulation in regions of low blood flow during the postischemic period*. Stroke, 1985. **16**(2): p. 224-34.
43. Stoll, G., et al., *An intravascular perspective on hyper-acute neutrophil, T-cell and platelet responses: Similarities between human and experimental stroke*. J Cereb Blood Flow Metab, 2022: p. 271678X221105764.
44. Giles, J.A., et al., *Neutrophil infiltration to the brain is platelet-dependent, and is reversed by blockade of platelet GPIIb/IIIa*. Immunology, 2018. **154**(2): p. 322-328.
45. Berndt, M.C., et al., *The vascular biology of the glycoprotein Ib-IX-V complex*. Thromb Haemost, 2001. **86**(1): p. 178-88.
46. Nieswandt, B., I. Pleines, and M. Bender, *Platelet adhesion and activation mechanisms in arterial thrombosis and ischaemic stroke*. J Thromb Haemost, 2011. **9 Suppl 1**: p. 92-104.
47. Pham, M., et al., *Sustained reperfusion after blockade of glycoprotein-receptor-Ib in focal cerebral ischemia: an MRI study at 17.6 Tesla*. PLoS One, 2011. **6**(4): p. e18386.
48. Schuhmann, M.K., et al., *Blocking of platelet glycoprotein receptor Ib reduces "thrombo-inflammation" in mice with acute ischemic stroke*. J Neuroinflammation, 2017. **14**(1): p. 18.
49. Kraft, P., et al., *Efficacy and Safety of Platelet Glycoprotein Receptor Blockade in Aged and Comorbid Mice With Acute Experimental Stroke*. Stroke, 2015. **46**(12): p. 3502-6.
50. De Meyer, S.F., et al., *Binding of von Willebrand factor to collagen and glycoprotein Iba1, but not to glycoprotein IIb/IIIa, contributes to ischemic stroke in mice--brief report*. Arterioscler Thromb Vasc Biol, 2010. **30**(10): p. 1949-51.
51. De Meyer, S.F., et al., *Platelet glycoprotein Iba1 is an important mediator of ischemic stroke in mice*. Exp Transl Stroke Med, 2011. **3**: p. 9.
52. Kleinschnitz, C., et al., *Deficiency of von Willebrand factor protects mice from ischemic stroke*. Blood, 2009. **113**(15): p. 3600-3.
53. Rayes, J., S.P. Watson, and B. Nieswandt, *Functional significance of the platelet immune receptors GPVI and CLEC-2*. J Clin Invest, 2019. **129**(1): p. 12-23.
54. Stegner, D. and B. Nieswandt, *Platelet receptor signaling in thrombus formation*. J Mol Med (Berl), 2011. **89**(2): p. 109-21.
55. Goebel, S., et al., *The GPVI-Fc fusion protein Revacept improves cerebral infarct volume and functional outcome in stroke*. PLoS One, 2013. **8**(7): p. e66960.
56. Bieber, M., et al., *Targeting platelet glycoprotein VI attenuates progressive ischemic brain damage before recanalization during middle cerebral artery occlusion in mice*. Exp Neurol, 2021. **344**: p. 113804.
57. Schuhmann, M.K., et al., *Targeting Platelet GPVI Plus rt-PA Administration but Not alpha2beta1-Mediated Collagen Binding Protects against Ischemic Brain Damage in Mice*. Int J Mol Sci, 2019. **20**(8).
58. Cherpokova, D., et al., *SLAP/SLAP2 prevent excessive platelet (hem)ITAM signaling in thrombosis and ischemic stroke in mice*. Blood, 2015. **125**(1): p. 185-94.
59. Bigalke, B., et al., *Expression of platelet glycoprotein VI is associated with transient ischemic attack and stroke*. Eur J Neurol, 2010. **17**(1): p. 111-7.
60. Ungerer, M., et al., *Novel antiplatelet drug revacept (Dimeric Glycoprotein VI-Fc) specifically and efficiently inhibited collagen-induced platelet aggregation without affecting general hemostasis in humans*. Circulation, 2011. **123**(17): p. 1891-9.
61. Groschel, K., et al., *Revacept, an Inhibitor of Platelet Adhesion in Symptomatic Carotid Artery Stenosis: Design and Rationale of a Randomized Phase II Clinical Trial*. TH Open, 2020. **4**(4): p. e393-e399.
62. Uphaus, T., et al., *Revacept, an Inhibitor of Platelet Adhesion in Symptomatic Carotid Stenosis: A Multicenter Randomized Phase II Trial*. Stroke, 2022: p. STROKEAHA121037006.
63. Stegner, D., V. Klaus, and B. Nieswandt, *Platelets as Modulators of Cerebral Ischemia/Reperfusion Injury*. Front Immunol, 2019. **10**: p. 2505.

-
64. Golebiewska, E.M. and A.W. Poole, *Platelet secretion: From haemostasis to wound healing and beyond*. *Blood Rev*, 2015. **29**(3): p. 153-62.
 65. Rendu, F. and B. Brohard-Bohn, *The platelet release reaction: granules' constituents, secretion and functions*. *Platelets*, 2001. **12**(5): p. 261-73.
 66. Linden, M.D., *Platelet flow cytometry*. *Methods Mol Biol*, 2013. **992**: p. 241-62.
 67. Gerrard, J.M., G.H. Rao, and J.G. White, *The influence of reserpine and ethylenediaminetetraacetic acid (EDTA) on serotonin storage organelles of blood platelets*. *Am J Pathol*, 1977. **87**(3): p. 633-46.
 68. Chicka, M.C., et al., *Role of Munc13-4 as a Ca²⁺-dependent tether during platelet secretion*. *Biochem J*, 2016. **473**(5): p. 627-39.
 69. Ren, Q., et al., *Munc13-4 is a limiting factor in the pathway required for platelet granule release and hemostasis*. *Blood*, 2010. **116**(6): p. 869-77.
 70. Savage, J.S., et al., *Munc13-4 is critical for thrombosis through regulating release of ADP from platelets*. *J Thromb Haemost*, 2013. **11**(4): p. 771-5.
 71. Stegner, D., et al., *Munc13-4-mediated secretion is essential for infarct progression but not intracranial hemostasis in acute stroke*. *J Thromb Haemost*, 2013. **11**(7): p. 1430-3.
 72. Blair, P. and R. Flaumenhaft, *Platelet alpha-granules: basic biology and clinical correlates*. *Blood Rev*, 2009. **23**(4): p. 177-89.
 73. Harrison, P., et al., *Uptake of plasma fibrinogen into the alpha granules of human megakaryocytes and platelets*. *J Clin Invest*, 1989. **84**(4): p. 1320-4.
 74. Noetzli, L.J. and J.E. Italiano, Jr., *Unlocking the Molecular Secrete(s) of alpha-Granule Biogenesis*. *Arterioscler Thromb Vasc Biol*, 2018. **38**(11): p. 2539-2541.
 75. Lo, R.W., et al., *NBEAL2 (Neurobeachin-Like 2) Is Required for Retention of Cargo Proteins by alpha-Granules During Their Production by Megakaryocytes*. *Arterioscler Thromb Vasc Biol*, 2018. **38**(10): p. 2435-2447.
 76. Gunay-Aygun, M., et al., *Gray platelet syndrome: natural history of a large patient cohort and locus assignment to chromosome 3p*. *Blood*, 2010. **116**(23): p. 4990-5001.
 77. Gunay-Aygun, M., et al., *NBEAL2 is mutated in gray platelet syndrome and is required for biogenesis of platelet alpha-granules*. *Nat Genet*, 2011. **43**(8): p. 732-4.
 78. Deppermann, C., et al., *The Nbeal2(-/-) mouse as a model for the gray platelet syndrome*. *Rare Dis*, 2013. **1**: p. e26561.
 79. Deppermann, C., et al., *Gray platelet syndrome and defective thrombo-inflammation in Nbeal2-deficient mice*. *J Clin Invest*, 2013.
 80. Morowski, M., et al., *Only severe thrombocytopenia results in bleeding and defective thrombus formation in mice*. *Blood*, 2013. **121**(24): p. 4938-47.
 81. Deppermann, C., et al., *Platelet secretion is crucial to prevent bleeding in the ischemic brain but not in the inflamed skin or lung in mice*. *Blood*, 2017. **129**(12): p. 1702-1706.
 82. Shattil, S.J., C. Kim, and M.H. Ginsberg, *The final steps of integrin activation: the end game*. *Nat Rev Mol Cell Biol*, 2010. **11**(4): p. 288-300.
 83. Beuker, C., et al., *Immune Cell Infiltration into the Brain After Ischemic Stroke in Humans Compared to Mice and Rats: a Systematic Review and Meta-Analysis*. *Transl Stroke Res*, 2021. **12**(6): p. 976-990.
 84. Shichita, T., et al., *Pivotal role of cerebral interleukin-17-producing gammadeltaT cells in the delayed phase of ischemic brain injury*. *Nat Med*, 2009. **15**(8): p. 946-50.
 85. Stoll, G., C. Kleinschnitz, and B. Nieswandt, *Combating innate inflammation: a new paradigm for acute treatment of stroke?* *Ann N Y Acad Sci*, 2010. **1207**: p. 149-54.
 86. Mestas, J. and C.C. Hughes, *Of mice and not men: differences between mouse and human immunology*. *J Immunol*, 2004. **172**(5): p. 2731-8.
-

87. Kim, J., et al., *Different prognostic value of white blood cell subtypes in patients with acute cerebral infarction*. *Atherosclerosis*, 2012. **222**(2): p. 464-7.
88. Buck, B.H., et al., *Early neutrophilia is associated with volume of ischemic tissue in acute stroke*. *Stroke*, 2008. **39**(2): p. 355-60.
89. Jickling, G.C., et al., *Targeting neutrophils in ischemic stroke: translational insights from experimental studies*. *J Cereb Blood Flow Metab*, 2015. **35**(6): p. 888-901.
90. Kumar, A.D., et al., *Leukocytosis in patients with neurologic deterioration after acute ischemic stroke is associated with poor outcomes*. *J Stroke Cerebrovasc Dis*, 2013. **22**(7): p. e111-7.
91. Strinitz, M., et al., *Immune Cells Invade the Collateral Circulation during Human Stroke: Prospective Replication and Extension*. *Int J Mol Sci*, 2021. **22**(17).
92. Essig, F., et al., *Local Cerebral Recombinant Tissue Plasminogen Activator Concentrations During Acute Stroke*. *JAMA Neurol*, 2021. **78**(5): p. 615-617.
93. Enzmann, G., et al., *The neurovascular unit as a selective barrier to polymorphonuclear granulocyte (PMN) infiltration into the brain after ischemic injury*. *Acta Neuropathol*, 2013. **125**(3): p. 395-412.
94. Metzler, K.D., et al., *Myeloperoxidase is required for neutrophil extracellular trap formation: implications for innate immunity*. *Blood*, 2011. **117**(3): p. 953-9.
95. Turner, R.J. and F.R. Sharp, *Implications of MMP9 for Blood Brain Barrier Disruption and Hemorrhagic Transformation Following Ischemic Stroke*. *Front Cell Neurosci*, 2016. **10**: p. 56.
96. Denorme, F., et al., *Neutrophil extracellular traps regulate ischemic stroke brain injury*. *J Clin Invest*, 2022. **132**(10).
97. Sorvillo, N., et al., *Extracellular DNA NET-Works With Dire Consequences for Health*. *Circ Res*, 2019. **125**(4): p. 470-488.
98. Essig, F., et al., *Immunohistological Analysis of Neutrophils and Neutrophil Extracellular Traps in Human Thrombemboli Causing Acute Ischemic Stroke*. *Int J Mol Sci*, 2020. **21**(19).
99. El Amki, M., et al., *Neutrophils Obstructing Brain Capillaries Are a Major Cause of No-Reflow in Ischemic Stroke*. *Cell Rep*, 2020. **33**(2): p. 108260.
100. Becker, K.J., *Anti-leukocyte antibodies: LeukArrest (Hu23F2G) and Enlimomab (R6.5) in acute stroke*. *Curr Med Res Opin*, 2002. **18 Suppl 2**: p. s18-22.
101. Krams, M., et al., *Acute Stroke Therapy by Inhibition of Neutrophils (ASTIN): an adaptive dose-response study of UK-279,276 in acute ischemic stroke*. *Stroke*, 2003. **34**(11): p. 2543-8.
102. Enlimomab Acute Stroke Trial, I., *Use of anti-ICAM-1 therapy in ischemic stroke: results of the Enlimomab Acute Stroke Trial*. *Neurology*, 2001. **57**(8): p. 1428-34.
103. Yilmaz, G., et al., *Role of T lymphocytes and interferon-gamma in ischemic stroke*. *Circulation*, 2006. **113**(17): p. 2105-12.
104. Kleinschnitz, C., et al., *Early detrimental T-cell effects in experimental cerebral ischemia are neither related to adaptive immunity nor thrombus formation*. *Blood*, 2010. **115**(18): p. 3835-42.
105. Schuhmann, M.K., et al., *B cells do not have a major pathophysiologic role in acute ischemic stroke in mice*. *J Neuroinflammation*, 2017. **14**(1): p. 112.
106. Ren, X., et al., *Regulatory B cells limit CNS inflammation and neurologic deficits in murine experimental stroke*. *J Neurosci*, 2011. **31**(23): p. 8556-63.
107. Schuhmann, M.K., et al., *CD84 Links T Cell and Platelet Activity in Cerebral Thrombo-Inflammation in Acute Stroke*. *Circ Res*, 2020. **127**(8): p. 1023-1035.
108. Zhang, H., et al., *CD4 T cell deficiency attenuates ischemic stroke, inhibits oxidative stress, and enhances Akt/mTOR survival signaling pathways in mice*. *Chin Neurosurg J*, 2018. **4**.
109. Kleinschnitz, C., et al., *Regulatory T cells are strong promoters of acute ischemic stroke in mice by inducing dysfunction of the cerebral microvasculature*. *Blood*, 2013. **121**(4): p. 679-91.

-
110. Schuhmann, M.K., et al., *CD28 superagonist-mediated boost of regulatory T cells increases thrombo-inflammation and ischemic neurodegeneration during the acute phase of experimental stroke*. J Cereb Blood Flow Metab, 2015. **35**(1): p. 6-10.
 111. Kraft, P., et al., *FTY720 ameliorates acute ischemic stroke in mice by reducing thrombo-inflammation but not by direct neuroprotection*. Stroke, 2013. **44**(11): p. 3202-10.
 112. Zhu, Z., et al., *Combination of the Immune Modulator Fingolimod With Alteplase in Acute Ischemic Stroke: A Pilot Trial*. Circulation, 2015. **132**(12): p. 1104-1112.
 113. Fu, Y., et al., *Impact of an immune modulator fingolimod on acute ischemic stroke*. Proc Natl Acad Sci U S A, 2014. **111**(51): p. 18315-20.
 114. Heindl, S., et al., *Chronic T cell proliferation in brains after stroke could interfere with the efficacy of immunotherapies*. J Exp Med, 2021. **218**(8).
 115. Langhauser, F., et al., *Blocking of alpha4 integrin does not protect from acute ischemic stroke in mice*. Stroke, 2014. **45**(6): p. 1799-806.
 116. Cannons, J.L., et al., *Optimal germinal center responses require a multistage T cell:B cell adhesion process involving integrins, SLAM-associated protein, and CD84*. Immunity, 2010. **32**(2): p. 253-65.
 117. Hofmann, S., et al., *The SLAM family member CD84 is regulated by ADAM10 and calpain in platelets*. J Thromb Haemost, 2012. **10**(12): p. 2581-92.
 118. Ruck, T., et al., *Isolation of primary murine brain microvascular endothelial cells*. J Vis Exp, 2014(93): p. e52204.
 119. nanoAnalytics. *Measure the transepithelial/transendothelial electrical resistance TEER of barrier forming cells automatically*.
 120. Zimmermann, L., et al., *Defining cerebral leukocyte populations in local ischemic blood samples from patients with hyperacute stroke*. J Cereb Blood Flow Metab, 2022. **42**(5): p. 901-904.
 121. Hatfield, R.H., et al., *Triphenyltetrazolium chloride (TTC) as a marker for ischaemic changes in rat brain following permanent middle cerebral artery occlusion*. Neuropathol Appl Neurobiol, 1991. **17**(1): p. 61-7.
 122. Gob, V., et al., *Infarct growth precedes cerebral thrombosis following experimental stroke in mice*. Sci Rep, 2021. **11**(1): p. 22887.
 123. Nadareishvili, Z., et al., *Post-Stroke Blood-Brain Barrier Disruption and Poor Functional Outcome in Patients Receiving Thrombolytic Therapy*. Cerebrovasc Dis, 2019. **47**(3-4): p. 135-142.
 124. Lakhan, S.E., et al., *Matrix metalloproteinases and blood-brain barrier disruption in acute ischemic stroke*. Front Neurol, 2013. **4**: p. 32.
 125. Cloutier, N., et al., *Platelets can enhance vascular permeability*. Blood, 2012. **120**(6): p. 1334-43.
 126. Heindl, B., et al., *Disparate effects of adhesion and degranulation of platelets on myocardial and coronary function in postischaemic hearts*. Cardiovasc Res, 1998. **38**(2): p. 383-94.
 127. Bender, M., et al., *Differentially regulated GPVI ectodomain shedding by multiple platelet-expressed proteinases*. Blood, 2010. **116**(17): p. 3347-55.
 128. Nieswandt, B. and S.P. Watson, *Platelet-collagen interaction: is GPVI the central receptor?* Blood, 2003. **102**(2): p. 449-61.
 129. Varga-Szabo, D., A. Braun, and B. Nieswandt, *Calcium signaling in platelets*. J Thromb Haemost, 2009. **7**(7): p. 1057-66.
 130. Kollikowski, A.M., et al., *Platelet Activation and Chemokine Release Are Related to Local Neutrophil-Dominant Inflammation During Hyperacute Human Stroke*. Transl Stroke Res, 2022. **13**(3): p. 364-369.
 131. Haarmann, A., et al., *Human Brain Endothelial CXCR2 is Inflammation-Inducible and Mediates CXCL5- and CXCL8-Triggered Paraendothelial Barrier Breakdown*. Int J Mol Sci, 2019. **20**(3).
-

-
132. Clapham, D.E., *Calcium signaling*. Cell, 2007. **131**(6): p. 1047-58.
 133. Dalal, P.J., W.A. Muller, and D.P. Sullivan, *Endothelial Cell Calcium Signaling during Barrier Function and Inflammation*. Am J Pathol, 2020. **190**(3): p. 535-542.
 134. Tirupathi, C., et al., *Role of Ca²⁺ signaling in the regulation of endothelial permeability*. Vascul Pharmacol, 2002. **39**(4-5): p. 173-85.
 135. Gelderblom, M., et al., *Temporal and spatial dynamics of cerebral immune cell accumulation in stroke*. Stroke, 2009. **40**(5): p. 1849-57.
 136. Stoll, G., S. Jander, and M. Schroeter, *Inflammation and glial responses in ischemic brain lesions*. Prog Neurobiol, 1998. **56**(2): p. 149-71.
 137. Finsterbusch, M., et al., *Measuring and interpreting platelet-leukocyte aggregates*. Platelets, 2018. **29**(7): p. 677-685.
 138. Organization, W.H. *Cardiovascular diseases (CVDs)*. 2021 11 June 2021; Available from: [https://www.who.int/news-room/fact-sheets/detail/cardiovascular-diseases-\(cvds\)](https://www.who.int/news-room/fact-sheets/detail/cardiovascular-diseases-(cvds)).
 139. Hankey, G.J., *Stroke*. Lancet, 2017. **389**(10069): p. 641-654.
 140. Wafa, H.A., et al., *Burden of Stroke in Europe: Thirty-Year Projections of Incidence, Prevalence, Deaths, and Disability-Adjusted Life Years*. Stroke, 2020. **51**(8): p. 2418-2427.
 141. Powers, W.J., et al., *Guidelines for the Early Management of Patients With Acute Ischemic Stroke: 2019 Update to the 2018 Guidelines for the Early Management of Acute Ischemic Stroke: A Guideline for Healthcare Professionals From the American Heart Association/American Stroke Association*. Stroke, 2019. **50**(12): p. e344-e418.
 142. Wollenweber, F.A., et al., *Functional Outcome Following Stroke Thrombectomy in Clinical Practice*. Stroke, 2019. **50**(9): p. 2500-2506.
 143. Rubiera, M., et al., *Computed Tomography Perfusion After Thrombectomy: An Immediate Surrogate Marker of Outcome After Recanalization in Acute Stroke*. Stroke, 2020. **51**(6): p. 1736-1742.
 144. Heye, N. and J. Cervos-Navarro, *Microthromboemboli in acute infarcts: analysis of 40 autopsy cases*. Stroke, 1996. **27**(3): p. 431-4.
 145. Deng, J., et al., *Arterial wall injury and miRNA expression induced by stent retriever thrombectomy under stenotic conditions in a dog model*. J Neurointerv Surg, 2021. **13**(6): p. 563-567.
 146. Heye, N., et al., *The topography of microthrombi in ischemic brain infarct*. Acta Neurol Scand, 1992. **86**(5): p. 450-4.
 147. Kaesmacher, J., et al., *Risk of Thrombus Fragmentation during Endovascular Stroke Treatment*. AJNR Am J Neuroradiol, 2017. **38**(5): p. 991-998.
 148. Caplan, L.R. and M. Hennerici, *Impaired clearance of emboli (washout) is an important link between hypoperfusion, embolism, and ischemic stroke*. Arch Neurol, 1998. **55**(11): p. 1475-82.
 149. Zhou, P., et al., *Interactions between neutrophil extracellular traps and activated platelets enhance procoagulant activity in acute stroke patients with ICA occlusion*. EBioMedicine, 2020. **53**: p. 102671.
 150. Zhang, W., et al., *The blood brain barrier in cerebral ischemic injury - Disruption and repair*. Brain Hemorrhages, 2020. **1**: p. 34-53.
 151. Knowland, D., et al., *Stepwise recruitment of transcellular and paracellular pathways underlies blood-brain barrier breakdown in stroke*. Neuron, 2014. **82**(3): p. 603-17.
 152. Battey, T.W., et al., *Brain edema predicts outcome after nonlacunar ischemic stroke*. Stroke, 2014. **45**(12): p. 3643-8.
 153. van Kranendonk, K.R., et al., *Hemorrhagic transformation is associated with poor functional outcome in patients with acute ischemic stroke due to a large vessel occlusion*. J Neurointerv Surg, 2019. **11**(5): p. 464-468.
-

154. Jickling, G.C., et al., *Hemorrhagic transformation after ischemic stroke in animals and humans*. J Cereb Blood Flow Metab, 2014. **34**(2): p. 185-99.
155. Sifat, A.E., B. Vaidya, and T.J. Abbruscato, *Blood-Brain Barrier Protection as a Therapeutic Strategy for Acute Ischemic Stroke*. AAPS J, 2017. **19**(4): p. 957-972.
156. Yang, G.Y. and A.L. Betz, *Reperfusion-induced injury to the blood-brain barrier after middle cerebral artery occlusion in rats*. Stroke, 1994. **25**(8): p. 1658-64; discussion 1664-5.
157. Braun, L.J., et al., *Platelets docking to VWF prevent leaks during leukocyte extravasation by stimulating Tie-2*. Blood, 2020. **136**(5): p. 627-639.
158. Feldmann, J., et al., *Munc13-4 is essential for cytolytic granules fusion and is mutated in a form of familial hemophagocytic lymphohistiocytosis (FHL3)*. Cell, 2003. **115**(4): p. 461-73.
159. Menager, M.M., et al., *Secretory cytotoxic granule maturation and exocytosis require the effector protein hMunc13-4*. Nat Immunol, 2007. **8**(3): p. 257-67.
160. van Holten, T.C., et al., *Quantitative proteomics analysis reveals similar release profiles following specific PAR-1 or PAR-4 stimulation of platelets*. Cardiovasc Res, 2014. **103**(1): p. 140-6.
161. Gu, X.L., et al., *Serum CXCL12 Levels as a Novel Predictor of Future Stroke Recurrence in Patients with Acute Ischemic Stroke*. Mol Neurobiol, 2016. **53**(5): p. 2807-2814.
162. Ghasemzadeh, M., et al., *The CXCR1/2 ligand NAP-2 promotes directed intravascular leukocyte migration through platelet thrombi*. Blood, 2013. **121**(22): p. 4555-66.
163. Matsumoto, K., et al., *Platelet CXCL4 mediates neutrophil extracellular traps formation in ANCA-associated vasculitis*. Sci Rep, 2021. **11**(1): p. 222.
164. Karel, M.F.A., et al., *Characterization of cerebral small vessel disease by neutrophil and platelet activation markers using artificial intelligence*. J Neuroimmunol, 2022. **367**: p. 577863.
165. Zaremba, J., P. Skrobanski, and J. Losy, *The level of chemokine CXCL5 in the cerebrospinal fluid is increased during the first 24 hours of ischaemic stroke and correlates with the size of early brain damage*. Folia Morphol (Warsz), 2006. **65**(1): p. 1-5.
166. Yu, M., et al., *CXC chemokine ligand 5 (CXCL5) disrupted the permeability of human brain microvascular endothelial cells via regulating p38 signal*. Microbiol Immunol, 2021. **65**(1): p. 40-47.
167. Borkham-Kamphorst, E. and R. Weiskirchen, *The PDGF system and its antagonists in liver fibrosis*. Cytokine Growth Factor Rev, 2016. **28**: p. 53-61.
168. Kazlauskas, A., *PDGFs and their receptors*. Gene, 2017. **614**: p. 1-7.
169. Sil, S., et al., *PDGF/PDGFR axis in the neural systems*. Mol Aspects Med, 2018. **62**: p. 63-74.
170. Ma, Q., et al., *PDGFR-alpha inhibition preserves blood-brain barrier after intracerebral hemorrhage*. Ann Neurol, 2011. **70**(6): p. 920-31.
171. Grosse, G.M., et al., *Circulating Cytokines and Growth Factors in Acute Cerebral Large Vessel Occlusion-Association with Success of Endovascular Treatment*. Thromb Haemost, 2022. **122**(4): p. 623-632.
172. Shen, J., et al., *PDGFR-beta restores blood-brain barrier functions in a mouse model of focal cerebral ischemia*. J Cereb Blood Flow Metab, 2019. **39**(8): p. 1501-1515.
173. Bieber, M., et al., *Blockade of Platelet Glycoprotein Ibalpha Augments Neuroprotection in Orai2-Deficient Mice during Middle Cerebral Artery Occlusion*. Int J Mol Sci, 2022. **23**(16).
174. Stegner, D., et al., *Loss of Orai2-Mediated Capacitative Ca(2+) Entry Is Neuroprotective in Acute Ischemic Stroke*. Stroke, 2019. **50**(11): p. 3238-3245.
175. Sandoval, R., et al., *Requirement for Ca2+ signaling in the mechanism of thrombin-induced increase in endothelial permeability*. Am J Physiol Lung Cell Mol Physiol, 2001. **280**(2): p. L239-47.

176. Brown, R.C. and T.P. Davis, *Calcium modulation of adherens and tight junction function: a potential mechanism for blood-brain barrier disruption after stroke*. Stroke, 2002. **33**(6): p. 1706-11.
177. Cruzalegui, F.H. and H. Bading, *Calcium-regulated protein kinase cascades and their transcription factor targets*. Cell Mol Life Sci, 2000. **57**(3): p. 402-10.
178. Kong, T., et al., *Role of the Extracellular Signal-Regulated Kinase 1/2 Signaling Pathway in Ischemia-Reperfusion Injury*. Front Physiol, 2019. **10**: p. 1038.
179. Schanbacher, C., et al., *ERK1/2 Activity Is Critical for the Outcome of Ischemic Stroke*. Int J Mol Sci, 2022. **23**(2).
180. Tirupathi, C., et al., *Ca²⁺ signaling, TRP channels, and endothelial permeability*. Microcirculation, 2006. **13**(8): p. 693-708.
181. Mendoza, C., et al., *Calcium regulates the interplay between the tight junction and epithelial adherens junction at the plasma membrane*. FEBS Lett, 2022. **596**(2): p. 219-231.
182. Stamenkovic, I., *Extracellular matrix remodelling: the role of matrix metalloproteinases*. J Pathol, 2003. **200**(4): p. 448-64.
183. Maestrini, I., et al., *Analysis of the association of MPO and MMP-9 with stroke severity and outcome: Cohort study*. Neurology, 2020. **95**(1): p. e97-e108.
184. Rosell, A., et al., *MMP-9-positive neutrophil infiltration is associated to blood-brain barrier breakdown and basal lamina type IV collagen degradation during hemorrhagic transformation after human ischemic stroke*. Stroke, 2008. **39**(4): p. 1121-6.
185. Zhang, S., et al., *Autophagy- and MMP-2/9-mediated Reduction and Redistribution of ZO-1 Contribute to Hyperglycemia-increased Blood-Brain Barrier Permeability During Early Reperfusion in Stroke*. Neuroscience, 2018. **377**: p. 126-137.
186. Zhong, C., et al., *Serum matrix metalloproteinase-9 levels and prognosis of acute ischemic stroke*. Neurology, 2017. **89**(8): p. 805-812.
187. Shi, K., et al., *tPA Mobilizes Immune Cells That Exacerbate Hemorrhagic Transformation in Stroke*. Circ Res, 2021. **128**(1): p. 62-75.
188. Wiedmeyer, C.E., D. Ruben, and C. Franklin, *Complete blood count, clinical chemistry, and serology profile by using a single tube of whole blood from mice*. J Am Assoc Lab Anim Sci, 2007. **46**(2): p. 59-64.
189. Shaw, B.C., et al., *Isolation and identification of leukocyte populations in intracranial blood collected during mechanical thrombectomy*. J Cereb Blood Flow Metab, 2022. **42**(2): p. 280-291.
190. Kolaczkowska, E. and P. Kubes, *Neutrophil recruitment and function in health and inflammation*. Nat Rev Immunol, 2013. **13**(3): p. 159-75.
191. Brandt, E., et al., *Platelet-derived CXC chemokines: old players in new games*. Immunol Rev, 2000. **177**: p. 204-16.
192. Smith, C., et al., *Increased levels of neutrophil-activating peptide-2 in acute coronary syndromes: possible role of platelet-mediated vascular inflammation*. J Am Coll Cardiol, 2006. **48**(8): p. 1591-9.
193. Schuhmann, M.K., et al., *Danger-associated molecular patterns are locally released during occlusion in hyper-acute stroke*. Brain Behav Immun Health, 2021. **15**: p. 100270.
194. Candelario-Jalil, E., R.M. Dijkhuizen, and T. Magnus, *Neuroinflammation, Stroke, Blood-Brain Barrier Dysfunction, and Imaging Modalities*. Stroke, 2022. **53**(5): p. 1473-1486.
195. Wang, Y.C., et al., *Myeloperoxidase: a new target for the treatment of stroke?* Neural Regen Res, 2022. **17**(8): p. 1711-1716.
196. Li, S., et al., *Change and predictive ability of circulating immunoregulatory lymphocytes in long-term outcomes of acute ischemic stroke*. J Cereb Blood Flow Metab, 2021. **41**(9): p. 2280-2294.
197. Nanda, N., et al., *Platelet aggregation induces platelet aggregate stability via SLAM family receptor signaling*. Blood, 2005. **106**(9): p. 3028-34.

-
198. Romero, X., et al., *Differential expression of SAP and EAT-2-binding leukocyte cell-surface molecules CD84, CD150 (SLAM), CD229 (Ly9) and CD244 (2B4)*. Tissue Antigens, 2004. **64**(2): p. 132-44.
 199. Rossaint, J., A. Margraf, and A. Zarbock, *Role of Platelets in Leukocyte Recruitment and Resolution of Inflammation*. Front Immunol, 2018. **9**: p. 2712.
 200. Cognasse, F., et al., *Platelets as Key Factors in Inflammation: Focus on CD40L/CD40*. Front Immunol, 2022. **13**: p. 825892.
 201. Simon, D.I., et al., *Platelet glycoprotein α IIb β 3 is a counterreceptor for the leukocyte integrin Mac-1 (CD11b/CD18)*. J Exp Med, 2000. **192**(2): p. 193-204.
 202. Weber, C. and T.A. Springer, *Neutrophil accumulation on activated, surface-adherent platelets in flow is mediated by interaction of Mac-1 with fibrinogen bound to α IIb β 3 and stimulated by platelet-activating factor*. J Clin Invest, 1997. **100**(8): p. 2085-93.
 203. Setianto, B.Y., et al., *Circulating soluble CD40 ligand mediates the interaction between neutrophils and platelets in acute coronary syndrome*. Heart Vessels, 2010. **25**(4): p. 282-7.
 204. Pluta, K., et al., *Platelet-Leucocyte Aggregates as Novel Biomarkers in Cardiovascular Diseases*. Biology (Basel), 2022. **11**(2).
 205. Marquardt, L., et al., *Leukocyte-platelet aggregates in acute and subacute ischemic stroke*. Cerebrovasc Dis, 2009. **28**(3): p. 276-82.
 206. Schrottmaier, W.C., et al., *Platelet-leukocyte interplay during vascular disease*. Atherosclerosis, 2020. **307**: p. 109-120.
 207. Ishikawa, M., et al., *CD40/CD40 ligand signaling in mouse cerebral microvasculature after focal ischemia/reperfusion*. Circulation, 2005. **111**(13): p. 1690-6.
 208. Lukasik, M., et al., *Upregulation of CD40 ligand and enhanced monocyte-platelet aggregate formation are associated with worse clinical outcome after ischaemic stroke*. Thromb Haemost, 2012. **107**(2): p. 346-55.

6 Appendix

6.1 Devices

Device	Manufacture
Bio RS-24 rotator	Hartenstein, Würzburg
BioPhotometer	Eppendorf, Hamburg
CellZScope	nanoAnalytics, Münster
ChemiDoc™ Touch Imaging System	Bio-Rad, Feldkirchen
Dry Block Thermostat Bio TDB-100	Hartenstein, Würzburg
DUOMAX 1030 shaker	Heidolph Instruments, Schwabach
Eppendorf Centrifuge 5415 R	Eppendorf, Hamburg
FACSLyric	BD Biosciences, Heidelberg
Hera Cell incubator	ThermoFisher, Dreiech
Heraeus Megafuge 1.0R	ThermoFisher, Dreiech
Heraeus Multifuge X1R Centrifuge	ThermoFisher, Dreiech
IKAR VIBRAX VCR basic shaker	Hartenstein, Würzburg
Laboratory shaker KS-10 Swip	Edmund Bühler, Bodelshausen
Labotect Incubator C60	Labotect Labor-Technik-Göttingen, Rosdorf
Leica DMI8	Leica, Wetzlar
MACSmix™ Tube Rotator	Miltenyi Biotec, Bergisch Gladbach
Mega Star 1.6R Centrifuge	VWR, Darmstadt
Microlitercentrifuge MIKRO 200	Andreas Hettich, Tuttlingen
Precision scale PFB	Kern & Sohn, Balingen-Frommern
Sysmex KX-21N Hematology Analyzer	Sysmex Europe, Norderstedt
TECAN Infinite M200PRO	Tecan Trading, Männedorf

6.2 Consumables, Kits

Consumables	Manufacture
μ-slide 8 well	Ibidi, Gräfelfing
Transwell 24 well plates, 0.4 μm pore size	Corning, New York, USA
Syringe filters 0.22 μm	Sarstedt, Nümbrecht

T25 cell culture flask	Greiner Bio-One, Frickenhausen
Capillaries for blood taking	Hartenstein, Würzburg
Transwell 24 well plates, 3.0 µm pore size	Corning, New York, USA
Nitrocellulose membrane 0.45 NC	GE Healthcare, Chicago, USA
Whatman Blotting paper, B003	Hartenstein, Würzburg
Cryovials, 2 ml	Biozym, Hessisch-Oldendorf
PDGF-AB Mouse Quantikine ELISA Kit	R&D Systems, Minneapolis, USA

6.3 Chemicals/Reagents

Chemicals, reagents	Manufacture
(di-)Sodium hydrogen phosphate (Na ₂ HPO ₄)	Roth, Karlsruhe
4-(2-hydroxyethyl)-1-piperazineethanesulfonic acid (HEPES)	Roth, Karlsruhe
Acetic acid	Roth, Karlsruhe
Ammonium chloride (NH ₄ Cl)	Merck, Darmstadt
Ammonium peroxodisulfate (APS)	Merck, Darmstadt
Apyrase	Merck, Darmstadt
B27 supplement	ThermoFisher, Dreiech
BD FACS™ Lysing Solution	BD Biosciences, Heidelberg
bFGF	PeproTech, Cranbury; USA
Bicinchoninic acid solution	Merck, Darmstadt
Bovine serum albumin (BSA)	Merck, Darmstadt
Bromphenol blue	Merck, Darmstadt
Clacium chloride (CaCl ₂)	Roth, Karlsruhe
Collagen from human placenta type IV	Merck, Darmstadt
Collagen related peptide (CRP)	Kindly provided by Bernhard Nieswandt
Collagenase Type 2 (CLS2)	Worthington, Columbus, USA
Collagenase/Dispase	Roche, Basel, Switzerland
Complete Protease Inhibitor	Roche, Basel, Switzerland
Copper (II) sulphate solution	Merck, Darmstadt
Deoxyribonuclease I from bovine pancreas	Merck, Darmstadt

DEPC water	Merck, Darmstadt
Dimethyl sulfoxide (DMSO)	Roth, Karlsruhe
DMEM high glucose	Merck, Darmstadt
Ethanol 100 %	Chemsolute, Renningen
Ethylene glycol tetraacetic acid (EGTA)	Merck, Darmstadt
Fetal calf serum (FCS)	ThermoFisher, Dreiech
Fibronectin bovine plasma	Merck, Darmstadt
Fura-2 acetoxymethyl ester (AM)	ThermoFisher, Dreiech
Glucose	Merck, Darmstadt
Glycerine	Roth, Karlsruhe
Glyoxal solution	Merck, Darmstadt
Heparin sodium salt from porcine intestinal mucosa	Merck, Darmstadt
Hydrochloride acid (HCl)	Merck, Darmstadt
Hydrocortisone	Merck, Darmstadt
Hydrogen peroxide 30%	Merck, Darmstadt
Immersol 518F immersion oil	ThermoFisher, Dreiech
Ionomycin calcium salt	Merck, Darmstadt
Isoflurane	CP Pharma, Burgdorf
Isopropanol	Merck, Darmstadt
L-Glutamine	Merck, Darmstadt
Magnesium chloride (MgCl ₂)	Roth, Karlsruhe
Methanol	VWR, Radnor, USA
Milk powder, fat free	Roche, Basel, Switzerland
NaCl	Roth, Karlsruhe
NaOH	Merck, Darmstadt
Nonidet TM P40 Substitute	Merck, Darmstadt
Paraformaldehyde (PFA)	Merck, Darmstadt
Penicillin/Streptomycin	Merck, Darmstadt
Percoll	GE Healthcare, Chicago, USA
Phosphatase inhibitor	Merck, Darmstadt
Phosphate buffered saline (PBS)	Merck, Darmstadt
Plasma derived Serum (PDS)	First Link UK
Pluronic F-127 20 % solution	ThermoFisher, Dreiech
Ponceau S Solution	Merck, Darmstadt

Potassium chloride (KCl)	Roth, Karlsruhe
Potassium decarbonate (KHCO ₃)	Roth, Karlsruhe
Precision Plus Western C Standards	BioRad, Hercules, USA
Precision Protein Strep Tactin-HRP Conjugate	BioRad, Hercules, USA
Prolong Gold with DAPI	Invitrogen, Waltham, USA
Prostacyclin (PGI ₂)	Merck, Darmstadt
Protease Inhibitor	Merck, Darmstadt
Puromycin dihydrochloride from Streptomyces alboniger	Merck, Darmstadt
RotiphoreseR Gel 30 (Acrylamide)	Roth, Karlsruhe
RPMI	Merck, Darmstadt
RPMI no glucose	ThermoFisher, Dreiech
Sodium azide (NaN ₃)	Merck, Darmstadt
Sodium hydrogencarbonate (NaHCO ₃)	Roth, Karlsruhe
Sodium citrate	Roth, Karlsruhe
Sodium dodecyl sulfate (SDS)	Roth, Karlsruhe
Sodium hydrogen phosphate (NaH ₂ PO ₄)	AppliChem, Darmstadt
Sodium hydroxide (NaOH)	Merck, Darmstadt
Tetramethylethylenediamine (TEMED)	Merck, Darmstadt
Thapsigargin	Life Technologie
Tissue Tek	Hartenstein, Würzburg
Tris(hydroxymethyl)aminomethane (Tris)	Roth, Karlsruhe
Tris/HCl	Roth, Karlsruhe
Tri-sodium citrate dihydrate	Roth, Karlsruhe
Triton X-100	Merck, Darmstadt
Trypsin-EDTA solution	Merck, Darmstadt
Tween ^R 20	Merck, Darmstadt
Water, sterile for cell culture	Merck, Darmstadt
Western Lighting Plus Enhanced Chemiluminescence (ECL)	Perkin Elmer, Rodgau
β-Mercaptoethanol	Merck, Darmstadt

6.4 Buffers, solutions and media

Puromycin containing MBMEC medium	DMEM high glucose 20% PDS 1% L-Glutamine 1% Penicillin/Streptomycin 0.05% bFGF 0.1% Heparin 0.1% Puromycin
Puromycin free MBMEC medium	DMEM high glucose 20% PDS 1% L-Glutamine 1% Penicillin/Streptomycin 0.05% bFGF 0.1% Heparin
RPMI MBMEC medium	RPMI high glucose 2% B27 1% Penicillin/Streptomycin
Freezing medium for MBMEC	60% FCS 10% DMSO 30% DMEM high glucose
Thawing medium for MBMEC	10% FCS DMEM high glucose

20 % BSA in DMEM	20% BSA DMEM high glucose
Percoll gradient	61.3% PBS (1x) 3.2% PBS (10x) 3.2% PDS 32% Percoll
Hydrocortisone Stock	2.8 mM Hydrocortisone 100% Ethanol
Coating Buffer for MBMEC	sterile ddH ₂ O Collagen from human placenta, Type IV Fibronectin
Glyoxal fixation Buffer	ddH ₂ O Pure Ethanol Glyoxal Acetic Acid pH 5
Phosphate buffered saline (PBS), pH 7.4	137 mM NaCl 2.7 mM KCl 8 mM Na ₂ HPO ₄ 1.5 mM NaH ₂ PO ₄ ddH ₂ O

Laemmli Sample Buffer (4x), reducing	62.5 mM Tris/HCl, pH 6.8 8% SDS 15% Glycerine 3% β -Mercaptoethanol Bromphenol blue ddH ₂ O
SDS Sample Buffer (2x), reducing	120 mM Tris, pH 6.8 10% SDS 20% Glycerine 20% β -Mercaptoethanol Bromphenol blue
RIPA Buffer, pH 7.4	25 mM Tris 150 mM NaCl 1% Nonidet P40 0.1% SDS ddH ₂ O
Lysis Buffer (Protein Purification)	RIPA Buffer Phosphataseinhibitor Proteaseinhibitor
Running Buffer (10x)	35 mM SDS 250 mM Tris 1.92 M Glycine ddH ₂ O

Separating Gel Buffer	30% Bisacrylamide 1.5 M Tris, pH 8.8 10% SDS 10% APS TEMED ddH ₂ O
Stacking Gel Buffer	30% Bisacrylamide 1 M Tris, pH 6.8 10% SDS 10% APS TEMED ddH ₂ O
Blotting Buffer (10x)	1.92 M Glycine 250 mM Tris ddH ₂ O
Blotting Buffer (1x)	ddH ₂ O 20% Methanol 10% Blotting Buffer (10x)
Washing Buffer (10x)	PBS (10x) 0.5% Tween
Washing Buffer (1x)	ddH ₂ O 10% Washing Buffer (10x)

Blocking Buffer	Washing Buffer (1x) 5% Fat-free dry milk powder
Incomplete Stripping Buffer	15% H ₂ O ₂ 85% Washing Buffer (1x)
Complete Stripping Buffer	100 mM Tris, pH 6.8 2% SDS 0.8% β-Mercaptoethanol ddH ₂ O
Splenocyte complete	1 M HEPES 25 μg/ml Gentamycin 50 μM Mercaptoethanol 5% FCS 2 mM L-Glutamine 1% NEAA (100x) DMEM high glucose
Splenocyte Washing Buffer	1% FCS 1% L-Glutamine 1% Pen/Strep DMEM high glucose

Tyrode's buffer, pH 7.3	134 mM NaCl
	0.34 mM Na ₂ HPO ₄
	2.9 mM KCl
	12 mM NaHCO ₃
	5 mM HEPES
	1 mM MgCl ₂
	5 mM Glucose
	0.35% BSA

FACS Buffer	PBS (1x)
	1% FCS
	0.09% Sodium azide

6.5 Antibodies

Primary Antibodies Western Blot

Antibody (anti-)	Host	Manufacture
β-Actin	mouse	Merck
Albumin	chicken	Abcam
p44/42 MAPK	rabbit	Cell Signalling
Phospho-p44/42 MAPK	rabbit	Cell Signalling
MMP9	rabbit	Abcam

Secondary Antibodies Western Blot

Antibody	Host	Manufacture
Anti-rabbit-HRP	donkey	Jackson Immuno R
Anti-mouse-HRP	donkey	Jackson Immuno R
Anti-chicken-HRP	goat	Abcam

Primary Antibodies Mouse Immunohistochemistry

Antibody (anti-)	Host	Manufacture
Albumin	rabbit	Abcam
CD31	rat	BioRad
ZO1	rabbit	Invitrogen

Primary Antibodies Human Immunohistochemistry

Antigen	Host	Manufacture
CD42b	rabbit	Abcam
Neutrophil Elastase	Mouse	Dako

Secondary Antibodies Immunohistochemistry

Antibody	Host	Manufacturer
Anti-rabbit AF594	goat	Invitrogen
Anti-rabbit AF647	Goat	Invitrogen
Anti-rabbit AF594	goat	Life Technologies
Anti-rat Dylight 488	donkey	Abcam
Anti-mouse AF488	Goat	Invitrogen

Antibodies for Flow Cytometry with Human Samples

Antibody	Clone	Isotype	Conjugate	Manufacture
CD3	SK7	mouse IgG1, κ	BALB/c FITC	BD Biosciences
CD16	B73.1	mouse IgG1, κ	BALB/c PE	BD Biosciences
CD56	NCAM16.2	mouse IgG2b, κ	BALB/c PE	BD Biosciences
CD45	2D1 (HLe-1)	mouse IgG1, κ	PerCP-Cy5.5	BD Biosciences
CD4	SK3	mouse IgG1, κ	BALB/c PE-Cy7	BD Biosciences

CD19	SJ25C1	mouse IgG1, κ	BALB/c	APC	BD Biosciences
CD8	Sk1	mouse IgG1, κ	BALB/c	APC-Cy7	BD Biosciences
CD41a	HIP8	mouse IgG1, κ		BV421	Biolegend

Antibodies for Flow Cytometry with Murine Samples

Antibody	Clone	Isotype	Conjugate	Manufacture
TruStain FcX™ Plus	S17011E	rat IgG2b, κ		Biolegend
Live/Dead			7-AAD	Biolegend
CD45	30-F11	rat (LOU) IgG2b, κ	V500-C	BD Biosciences
CD3	17A2	rat IgG2b, κ	APC-Cy7	Biolegend
CD11b	M1/70	rat IgG2b, κ	BV785	Biolegend

Platelet/Endothelial cell agonists

Agonist	Manufacture
Adenosine 5'-diphosphate (ADP)	Hart Biologicals, Hartlepool, UK
Collagen-related peptide (CRP)	Kindly provided by Bernard Nieswandt
CXCL12	Bio Techne, Minneapolis, USA
CXCL5	PeptoTech, Cranbury; USA
CXCL7	Biolegend, San Diego, USA
CXCL8	PeptoTech, Cranbury; USA
Human thrombin	Roche, Basel, Switzerland
PDGF-AB	Biolegend, San Diego, USA
PDGF-BB	Biolegend, San Diego, USA
PDGF antibody	R&D Systems, Minneapolis, USA
PF4	Kindly provided by David Stegner
VEGF-121	Biolegend, San Diego, USA
VEGF-165	Biolegend, San Diego, USA

6.6 Software

Software	Manufacture
BD FACSuite™ Clinical Software V1.4	BD Biosciences, Heidelberg
BD FACSuite™ Research Software V1.4	BD Biosciences, Heidelberg
BioRender	Biorender AG, Toronto, Canada
CellZscope 2.2.1	nanoAnalytics, Münster
ChemDraw 20.0	PerkinElmer, Waltham, USA
FlowJo 10.8.0	BD Biosciences, Heidelberg
GraphPad Prism 9.3.0.463	GraphPad Software, San Diego, USA
Image Lab 5.2.1	Bio-Rad, Feldkirchen
ImageJ	NIH, Bethesda, USA
TECAN i-control 2.0	Tecan Trading AG, Männedorf

7 Abbreviations

°C	Degree Celcius
μM	μMol
2-PM	2-photon intravital microscopy
ACA	Anterior cerebral artery
ADP	Adenosine diphosphate
AJ	Adherens junctions
AMPA	α-amino-3-hydroxy-5-methyl-4-isoxazolepropionic acid
ANCA	Anti-neutrophil cytoplasmic antibody
ANOVA	Analysis of variance
APC	allophycocyanin
APS	Ammonium peroxodisuophate
ATP	Adenosine triphosphate
BBB	Blood brain barrier
BCA	Bicinochonic acid
bFGF	Basic fibroblast growth factor
BSA	Bovine serum albumin
BV	Brilliant violet
c	contralateral
CBF	Cerebral blood flow
CCA	Common carotid artery
CD	Cluster of differentiation
CLS2	Collagenase Type2
CNS	Central nervous system
CPDA1	Citrate-phosphate-dectrose-adenine 1
CRP	Collagen-related peptide
CXCL	C-X-C motif ligand
Cy	Cyanine
d	Day
DAMP	Danger-associated molecular pattern
DAPI	4',6-Diamidino-2-Phenylindole
DMEM	Dulbecco's modified eagle's medium
DMSO	dimethylsulfoxide

ECL	Enhance chemiluminescence
ECM	Extracellular matrix
ECs	Endothelial cells
EDTA	Ethylenediaminetetraacetic acid
ELISA	Enzyme linked immune sorbent assay
ERK	Extracellular signal-regulated kinase
FACS	Fluorescence activated cell sorting
FCS	Fetal calf serum
FITC	Fluorescein-5-isothiocyanate
FOXP3	Forkhead box P3
FSC	Forward scatter
FTY720	Fingolimod
g	Gramme
GP	Glycoprotein
h	Hour
HEPES	2-[4-(2-hydroxyethyl)piperazin-1-yl]ethanesulfonic acid
HMGB1	High-mobility group box 1
HRP	Horseradish peroxidase
HT	Haemorrhagic transformation
i	ipsilateral
I/R injury	Ischemia-reperfusion injury
ICA	Internal carotid artery
ICH	Intracranial haemorrhage
IL	Interleukin
IS	Ischemic stroke
ITAM	Immunoreceptor tyrosine-based activation motif
kDa	Kilo Dalton
LVO	Large-vessel occlusion
MAPK	Mitogen-activated protein kinase
MBMEC	Murine brain microvascular endothelial cells
MCA	Middle cerebral artery
ME	mercaptoethanol
min	Minutes
MKs	Megakaryocytes
MMP	Matrix metalloproteinase

MPO	Myeloperoxidase
MS	Multiple sclerosis
MT	Mechanical thrombectomy
Nbeal2	Neurobeachin-like 2
NETs	Neutrophil extracellular traps
NK cells	Natural killer cells
Nm	Nano meters
NMDA	N-methyl-D-aspartate
NVU	Neurovascular unit
o/n	Over night
PAGE	Polyacrylamide gel electrophoresis
PBS	Phosphate buffered saline
PCA	Posterior cerebral artery
PDGF	Platelet derived growth factor
PDGF-NAb	Platelet derived growth factor neutralization antibody
PDS	Plasma derived serum
PE	Phycoerythrin
Pen/Strep	Penicillin/Streptomycin
PerCP	Peridinin-chlorophyll-protein
PF-4	Platelet factor 4
PGI ₂	Prostacyclin
PLA	Platelet-leukocyte aggregates
PMA	Platelet-monocyte aggregates
pMCAO	Permanent middle cerebral artery occlusion
PMN	Polymorphnuclear leukocytes
PRP	Platelet rich plasma
Rag1	Recombinant activating gene 1
RIPA	radio immunoprecipitation assay
ROS	Reactive oxygen species
rpm	Rounds per minute
RT	Room temperature
rt-PA	Recombinant tissue plasminogen activator
s	Seconds
sCD84	Soluble CD84
SD	Standard deviation

SDS	Sodium dodecyl sulfate
SDS-PAGE	SDS-acrylamide gel electrophoresis
SLAP	Src-like adaptor proteins
SSC	Sideward scatter
TEER	Transendothelial electrical resistance
TEMED	Tetramethylethylenediamine
TIA	Transient ischemic attack
TJ	Tight junctions
tMCAO	Transient middle cerebral artery occlusion
T _{reg}	Regulatory T cells
TRIS	Trishydroxymethylaminomethane
TTC	2,3,5-triphenyltetrazolium chloride
U	Units
vWF	Von Willebrand factor
WT	Wild type

8 Creative Commons License

This thesis contains content from published scientific publications. Illustrations displayed in the introduction and discussion have been adopted or modified from Campbell *et al.* [8], Fluri *et al.* [26], Sweeney *et al.* [35], Stegner *et al.* [63], or Stoll *et al.* [16]. These publications were either distributed under the terms of the Creative Commons Attribution License (<https://creativecommons.org/licenses>) or permission was gathered by the copyright keeper. The former also applies to parts of the result section, which contains data that is published under Göb *et al.* [122] and Zimmermann *et al.* [120].

9 Curriculum vitae

10 Acknowledgements

First and foremost, I would like to thank my primary supervisor Michael Schuhmann for giving me the opportunity to do my PhD thesis in his laboratory and on this outstanding thesis project. I am grateful for his excellent supervision, constant support and advice. Thank you for the trust and confidence you placed in my abilities, which let me grow throughout the time of my thesis.

I would also express my gratitude to my thesis committee members David Stegner, Katrin Heinze and Prof Dr. Mirko Pham for your advice, the constant motivation and the fruitful discussions during our committee meetings.

Furthermore, I would like to thank Guido Stoll for the enthusiastic support throughout my thesis and the constructive input.

I would like to express my special thanks to all people shaping my way and for their unconditional support during my thesis: Michael Bieber, Sarah Hopp-Krämer, Carine Nguemeni, Martina Wilhelm, Sarah Beck, Maximilian Bellut, Alexander Kollikowski, Susanne Hellmig, Gabriele Köllner, Sabrina Braunschweig, the team of the CSF laboratory and the Flachbau crew.

Especially, I want to thank Vanessa Göb for the great cooperation within the B06 project, the constant commitment and the friendly relationship.

Another special thank goes to the PhD students of the platelet literature seminar (Experimental Biomedicine Chair I) for the valuable discussions on platelet/ MK functions in various pathological settings.

I would also like to thank my family for the unceasing encouragement and support throughout so many years. Without your support, it would not have been possible to take this path.

But my warmest thanks are owed by my husband Thomas and Laika for constant encouragement, support, patience, and love.

11 Publications

Haarmann A., **Zimmermann L.**, Bieber M., Silwedel C., Stoll G., Schuhmann M.K. Regulation and release of vasoactive endoglin by brain endothelium in response to hypoxia/reoxygenation in stroke. *Int. J. Mol. Sci.* 2022; 23(13):7085.

Bellut M., Raimondi A.T., Haarmann A., **Zimmermann L.**, Stoll G., Schuhmann M.K. NLRP3 inhibition reduces rt-PA induced endothelial dysfunction under ischemic conditions. *Biomedicines.* 2022; 10(4):762.

Zimmermann L.*, Pham M.*, März A.G., Kollikowski A.M., Stoll G., Schuhmann M.K. Defining cerebral leukocyte populations in local ischemic blood samples from patients with hyperacute stroke. *J Cereb Blood Flow Metab.* 2022; 42(5):901-904.

Kollikowski A.M., Pham M., März A.G., **Papp L.**, Nieswandt B., Stoll G., Schuhmann M.K. Platelet Activation and Chemokine Release Are Related to Local Neutrophil-Dominant Inflammation During Hyperacute Human Stroke. *Transl Stroke Res.* 2022; 13(3):364-369.

Göb V., Voll M.G., **Zimmermann L.**, Hemmen K., Stoll G., Nieswandt B., Schuhmann M.K., Heinze K.G., Stegner D. Infarct growth precedes cerebral thrombosis following experimental stroke in mice. *Sci Rep.* 2021;11(1):22887.

Bellut M., **Papp L.**, Bieber M., Kraft P., Stoll G., Schuhmann M.K. NLRP3 inflammasome inhibition alleviates hypoxic endothelial cell death in vitro and protects blood-brain barrier integrity in murine stroke. *Cell Death Dis.* 2021;13(1)20.

Schuhmann M.K., **Papp L.**, Stoll G., Blum R., Volkmann J., Fluri F. Mesencephalic Electrical Stimulation Reduces Neuroinflammation after Photothrombotic Stroke in Rats by Targeting the Cholinergic Anti-Inflammatory Pathway. *Int J Mol Sci.* 2021;22(3):1254.

Bohr A., Schuhmann M.K., **Papp L.**, Volkmann J., Fluri F. Deep Brain Stimulation for Stroke: Continuous Stimulation of the Pedunculopontine Tegmental Nucleus has no Impact on Skilled Walking in Rats After Photothrombotic Stroke. *Curr Neurovasc Res.* 2020;17(5):636-643.

Schuhmann M.K., Stoll G., Bieber M., Vögtle T., Hofmann Sebastian, Klaus V., Kraft P., Syhan M., Kollikowski A.M., **Papp L.**, Heuschmann P.U., Pham M., Nieswandt B., Stegner D. CD84 Links T Cell and Platelet Activity in Cerebral Thrombo-Inflammation in Acute Stroke. *Circ Res.* 2020;127(8):1023-1035.

Schuhmann M.K., Stoll G., **Papp L.**, Bohr A., Volkmann J., Fluri F. Electrical Stimulation of the Mesencephalic Locomotor Region Has No Impact on Blood-Brain Barrier Alterations after Cerebral Photothrombosis in Rats. *Int J Mol Sci.* 2019;20(16):4036.

12 Affidavit

I hereby confirm that my thesis entitled “Platelets as modulators of blood-brain barrier disruption and inflammation in the pathophysiology of ischemic stroke” is the result of my own work. I did not receive any help or support from commercial consultants. All sources and/or materials applied are listed and specified in the thesis.

Furthermore, I confirm that this thesis has not yet been submitted as part of another examination process neither in identical nor in similar form.

Würzburg, Oktober 2022

.....

Zimmermann, Lena

13 Eidessattliche Erklärung

Hiermit erkläre ich an Eides statt, die Dissertation „Thrombozyten als Modulatoren der Blut-Hirn-Schrankenstörung und Inflammation in der Pathophysiologie des ischämischen Schlaganfalls“ eigenständig, d.h. insbesondere selbständig und ohne Hilfe eines kommerziellen Promotionsberaters, angefertigt und keine anderen als die von mir angegebenen Quellen und Hilfsmittel verwendet zu haben.

Ich erkläre außerdem, dass die Dissertation weder in gleicher noch in ähnlicher Form bereits in einem anderen Prüfungsverfahren vorlegen hat.

Würzburg, Oktober 2022

.....

Zimmermann, Lena